NOTE TO USERS

VIBRATION ANALYSIS OF A HAND-GRINDER SYSTEM UNDER WHEEL UNBALANCE EXCITATION

LakshmiNarayana Naga Nemani

A Thesis
in
The Department
of
Mechanical and Industrial Engineering.

Presented in Partial Fulfillment of the Requirements
for
The Degree of Master of Applied Science
at
Concordia University
Montreal, Quebec, Canada

April 2005

Your file Votre référence
ISBN: 0-494-04424-1
Our file Notre référence
ISBN: 0-494-04424-1

ABSTRACT

VIBRATION ANALYSIS OF A HAND-GRINDER SYSTEM UNDER WHEEL UNBALANCE EXCITATION

LakshmiNarayana Naga Nemani

Use of hand-held grinding machines can cause excessive vibrations of the hand-arm system. Continued use of these vibrating tools has been found to be connected with various patterns of diseases affecting the blood vessels, nerves, bones, joints and muscles of the hand and forearm. The most severe symptom of prolonged exposure to hand-transmitted vibrations is the Vibration Induced White Finger (VWF) disease. The development of these disorders depends on the level of acceleration produced by the tool. In this thesis, the tool vibrations transmitted to the operator's hand and arm is investigated. A grinder model is developed and the calculated natural frequencies have been validated through laboratory experiments. Further, a two degrees-of-freedom (DOF) lumped parameter model of the human hand-arm system is developed, along each of the three orthogonal directions in order to identify the parameters of the hand-arm vibration (HAV) models using the reported mechanical impedance data and nonlinear programming based optimization technique. A complex eigenvalue analysis is performed in order to identify the damped natural frequencies and damping ratios of the hand-arm, which shows that the human hand-arm is a heavily damped system. Using the above information, an analytical model of the coupled hand-tool model with 14 degrees-of-freedom is developed to study the hand-transmitted vibration caused by the rotating unbalance of the grinding wheel. The simulation results obtained for different mass unbalances suggest that the magnitude of hand-transmitted vibration increases

considerably with increase in the mass unbalance. The results of the parametric study suggest that an increase in machine casing weight can help reduce the magnitudes of hand-transmitted vibration, but a heavier tool would be undesirable. Variations in the bearing damping do not influence the magnitude of transmitted vibration. The effect of hand-handle interface properties have also been studied by introducing visco-elastic properties representing anti-vibration glove. The resulting 17-DOF analytical model of the coupled hand-tool system is used to study the performance characteristics of the anti-vibration gloves materials. The study concludes that anti-vibration gloves can attenuate the hand-transmitted vibration at certain speeds.

ACKNOWLEDGEMENTS

I am sincerely grateful to my supervisors, Dr. Rama Bhat and Dr. Subhash Rakheja for their support, guidance and encouragement during all stages of this research.

I wish to thank members of the faculty and staff of CONCAVE Research Centre and the Department of Mechanical and Industrial Engineering at Concordia University for their help during the course of this work.

The Financial support by the Mechanical and Industrial Engineering Department at Concordia University through the Natural Sciences and Engineering Research Council is further acknowledged.

I also want to thank my colleagues, friends and fellow students for their help and useful discussions during this work.

Finally, I would like to thank my parents, brothers and other family members for their love, encouragement and constant motivation throughout the course of this investigation.

DEDICATION

I DEDICATE THIS THESIS TO LORD SRI VENKATESWARA

TABLE OF CONTENTS

APPENDIX D
EIGEN VECTORS OF 17 DEGREE-OF-FREEDOM HAND-GRINDER MODEL

LIST OF FIGURES

LIST OF TABLES

LIST OF ABBREVIATIONS AND SYMBOLS

a_0	Distance between the centre of gravity and grinding wheel
a_1	Distance between the centre of gravity and bearing no#1
b_1	Distance between the centre of gravity and bearing no#2
c_1	Distance between the centre of gravity and O-ring
d_1	Distance between the centre of gravity and retainer spring
[C]	Damping coefficient matrix
C_{bx1}	Damping coefficient of bearing no#1 along the X-axis (Ns/m)
C_{bx2}	Damping coefficient of bearing no#2 along the X-axis (Ns/m)
C_{by1}	Damping coefficient of bearing no#1 along the Y-axis (Ns/m)
C_{by2}	Damping coefficient of bearing no#2 along the Y-axis (Ns/m)
C_{bz1}	Damping coefficient of bearing no#1 along the Z-axis (Ns/m)
C_{bz2}	Damping coefficient of bearing no#2 along the Z-axis (Ns/m)
C_g	Damping coefficient of anti-vibration gloves (Ns/m)
$C_{hx1}, C_{hx2}, C_{hx3}$	Damping coefficients of hand-arm along the X-axis (Ns/m)
$C_{hy1}, C_{hy2}, C_{hy3}$	Damping coefficients of hand-arm along the Y-axis (Ns/m)
$C_{hz1}, C_{hz2}, C_{hz3}$	Damping coefficients of hand-arm along the Z-axis (Ns/m)
C_0	Damping coefficient of O-ring (Ns/m)
C_{sr}	Damping coefficient of retainer spring (Ns/m)
C_g	Damping coefficient of anti-vibration gloves (Ns/m)

$E(\bar{\lambda})$	Objective function for the minimization of error
F_{tx}	Force transmitted along the X-axis (N)
F_{ty}	Force transmitted along the Y-axis (N)
F_{tz}	Force transmitted along the Z-axis (N)
F_{tx3}	Force transmitted to the base along the X-axis (N)
F_{ty3}	Force transmitted to the base along the Y-axis (N)
F_{tz3}	Force transmitted to the base along the Z-axis (N)
I_x	Moment of inertia around X-axis ($kg.m^2$)
I_y	Moment of inertia around Y-axis ($kg.m^2$)
I_z	Moment of inertia around Z-axis ($kg.m^2$)
j	Imaginary Unit ($j = \sqrt{-1}$)
[K]	Spring stiffness matrix
K_{bx1}	Stiffness coefficient of bearing no#1 along the X-axis (N/m)
K_{bx2}	Stiffness coefficient of bearing no#2 along the X-axis (N/m)
K_{by1}	Stiffness coefficient of bearing no#1 along the Y-axis (N/m)
K_{by2}	Stiffness coefficient of bearing no#2 along the Y-axis (N/m)
K_{bz1}	Stiffness coefficient of bearing no#1 along the Z axis (N/m)
K_{bz2}	Stiffness coefficient of bearing no#2 along the Z axis (N/m)
K_g	Stiffness of anti vibration gloves (N/m)
$K_{hx1}, K_{hx2}, K_{hx3}$	Stiffness coefficients of hand-arm along the X-axis

$K_{hy1}, K_{hy2}, K_{hy3}$	Stiffness coefficients of hand-arm along the Y-axis
$K_{hz1}, K_{hz2}, K_{hz3}$	Stiffness coefficients of hand-arm along the Z-axis
K_0	Stiffness coefficient of O-ring (N/m)
K_{sr}	Stiffness coefficient of retainer spring (N/m)
m_d	Mass of the shaft-disc (kg)
M_g	Mass of anti-vibration gloves (kg)
m_u	Mass of the unbalance (kg)
$M_{hx1}, M_{hx2}, M_{hx3}$	Hand mass along the X-axis (kg)
$M_{hy1}, M_{hy2}, M_{hy3}$	Hand mass along the Y-axis (kg)
$M_{hz1}, M_{hz2}, M_{hz3}$	Hand mass along the Z-axis (kg)
[M]	Mass matrix
W_d	Energy dissipated (J)
ξ	Damping ratio
ω_n	Natural frequency (Hz)
ω_d	Damped frequency (Hz)
ϕ	Impedance phase angle in degrees
α	Rotation of the model around Z-axis (rad)
β	Rotation of the model around Y-axis (rad)
$\dot{\alpha}$	Precessional velocity around Z-axis (rad/sec)
$\dot{\beta}$	Precessional velocity around Y-axis (rad/sec)

CHAPTER 1
LITERATURE REVIEW AND OBJECTIVES

1.1 Introduction

Extended exposure to vibration generated by the hand-held power tools can cause pathological damage to the tissues and organs within the human hand and arm. Vibration induced health problems have been widely reported among workers who use hand-held power tools, such as chain saws, chipping hammers and grinders [1]. These power tools are known to transmit considerable levels of vibration to the operator's hand and arm. These high amplitude vibrations predominate in a wide frequency range, 10-2000 Hz, and are often limited to the hand-arm of the operators [2, 3]. The severe health risks posed by prolonged occupational exposure to the vibrations of hand-held power tools, supported by the findings of the epidemiological studies have prompted considerable efforts to enhance an understanding of the dynamic response characteristics of the human hand-arm system. Prolonged exposure to vibration transmitted to the operators of hand-held power tools has been related to symptoms of vibration white finger (VWF) disease also known as "Raynaud's Phenomenon of Occupational Origin". Many epidemiological and clinical studies have established the prevalence rates and vibration related symptoms, such as VWF disease, loss of muscle strength, injuries to bones, and joints and disorders of central nervous system [4,5].

Many epidemiological studies have established a strong relationship between the effects of hand-transmitted vibration (HTV) and the white finger attacks [6]. The first symptoms of VWF disease are related to intermittent tingling and numbness of the

fingers. With continued exposure, the tingling is followed by an attack of finger blanching in the first instance, confined to a finger tip, which subsequently propagates to the base of the finger. In view of the severity of the hand-arm vibration disease, caused by prolonged exposure to hand-held power tool vibration, considerable efforts have been made to understand the hand arm vibration syndrome. These studies have been directed towards enhancing an understanding of the bio-dynamic response of the hand-arm, hand-arm syndrome etiology, dose-response standards, and to develop methods to control transmission of vibration to the hand.

Owing to the potentially severe health effects of exposure to hand-transmitted vibration, considerable efforts have also been made to reduce the magnitudes of vibration in the hand-held machines. The major approach to the elimination or reduction of the vibration acceleration exposure levels are (i) reduction at the source and (ii) reduction during transmission. Reductions in the source vibration have been realized through tool operation at suitable speeds, tool and drive maintenance, and through improved designs of the drives [7]. A suitable vibration-isolation system for a hand held vibrating tool must satisfy the following conditions: it must simultaneously reduce vibration in different directions, not influence the operation of the power tool nor increase significantly its weight. The attenuation of HTV is primarily attained using two methods: (i) isolation of the tool handle from the source of vibration, and (ii) isolation of the hand from the tool handle. Tool-handle isolators, integrated within chain saws, have proven effective in attenuating the tool vibration transmitted to the operators [8,9]. The general implementation of such isolators, however, has been limited because of the design complexities of many tools [10]. Alternatively, handle grips and antivibration gloves

have been recommended for isolating the hand from the vibrating handle. Investigators have noted that at low frequencies (around 10 Hz) individuals perceived the sensation of vibration (due to vibration directed into the hand) all the way upto the shoulder and in some cases in the upper part of the torso, neck and head. As the vibration frequency was increased, the sensation of vibration tended to move down the arm until at frequencies above 100 Hz to 150 Hz, the sensation was primarily localized to the fingers [2, 3]. A series of studies performed on assessment of gloves have concluded that the gloves provide either negligible or limited isolation from vibration [11-13]. The control of vibration caused by operation of a hand-held power tool necessitates knowledge of its dynamic behavior and dynamic interactions of the components within the tool. Few studies have attempted to study the dynamic behavior of power tools and dynamic interactions among the components [14].

This dissertation concerns with the vibration behaviour of rotary hand-held tool, particularly a grinder. A hand-held grinder transmits comprehensive magnitudes of vibration to the operators hands, arising from many sources. These include the rotary unbalance of the grinding wheel that may vary with the usage, dynamic interactions associated with the grinding process, dynamic interaction among the electric/pneumatic drive and gear transmission, etc. The rotating unbalance tends to cause considerable vibration at a relative low frequency to which human hand-arm system is more sensitive. The biodynamic model of the human hand-arm system will be developed and integrated to the grinder model in order to derive the coupled hand-tool model. This dissertation research involves the analysis of vibration transmitted to the operators hand due to rotating unbalance of the grinding wheel.

1.2 Effects of Prolonged Exposure to Hand-Transmitted Vibration

Effects of occupational exposure to hand-transmitted vibration have been the focus of many epidemiological and clinical investigations [1,15]. The symptoms and effects of prolonged exposure to hand-transmitted vibration may be grouped as:

i. Neural and vascular effects.

ii. Muscular effects.

iii. Bone and joint effects and

iv. Effects on central nervous system.

Apart from the health and safety risks, the above mentioned effects of hand-transmitted vibration are known to decrease the performance and productivity of workers.

1.2.1 Epidemiological Studies

It has been well known that work involving vibrating tools may result in specific injuries to the hand-arm segment. Epidemiological studies conducted in several countries, showed that millions of industrial workers are being exposed to hand vibration throughout the world. Epidemiology surveys of vibration-exposed workers have shown that the prevalence of peripheral sensorineural disorders varies from a few percent to more than 80% and that symptoms and signs of sensory loss can effect users of a wide range of tool types [4, 5]. An extensive study in the U.S. estimated that of the 8 million workers exposed to vibration, approximately 7 million are exposed to whole body vibration and 1 million are exposed to hand-arm vibration [16]. In Canada an estimate made by the National Research Council of Canada indicated that approximately 200,000 workers are exposed to hand-arm vibration [17]. Studies conducted in Great Britain also

supported the findings of North America, with respect to the exposed population of [18]. The results of the study, presented in Figure 1.1, reveal that approximately 700,000 workers are exposed to occupational hand-arm vibration in different industries in Great Britain. The results of Figure 1.1, also reveal that, about 365,000 of the workers in Mechanical Engineering field, 125,000 workers in construction field, 60000 in the Agriculture, Forestry and in Shipbuilding sector, are also exposed to hand-arm vibrations. The workers in the concrete industry are least exposed to hand-arm vibration in Great Britain.

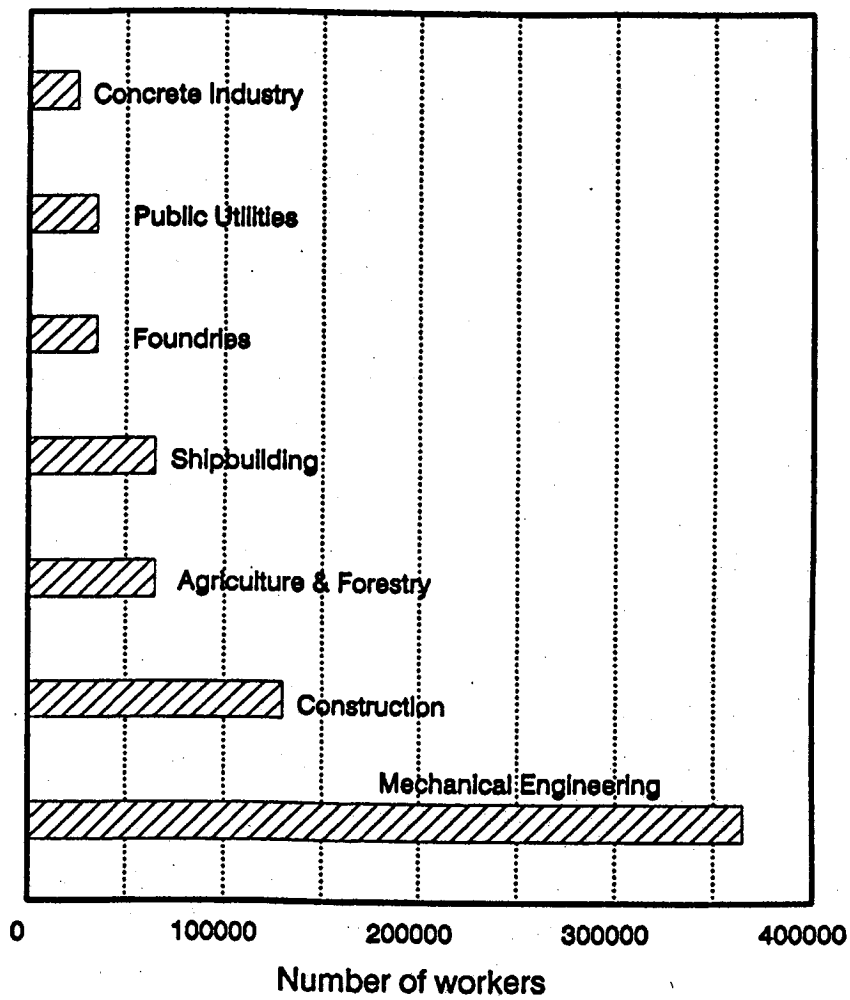

Figure 1.1: Workers exposed to hand-arm vibration in Great Britain [18]

Epidemiological studies have concentrated on three tool categories:

i. Pneumatic tools (chippers, grinders, jackhammers, riveters, and drills).

ii. Electrically operated tools (sanders, pedestal grinders, impact hammers), and

iii. Chain saws.

Many investigators have performed numerous field measurements to characterize the nature of vibration generated by different hand-held power tools, during operation. The studies conducted by investigators revealed that the magnitudes of vibration encountered on different tools vary significantly, from 10 m/s^2 weighted to 2014 m/s^2 unweighted, depending upon the tool, application, speed, feed, location of point of measurements, etc. [19-21]. The dominant frequencies of vibration, however, appear in the 25-320 Hz range, irrespective of the tool and the operating conditions.

All the epidemiological studies have reported the prevalence of HAV syndrome among the population of workers exposed to hand-arm vibration, independent of the level and nature of vibration exposure. The wide range of health effects and disorders associated with exposure to these high levels of hand-transmitted vibration have been grouped into five types of disorders, as summarized in Table 1.1. The prevalence of VWF symptoms among the operators using different tools is illustrated in Table 1.2. It must be noted that some types of tools appear more than once in Table 1.2, which yield vast differences in the acceleration levels due to differences in their size and capacity. While the measured acceleration levels differ considerably for different tools, the magnitudes are evidently very high irrespective of the type of tool.

The National Institute of Occupational Safety and Health (NIOSH), in the U.S. has established a linear relationship between the measured acceleration levels and the

Table 1.1 Types of disorders associated with hand-transmitted vibration exposure [6]

Type	Disorder
A	Vascular disorders
B	Bone and joint disorders
C	Peripheral neurological disorders
D	Muscle disorders
E	Other disorders (e.g. of the whole-body and central nervous system)

Table 1.2 Acceleration levels measured on different tools and associated VWF rates reported in different studies

Tool Type (Reference)	Acceleration Level (m/s^2)*	Prevalence of VWF Symptoms (%)
Chipping hammer [23]	2014	80
Riveter [24]	1183	75
Chipping hammer [25]	424	45
Pedestal grinder [26]	382	86
Chipping hammer [27]	378	64
Jack-leg drill [28]	362	50
Jack-leg drill [29]	339	70
Jack-leg drill [30]	335	80
Chipping hammer [31]	251	47
Grinder [32]	205	31
Pavement breaker [33]	195	10
Pedestal grinder [34]	125	96
Pedestal grinder [35]	122	100
Jack-leg drill [36]	121	72
Chain saw [30]	75	38
Jack-leg drill [36]	20#	45
Hand grinder [38]	20	35
Riveter [39]	10#	25

* Unweighted Acceleration except as mentioned

Weighted Acceleration as per ISO- 4 hour value

prevalence of vascular symptoms based on (i) epidemiologic data derived from field investigations, (ii) data from clinical examinations of workers who have used vibrating tools, and (iii) data derived from laboratory studies [22]. While the epidemiological studies do not provide a relationship between the vibration levels and the occurrence of HAV syndrome among the power tool operators, these studies provide ample evidence that the use of vibration producing, hand-held tools is associated with the development of HAV syndrome.

1.2.2 Factors that Influence Hand-Arm Vibration Severity

Human response to vibration exposure depends on several factors, such as direction, intensity, duration of vibration, frequency range of vibration, working posture and grip force, when power tools are used. The factors affecting the severity of HTV exposure have been grouped in three categories:

i. Physical factors related to nature, duration and patterns of vibration exposure.
ii. Biodynamic factors related to coupled hand-tool system, such as hand forces, and postural effects and hand-arm response to vibration.
iii. Individual factors that relate to health and condition of the tool and the operator.

A complete listing of the many factors known or believed to influence the severity of vibration exposure is given in Table 1.3. Among these factors, the physical factors such as the frequency, magnitude, duration and direction of the vibration, are considered to be the most important for engineering design and analysis of the tools and risk assessment. The Biodynamic and Individual factors related to hand grip forces, contact area, postures

of the hand, intensity and duration of exposure will also effect the hand-transmitted vibration. The severity of individual factors may be influenced by biological susceptibility to vibration and the determination of vibration dosage and exposure requires measurement of vibration amplitudes and frequencies entering the hand in all directions, as a function of time for hand grip forces in well defined postures. Further more, earlier disease or prior injuries to the fingers or hands, the size and weight of the hand and arm as well as working methods can influence the severity of the effects from vibration. The monitoring of all these factors for each worker including posture and other factors, is difficult. It is therefore necessary to reduce the problem to manageable proportions, by identifying those factors that significantly contribute to the severity of

Table 1.3 Summary of factors affecting hand-transmitted vibration [40]

Physical	▪ Dominant vibration amplitudes, frequencies and direction entering hand. ▪ Years of employment involving vibration exposure. ▪ Total duration of exposure each work day. ▪ Temporal pattern of exposure each work day. ▪ Non occupational exposure of the hand.
Biodynamic	• Hand grip forces. • Contact area, location of hand in contact with source of vibration. • Posture. • Other factors influencing the hand-handle coupling (e.g. texture of handle etc.)
Individual	• Factors influencing intensity and duration of exposure (e.g. state of tool, maintenance, operator control of tool, machine work rate, skill and productivity). • Biological susceptibility to vibration. • Vasoconstrictive agents affecting the peripheral circulation(e.g. smoking, drugs, etc) • Predisposing disease or prior injuries of the fingers or the hands. • Hand size and weight.

vibration exposure. The hand-arm vibration response is thus often characterized by the acceleration of the source [41, 42]. Two coordinate systems, anatomical and basic centric have been defined for characterizing the vibration occurring in different directions, as shown in Figure 1.2 [43].

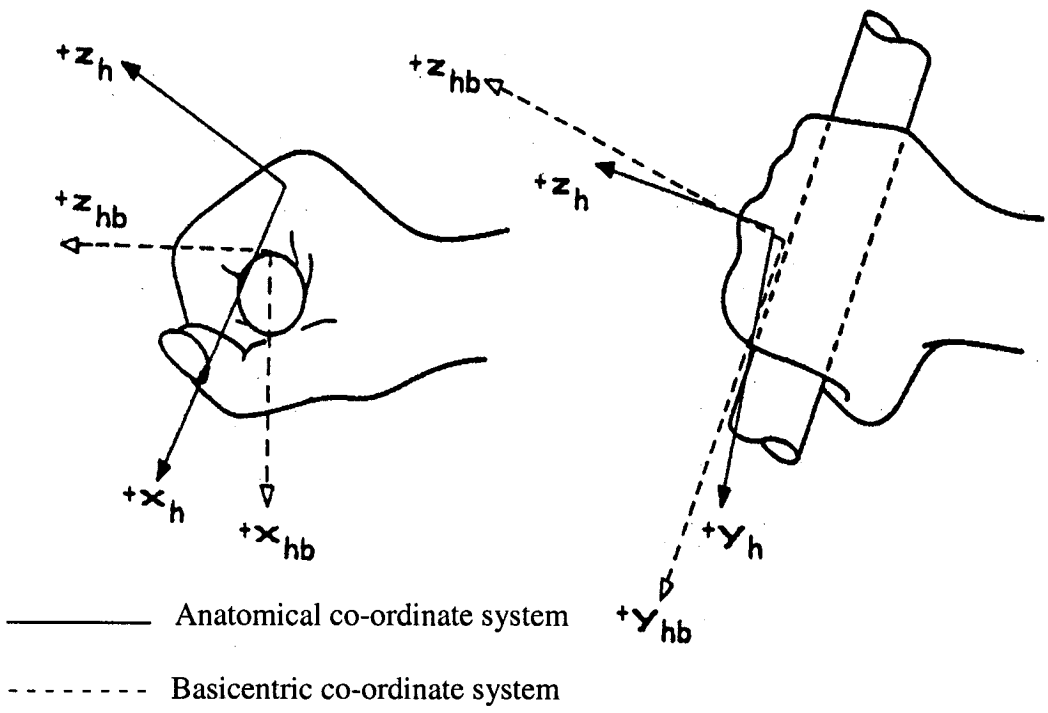

Figure 1.2: Reference coordinate system proposed in ISO-8727 [43]

Exposures to hand-transmitted vibration are complex and cannot be quantified simply. Vibration occurs in three translational axes, may differ at the two hands and may vary along the length of a tool handle. The vibration received by an operator will depend on the technique of tool use and vary according to the dynamic response of fingers, hands and arms. The International Standard ISO-5349 (1986) [41], prior to its recent revision in 2001, recommended the assessment of hand-transmitted vibration (HTV) along the axis

of the dominant vibration. Hand-held power tools, in general, transmit vibration to the human hand along all the three translational directions. The vibration along one direction may differ greatly from that in other directions due to significant variations in the working posture and the task. Many investigators have recommended measurements along all the three axes and assessment on the basis of the vector sum of the three components [44, 45]. The revised standard, ISO-5349 (2001) [42] also recommends the use of vector sum or the root-sum-of-square of the acceleration components. It is thus believed that the HTV along all the three directions is equally important. The standard, however, provides identical frequency weighting for all three axes as shown in Figure 1.3. The frequency weighting reflects the assumed importance of different frequencies in causing injury to the hand.

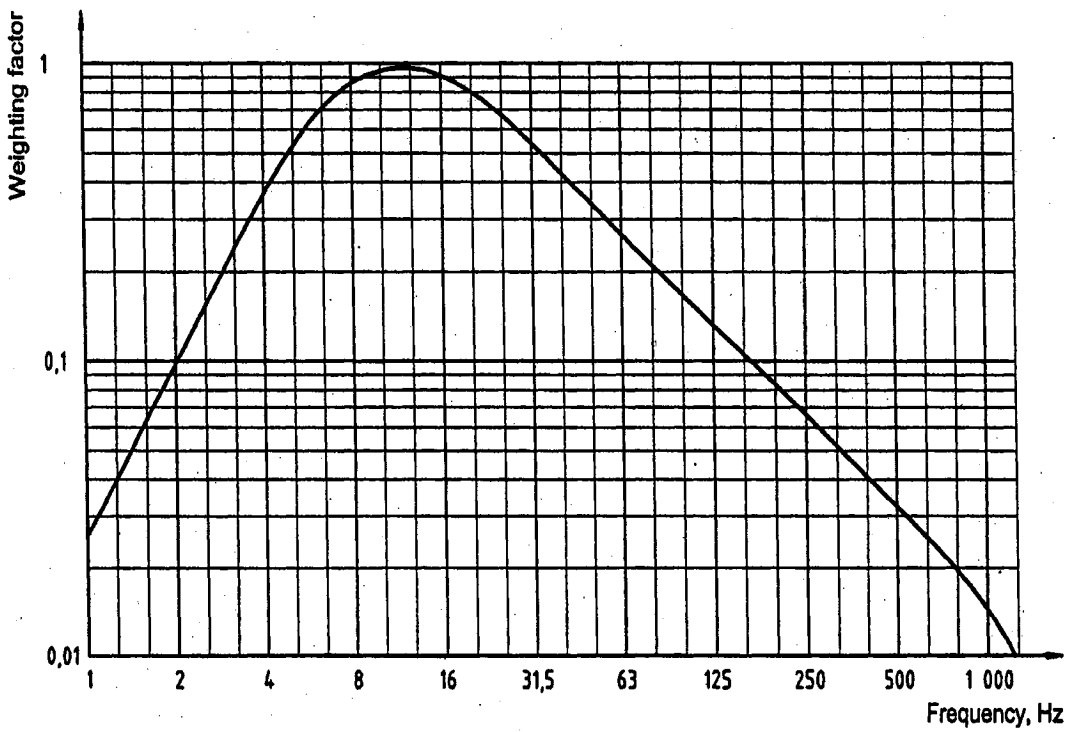

Figure 1.3: Frequency weighting function proposed in ISO-5349-1 [42]

The magnitudes of HTV arising from different tools vary depending upon the power and the size of the tool, type of tool, task speed, grip and feed forces, measurement location, etc. The measured acceleration data is frequently expressed in terms of its root mean square (rms) value, computed from:

$$a_{rms} = \sqrt{\frac{1}{T}\int a^2(t)dt}$$

where a_{rms} is the rms acceleration, a(t) is the instantaneous acceleration and T is the duration of the measured sample considered.

Daily exposure duration of the hand-transmitted vibration can be described as the total time for which the hands are exposed to vibration during the working day. Daily vibration exposure is derived from magnitude of the vibration (vibration total value) and the daily exposure duration [42]. In order to facilitate comparisons between daily exposures of different durations, the daily vibration exposure shall be expressed in terms of the 8-h energy-equivalent frequency-weighted vibration total value (A(8)). Such measure is valuable in giving a simple numerical indication of the severity of exposure.

1.2.3 HAV Standards

High levels of hand-transmitted vibration, high rates of prevalence of VWF symptoms among the exposed workers, and the severe health effects of hand-arm vibration, have all prompted efforts to develop standards to assess the vibration exposure levels. These efforts have achieved only moderate success since the etiology of VWF is not yet fully understood. Certain norms with regard to measurements, evaluations and reporting methods, however, have been established. All standards suggest that vibration

exposure be expressed in terms of rms acceleration in m/s^2 in the 1/3 octave frequency bands with center frequencies ranging from 6.3 Hz to 1250 Hz. Figure 1.4 shows the threshold values recommended by the International Standard Organization ISO-5349 [42]; British Standards Institute BSI-[46]; American National Standard Institute ANSI [47]; and American Conference of Government Industrial Hygienist ACGIH [48]. In ISO 5349 the total daily exposure to vibration is expressed in terms of the 'energy-equivalent' frequency weighted acceleration. It also offers a dose-effect relationship between the 4h energy-equivalent frequency-weighted acceleration, in the dominant axis of vibration, and the exposure period before the onset of vascular disorders. ACGIH has established threshold limit values (TLV) for hand-arm vibration. The standards of ACGIHL TLV in Figure1.4 represents the acceleration, values that should not be exceeded for various total daily exposure times. However, the TLV does not provide guidance for estimating the risk that any group of workers has for developing HAVS within given period when exposed to various frequency-weighted, component acceleration levels. An American National Standard (ANSI S3.34-1986) is consistent with ISO 5349 (1986b) in that it specifies the same dependencies on vibration frequency and daily exposure duration. It is suggested in this standard that the 4-8 hour exposure zone would yield latent period of 10-20 years before vascular symptoms develop in 10% of the exposed population. In BSI it is suggested that for normal tool usage vascular symptoms do not usually occur with frequency-weighted acceleration magnitudes below about $1\,m/s^2$. The limits recommended in all these standards follow the identical frequency distribution, suggests that the hand-arm system is more sensitive to vibration occurring at lower frequencies. All these curves have a horizontal portion over a low frequency range for constant

acceleration in that range. As the frequency increases, the curves show acceleration changes and is proportional to frequency. Acceleration values falling below each respective curve for a given exposure time are acceptable exposures.

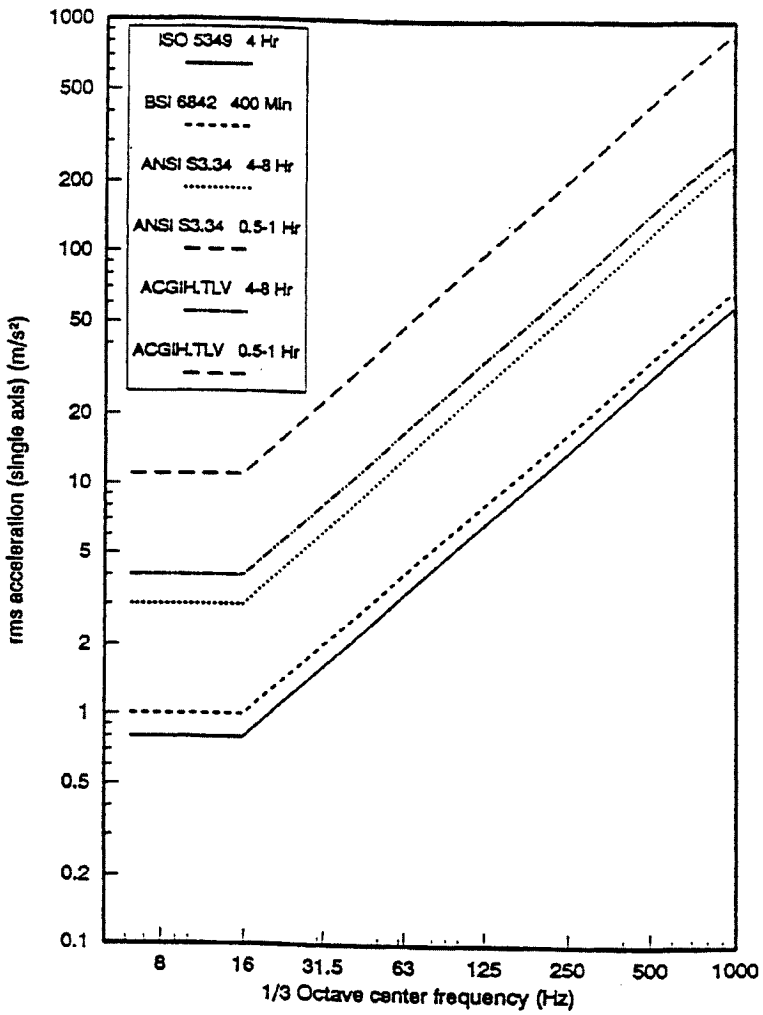

Figure 1.4: Hand-Arm vibration limits proposed by different organizations [22]

1.2.4 HAV Models

Vibrations have first of all a mechanical effect on the human hand-arm system due to the dynamic properties of the system. As a consequence of these mechanical effects, physiological effects occur depending upon several factors, such as intensity, frequency, direction and duration. Therefore, it is necessary to determine the dynamic properties of

the hand-arm system in order to understand the physiological effects. The hand-arm vibration (HAV) models when integrated with the analytical model of a power tool, could permit efficient evaluations of the tool design factors and vibration attenuation devices. All the engineering studies have mostly concentrated on the design of effective protective devices and tools [49] and emphasized the need to enhance thorough understanding of the biodynamic response behavior of the hand-arm system. Since the human hand-arm system is a very complex system, the hand-arm responses to vibration are mostly evaluated at the driving-point, which is the hand-handle interface. Many studies have reported the biodynamic responses in terms of to-the-hand and through-the-hand-arm response functions. The to-the-hand function relates the vibration in the vicinity of the hand to the force at the driving point. This function may be expressed as, the apparent mass (APMS), the ratio of force to driving-point acceleration; the dynamic stiffness, the complex ratio of force to displacement at the driving-point; the driving-point mechanical impedance (DPMI), the ratio of force to driving point velocity. The to-the-hand biodynamic response of the hand-arm has also been expressed as the energy absorbed by the hand and arm [50-53].

The through-the-hand-arm response function describes the transmission of vibration and is expressed as the ratio of motion magnitude at a specific segment of the hand-arm system to that at the hand-handle interface. Few studies have been conducted to describe the through-the-hand-arm response function in terms of vibration transmissibility of the hand-arm system [10, 54-58]. These studies describe the vibration transmissibility of different segments of the hand-arm system, such as the metacarpal bones, wrist, elbow and shoulder. The majority of these studies were performed using miniature and

subminiature accelerometers attached to the skin. The measurement of vibration transmitted to parts of upper limbs, has posed difficulties caused by attaching transducers to the skin and the flexibility of skin. These studies have also concluded that magnitudes of vibration transmitted to the hand-arm decrease with increasing frequency and the distance from the vibration source. The primary objective of the studies in biodynamic response of the human hand and arm is to develop analytical models of the hand and arm for use in modeling the vibration response characterictics of vibrating hand tools

The reported biodynamic responses exhibit considerable differences among them, which have been partly attributed to variations in intrinsic variables (such as body size, body posture and muscle tension) and extrinsic variables (such as frequency of vibration, amplitude of vibration, time history of vibration, direction of vibration, type of grip used to clasp a vibrating handle), test conditions and methodologies [59]. The International Standard describes the mechanical impedance of the human hand-arm system at the driving point. Values of the impedance, expressed as modulus and phase, are provided for three orthogonal, translatory directions of excitation that correspond to the x_h-, y_h- and z_h-axes, as shown in Figure 1.2 [43].

Many analytical and experimental studies have been undertaken to characterize the vibration response behaviour of the hand-arm system. The reported biodynamic models have been developed on the basis of the impedance or apparent mass properties of the hand-arm system. These reported HAV models can be classified in to two broad groups based on their structure: lumped-parameter models [19, 60-66] and distributed-parameter models [67]. The lumped parameter models include the linear single-DOF [66], linear two-DOF [60-63], and linear and non-linear three and four-DOF models [19, 61-65].

These models provide little insight into the pathological changes caused by HTV, as the models neglected the dynamic coupling effects of the hand and arm and do not adequately represent the biomechanical properties of the human hand and arm. These models failed to characterize the vibration transmitted to the hand and the arm. The applicability of the reported models for analyses of the coupled hand-tool system, has been compared in a recent study [68] using three different criteria: (i) The ability of the model to characterize the driving-point mechanical impedance [50]; (ii) The magnitude of model deflection under a static feed force; (iii) The natural vibration behaviour of the human hand and arm in terms of natural frequencies and damping ratios. The study concluded that the vast majority of the reported models could not be applied for development of mechanical hand-arm simulator or for the assessment of dynamic behavior of the coupled hand-tool system, because these models involve very light masses, in the 1.2-4.8 gm range, and exhibit low frequency vibration modes.

1.3 Power Tools

Vibration-induced white finger (VWF) is not restricted to users of a finite set of tools. Prolonged exposure to moderate or high magnitudes of vibration should be considered as a potential cause. This section gives a general idea of the main types of power tools and where they are used. The frequencies and magnitudes of hand-transmitted vibration caused by the operation of hand-held power tools are known to vary over a wide range, depending upon the type of tool, operation, and hand-tool orientation, as illustrated in Table1.4. A wide variety of tools involve metal-to-metal which include riveting, hammering, drilling, chipping and chiseling. Grinding machines are used where material

removal is the primary task, from heavy grinding on large components, to precision die grinding. Grinding machines are suitable for rough or fine sanding of castings. Power outputs can range from 0.1 to 4.5 kW. The dominant vibration frequency (range of vibration) for grinders is 20-205 Hz, as shown in Table1.4 and the acceleration levels associated with these frequency ranges vary from 40-63 (m/s^2). Imbalance in the grinding wheel is one of the primary causes for high levels of vibration. The percussive tools yield vibration at considerably higher frequencies, which may be attributed to repetitive impacts of the tool with the workpiece and the impacts of the tool components occurring within the tool. Percussive tools use the blow energy from an accelerated piston to create high forces. Using the tool may, however, involve risk of injury from noise and vibration. There are three different types of percussive tools: chipping hammers, scalers and

Table 1.4: Dominant ranges of frequencies and magnitudes of vibration generated by different power tools [19, 20]

Tool	Dominant frequency; Range of Vibration (Hz)	Reported acceleration levels (m/s^2)
Chipping hammers	25-125	251-2,014
Riveters	50-200	10^w -1,183
Pedestal grinders	≈ 250	125-382
Jackleg drills	6-1,250	121-362
Grinders	20-205	40-63
Chain saws	63-150	$2.7^w - 11^w$
Orbital sanders	60-100	$2.5^w - 5.0^w$
Stationary grinders	< 250	$2.2^w - 5.4^w$
Representative tools often used in automobile manufacturing (e.g., palm orbital sanders, reciprocating sanders, polishers, heavy-duty grinders)	20-160	10-300

w- Frequency-weighted rms acceleration

riveting hammers. Chipping hammers are commonly used in foundries, while the riveting hammer is mainly used in the aerospace industry. High noise levels are a typical problem with percussive tools. Srewdrivers are used to assemble parts in designs where the products need to be dismantled easily. Most screwdrivers are provided with either a straight or pistol grip. The surface of the straight handle has a rough texture to prevent it from rotating in the hand due to the reaction torque when tightening. Impact wrenches are used in after-sales service applications. The main advantage of impact wrenches is their capability to unscrew rusty bolts. Another advantage of these tools is their small size in relation to their torque level. Although they generate very high torque, they are relatively light and compact. Rotary tools may transmit dynamic torque and high reaction forces in the operator's hand and arm. The nut-runners that account for 75% of the hand-held power tools used in the automobile industry impose considerable moments on the hand and arm [69]. The exposure to dynamic torque and vibration generated by such tools has been related to the occurrence of cumulative trauma disorders among workers [70, 71]. Angle nutrunners are used at assemble workstations for repetitive assembly of joints. These are more accurate and give low noise levels than impact wrenches.

1.4 Scope and Objectives of the Thesis

Numerous studies, reviewed in the previous sections, have identified several health risks associated with prolonged exposure to hand-held power tool vibration. It is thus extremely vital to control the levels of hand-transmitted vibration to reduce the health risks associated with operation of hand-held power tools. The primary objective of this thesis is to investigate the vibration behavior of a hand-held grinder due to mass

unbalance. This thesis focuses on the development of analytical model of the grinder coupled with the human hand-arm to study the effects of mass unbalance. In order to develop logical standards and to design hand tools with low vibration levels, it is necessary to understand the coupled response of the hand and the vibrating tool. The specific objectives of this thesis are thus formulated as:

a. To develop an analytical model of a grinder under excitations caused by the grinding wheel unbalance.
b. To develop linear HAV model and identify the model parameters on the basis of the standardized impedance data.
c. Perform modal analysis of the HAV model to obtain the natural frequencies and damping ratio of the human hand-arm.
d. To develop analytical model of coupled hand-grinder system and perform free and forced vibration analyses as functions of the magnitude of rotating unbalance.
e. To study the effect of anti-vibration gloves on the hand-transmitted vibration.
f. To study the effects of mass unbalance on the force transmitted to the hand.

1.5 Overview of the Thesis

A study of vibration behavior of a coupled hand-tool system involves systematic analysis of the tool dynamics and vibration, biodynamic modeling of the human hand and arm, analysis of the coupled hand-tool model, and analysis of design and operating factors on the nature of hand-transmitted vibration. A grinder model having 5 DOF is developed in Chapter 2 which will be used for coupled hand-tool system analysis. The identification of the system parameters by using simple uncoupled model of the grinder

along with conducting experiments are also described. The natural frequencies and damping ratios of the system are further discussed.

In Chapter 3, the Human hand-arm system characterized by a two degrees-of-freedom lumped parameter model, along each of the three orthogonal directions is described. The model consists of rigid masses and linear visco-elastic elements. The model parameters are identified from the measured DPMI (Driving Point Mechanical Impedance) using a curve fitting approach and non-linear programming based constrained optimization algorithm. Eigenvalue analysis is performed to determine the natural frequencies, damping ratio of the heavily damped hand-arm system.

In Chapter 4, a coupled hand-tool model based on the models of the grinder and the human hand-arm system is derived. Eigenvalue analysis is performed to determine the natural frequencies and damping ratios of the coupled hand-tool model. Parametric studies are carried out and the response of the coupled hand-tool model is derived. The results of the experiments conducted in a previous study are also presented in this chapter and the coupled hand-tool model is validated using these results.

The conclusions drawn and recommendations for the future work are finally described in Chapter 5.

CHAPTER 2
DEVELOPMENT OF GRINDER MODEL AND EXPERIMENTAL INVESTIGATIONS

2.1 Introduction

Hand-Held grinding tools are widely used in the manufacturing sector, which may include vertical and horizontal grinders, that are mostly operated using pneumatic drives with air pressure ranging from 90 to 110 (psi). As with other machine tools, grinding machine vibrations could be classified into two types: forced and self-excited vibrations. Forced vibrations are caused by periodic disturbances which are external to the cutting processes such as, from an unbalanced wheel or spindle, electric motors, bearings and pneumatic systems. The causes of self-excited vibrations are much more complex than those of the forced vibrations [72]. Irregularities in the cutting process cause variations in the cutting force which can dynamically excite the machine-tool structure. Self-excited vibrations are generally associated with natural vibration modes of the machine-tool structure. In grinding, the local deformations between the wheel and the work piece have the effect of raising the chatter frequencies above the resonant frequencies of the machine structure [73-76]. Experimental characterization of chatter in grinding is quite difficult because the grinding process is influenced by many parameters, and the amplitudes of self-excited vibrations are very small and appear in conjunction with those caused by the forced vibrations from various sources. While the chatter frequencies depend on the natural frequencies of the grinding wheel-spindle system, they are, however, all rather higher than the natural frequencies [77]. The grinding wheels also exhibit considerable mass unbalance due to dirt build up, non-uniform wear, uneven weight distribution, etc.

Such unbalance not only causes considerable vibration at relatively lower frequencies associated with the operation speed but also yields poor quality of the work piece or manufactured product. Owing to extreme complexities associated with characterization of cutting forces, the role of rotating mass unbalance on the nature of the HTV alone is considered in this study.

2.2 Description of the Tool

A hand-held angle grinder, manufactured by Atlas Copco and pictorially shown in Figure 2.1, is considered in this study for the analysis of hand-transmitted vibration. The tool is designed with two handles, a support handle allowing the tool to be held in different ways and a trigger handle which consists of pneumatic drive. The support handle is adjustable so that different angles can be set between the support handle and the trigger handle. Thus, the operator can customize the machine to suit the working conditions and the task. The grinding wheel and the spindle is supported between two closely spaced bearings, as shown in Figure 2.2. A wheel guard is attached to the grinder that covers half of the rotor in order to ensure safety during operation. The free speed of the grinding wheel and spindle is 12000 rpm and the speed of the pneumatic motor is 60000 rpm. The rotating speed may decrease during cutting operation, depending upon the cutting force, feed force and the supply pressure. The vibration transmitted to the handle arises from the dynamic interaction of the rotor with the work surface and mass unbalance inherent in the rotor. An analytical model of the shaft-rotor system is formulated in this chapter to study the vibration caused by the mass unbalance and the force transmission along all the three translational axes.

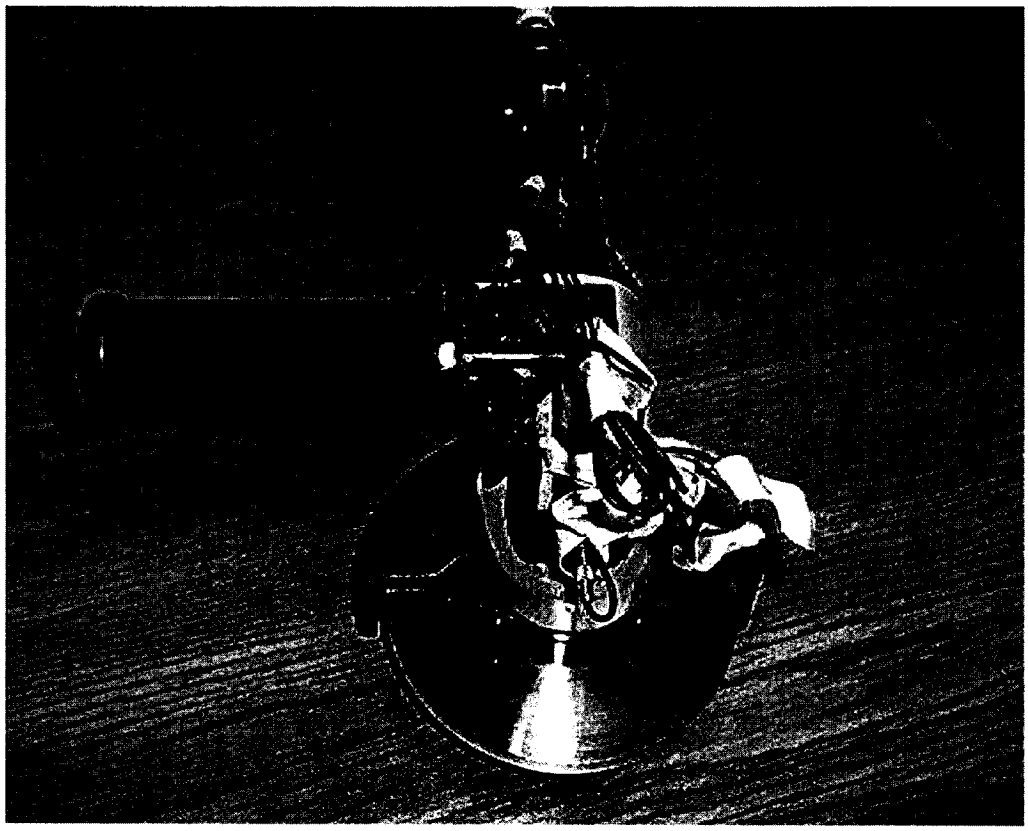

Figure 2.1: A pictoral view of the pneumatic angle grinder

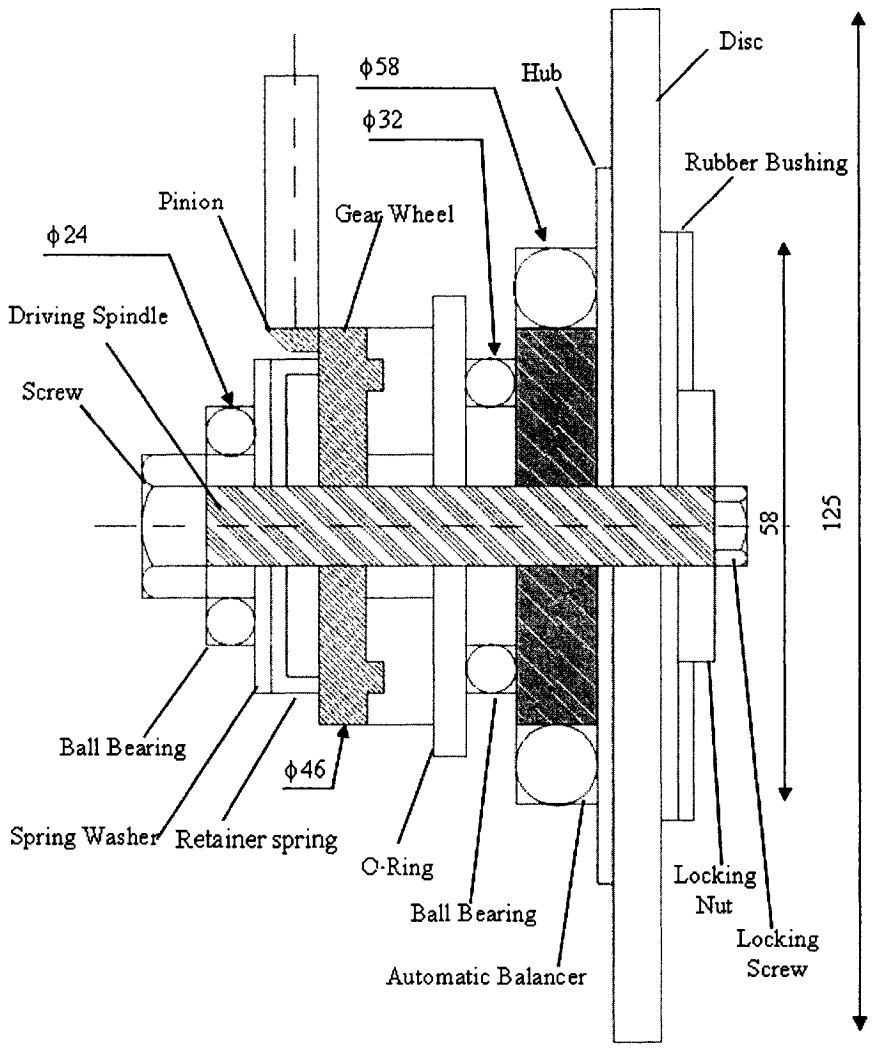

Figure 2.2: Cross sectional view of the angle grinder

2.3 Modeling Considerations

A coupled hand-tool system is quite complex that requires systematic considerations of tool behaviour, response of the biological system and the coupling effects. It has been suggested that the human hand-arm affects the vibration behaviour of the tool in a significant manner through absorption of energy within the biological system [22, 78]. In this study, an analytical model of an angle grinder alone is initially formulated to gain insight into the design features of the tool and its vibration behaviour. A mechanical-equivalent model of the human hand and arm is then formulated on the basis of reported driving-point mechanical impedance characteristics. The hand-arm models oriented along the x_h-, y_h- and z_h-axes are integrated to the tool model in order to derive the analytical model of the coupled hand-tool system.

A cross-sectional view of the angle grinder considered in the study is shown in Figure 2.2. The grinder consists of a grinding wheel attached to the shaft. The grinding wheel and the shaft are driven by a turbine pneumatic motor drive through a pair of bevel gears. Figure 2.3 shows a model representation of the shaft and the disc supported by a pair of deep groove radial ball bearings located at points p and q along the shaft, an O-ring and a retainer spring located at points r and s. The grinding wheel is mounted at the end of the shaft, as shown. The distances between the centre of gravity (cg) of the shaft-disc assembly and the bearing-1, bearing-2 (located at p and q, respectively), the O-ring and the retainer spring (located at r and s) are represented by a_1, b_1, c_1 and d_1, respectively. The distance between the centre of the grinding wheel (w) and the centre of gravity of the shaft-disc (cg) is represented by a_0.

The grinding machine spindle system is modeled by a five degrees-of-freedom (DOF) dynamical system, including the motions z_d and y_d, along the radial directions (Z-axis and Y-axis), x_d along the axial direction (X-axis), and the angular motions α and β about the Z- and Y-axes, respectively. The machine body to which handles are attached is assumed to be fixed, and the forces and motions caused by the gear drive and the pneumatic system are ignored. The bearings, O-ring and retainer spring are characterized by linear stiffness and damping elements, while identical properties are considered along the Z- and Y-axes assuming symmetry about the X-axis. The effect of cross coupling in Z-, Y- and X- axes is neglected. The contributions due to the flexibility of the disc and the shaft are also neglected in the model. The effect of Automatic Balancing Unit, as illustrated in Figure 2.2, is also not considered in the present study. As shown in Figure 2.3, the mass due to shaft and disc assembly is represented by m_d, and I_z and I_y represent the mass moments of inertia about the Z- and Y-axes, respectively. Let m_u be the mass unbalance at an eccentricity *e*. K_{b1} and C_{b1} are the constant spring rate and damping coefficient of bearing-1 located at *p*. Similarly K_{b2} and C_{b2} represent the constant spring rate and damping coefficient of bearing-2 located at *q*. The properties of these two bearings are assumed to be same, such that $K_{b1} = K_{b2}$ and $C_{b1} = C_{b2}$ along both the axes. K_0, C_0, K_{sr} and C_{sr} represent the visco-elastic properties of the O-ring and the retainer spring, respectively, whose values are obtained from the literature [79]. The bearings are assumed to possess constant properties, while the clearance effects are assumed to be negligible. The visco-elastic properties of the O-ring and the retainer spring are assumed to be equal along all the three axes (X-, Y- and Z-).

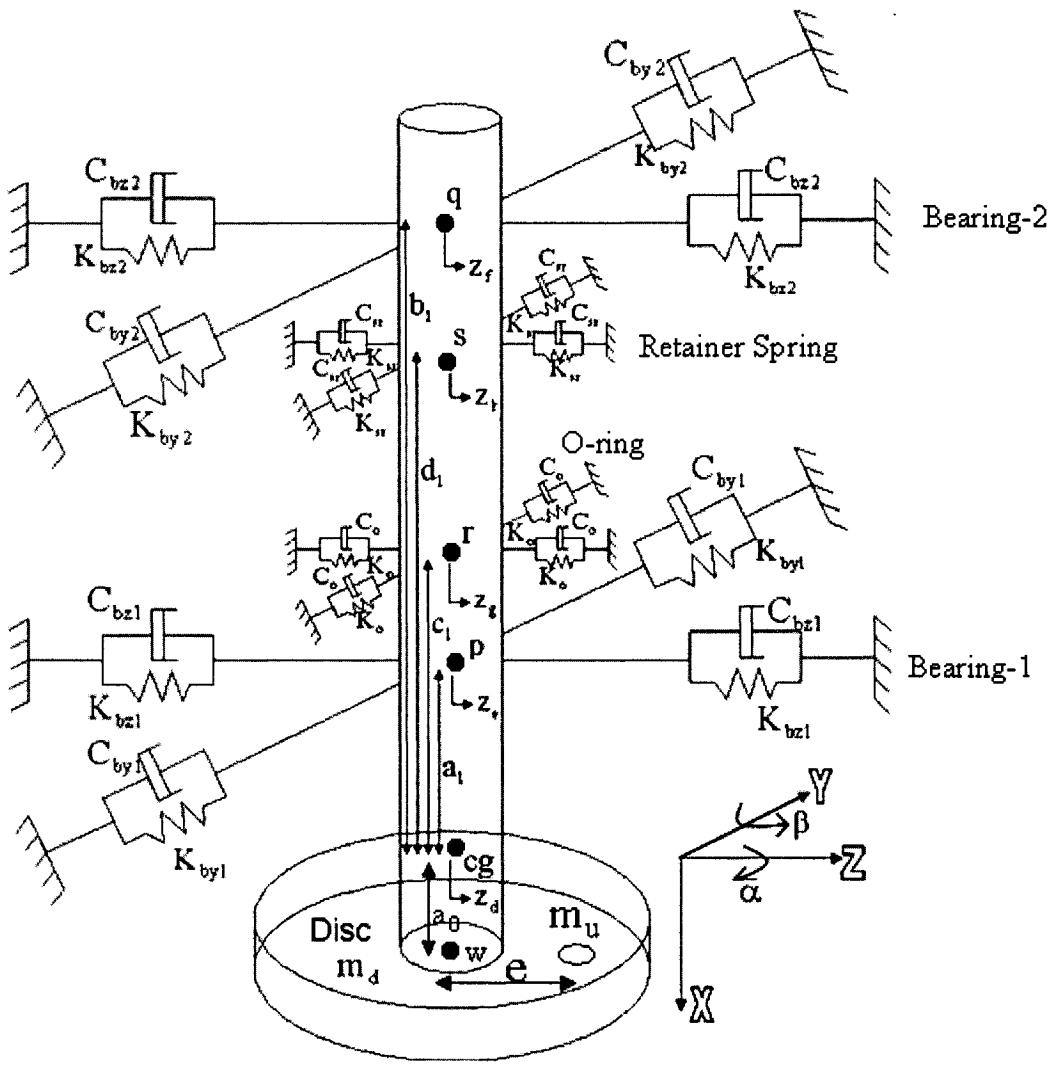

Fig 2.3: Five degrees of freedom for grinding spindle

2.4 Equations of Motion for Angle Grinder

The equations of motion for grinder model are derived along the radial (Z- and Y-) and axial (X) directions under the presence of a rotating mass unbalance excitation along the radial direction. The axial motions of the shaft are believed to be attributed mostly to the cross coupling between the motions along the three orthogonal axes and the coupled motions caused by the gear drive and the pneumatic drive system. The effects of the cross coupling and the motions due to gear and pneumatic drives on the axial motion are

considered by introducing an additional excitation component arising from the disc unbalance. Owing to the lack of appropriate data, it is assumed that 15% of the mass unbalance would account for the axial excitation component. Moreover, the gyroscopic effects are also considered in the model formulation.

Equations of Motion along the Z-axis

The centroidal motion of the shaft-disc assembly along the Z-axis can be related to the motion of the shaft in the vicinity of the bearing supports (z_e, z_h), O-ring (z_f), retainer spring (z_g) and to its rotation β about the Y-axis. Assuming rigid shaft and disc assembly, these motion coordinates can be expressed as:

$$z_d = z_e - a_1\beta$$

$$z_d = z_h - b_1\beta$$

$$z_d = z_f - c_1\beta$$

$$z_d = z_g - d_1\beta$$

where z_d is the centroidal motion of the shaft and disc.

The grinding wheels exhibit considerable mass unbalance due to dirt build up and non-uniform wear. In order to represent the mass unbalance of the grinding wheel, an additional mass m_u, which represents the mass unbalance of the grinding wheel, is considered with an eccentricity e, such that the total mass of the shaft and disc assembly is:

$$M = m_d + m_u$$

The equation of motion for the translational motion along the Z-axis of the shaft-disc assembly is written as:

$$M\ddot{z}_d + 2(K_{bz1} + K_{bz2} + K_0 + K_{sr})z_d + 2(C_{bz1} + C_{bz2} + C_0 + C_{sr})\dot{z}_d + 2(a_1K_{bz1} + b_1K_{bz2} + c_1K_0 + d_1K_{sr})\beta + 2(a_1C_{bz1} + b_1C_{bz2} + c_1C_0 + d_1C_{sr})\dot{\beta} = m_u e\omega^2 \sin(\omega t) \tag{2.1}$$

where K_{bz1} and K_{bz2} represent the constant spring rates of bearings 1 and 2, respectively, and C_{bz1} and C_{bz2} represent the corresponding damping coefficients, along the Z-axis. The stiffness and damping coefficients of the O-ring are represented by constant coefficients K_0 and C_0, while K_{sr} and C_{sr} are those of the retainer spring.

The equation of motion describing the rotational motion of the shaft-disc assembly about the Y-axis (β) is written as:

$$I_y\ddot{\beta} + 2(a_1K_{bz1} + b_1K_{bz2} + c_1K_0 + d_1K_{sr})z_d + 2(a_1C_{bz1} + b_1C_{bz2} + c_1C_0 + d_1C_{sr})\dot{z}_d + 2(a_1^2K_{bz1} + b_1^2K_{bz2} + c_1^2K_0 + d_1^2K_{sr})\beta + 2(a_1^2C_{bz1} + b_1^2C_{bz2} + c_1^2C_0 + d_1^2C_{sr})\dot{\beta} = -a_0m_u e\omega^2 \sin(\omega t) + I_x\omega\dot{\alpha} \tag{2.2}$$

where the term $I_x\omega\dot{\alpha}$ represents the gyroscopic effect.

Equations of Motion along the Y-axis

The centroidal motion of the shaft-disc assembly along the Y-axis of the shaft in the vicinity of the bearing supports (y_e, y_h), O-ring (y_f), retainer spring (y_g) can be related to its rotation α about the Z-axis. Assuming rigid shaft and disc assembly, these motion coordinates can be expressed as:

$$y_d = y_e + a_1\alpha$$

$$y_d = y_h + b_1\alpha$$

$$y_d = y_f + c_1\alpha$$

$$y_d = y_g + d_1\alpha$$

where y_d is the centroidal motion of the shaft and disc.

The equation of motion for the translational motion of the shaft-disc assembly along the Y-axis is written as:

$$M\ddot{y}_d + 2(K_{by1} + K_{by2} + K_0 + K_{sr})y_d + 2(C_{by1} + C_{by2} + C_0 + C_{sr})\dot{y}_d - 2(a_1K_{by1} + b_1K_{by2} + c_1K_0 + d_1K_{sr})\alpha - 2(a_1C_{by1} + b_1C_{by2} + c_1C_0 + d_1C_{sr})\dot{\alpha} = m_u e\omega^2 \cos(\omega t) \tag{2.3}$$

where K_{by1} and K_{by2} represent the constant spring rates of bearings 1 and 2 respectively, and C_{by1} and C_{by2} represent the corresponding damping coefficients, along the Y-axis.

The equation of motion for the rotational motion of the shaft-disc assembly about the Z-axis (α) is written as:

$$I_z\ddot{\alpha} - 2(a_1K_{by1} + b_1K_{by2} + c_1K_0 + d_1K_{sr})y_d - 2(a_1C_{by1} + b_1C_{by2} + c_1C_0 + d_1C_{sr})\dot{y}_d + 2(a_1^2K_{by1} + b_1^2K_{by2} + c_1^2K_0 + d_1^2K_{sr})\alpha + 2(a_1^2C_{by1} + b_1^2C_{by2} + c_1^2C_0 + d_1^2C_{sr})\dot{\alpha} = a_0m_u e\omega^2 \cos(\omega t) - I_x\omega\dot{\beta} \tag{2.4}$$

where the term $I_x\omega\dot{\beta}$ represents the gyroscopic effect.

Equation of Motion along the X-axis

Let x_d be the centroidal motion of the shaft-disc assembly along the X-axis. The lumped effect of cross coupling, vibration of the gear and the pneumatic drive, is represented as a function of the mass unbalance as described earlier. An equivalent

excitation along the X-axis ($0.15m_u e\omega^2$) is considered and the equation of motion for shaft-disc assembly along the axial direction is written as:

$$M\ddot{x}_d + (K_{bx1} + K_{bx2} + K_0 + K_{sr})x_d + (C_{bx1} + C_{bx2} + C_0 + C_{sr})\dot{x}_d = (0.15m_u e\omega^2)\sin(\omega t) \tag{2.5}$$

where K_{bx1} and K_{bx2} represent the constant spring rates of bearings 1 and 2 respectively, and C_{bx1} and C_{bx2} represent the corresponding damping coefficients, along the X-axis.

2.5 Model Parameters

As shown in Figure 2.2, the shaft is supported by two different ball bearings. The lower bearing located at point p, on the shaft is larger than the upper bearing located at point q. Table 2.1 shows the manufacturer's dimensional specifications of these bearings. The geometric and inertial parameters of the tool were measured and summarized in Table 2.2. The stiffness properties of the bearings are estimated from the frequency response of the angle grinder, measured in the laboratory. Despite the dimensional differences in the bearings, the stiffness and damping properties of the bearings are assumed to be identical.

Table 2.1 Specifications of the ball bearings of the tool

Bearing Number	Bore Diameter (mm)	Outer Diameter (mm)	Width (mm)	No. of Balls
609:Upper	9	24	7	7
6002: Lower	15	32	9	9

Table 2.2 Geometric and Inertial properties of the model

Parameter	Value
a_1	$8.33 * 10^{-3}$ m
b_1	$42.08 * 10^{-3}$ m
c_1	$15.0 * 10^{-3}$ m
d_1	$40.0 * 10^{-3}$ m
a_0	$15.67 * 10^{-3}$ m
I_z	$3.76 * 10^{-4}$ kg.m^2
I_y	$3.76 * 10^{-4}$ kg.m^2
I_x	$7.52 * 10^{-4}$ kg.m^2
m_d	0.395 kg
M_b	3.5 kg
K_0	20 N/m
C_0	30 Ns/m
K_{sr}	175 N/m
C_{sr}	7 Ns/m

In order to carry out vibration tests, the angle grinder was mounted on an electro-dynamic shaker, made by Unholtz-Dickie Corporation, through a fixture shown in Figure 2.4. A single-axis accelerometer, oriented along the Z-axis, was installed on the grinder body to measure the vibration transmitted to the body. Another single-axis accelerometer was also installed on the shaker head to measure the excitation signal along the Z-axis. The accelerometer signals, conditioned by the charge amplifiers, were acquired in a two-channel signal analyzer (B & K-2035). The electro-dynamic shaker was driven by a

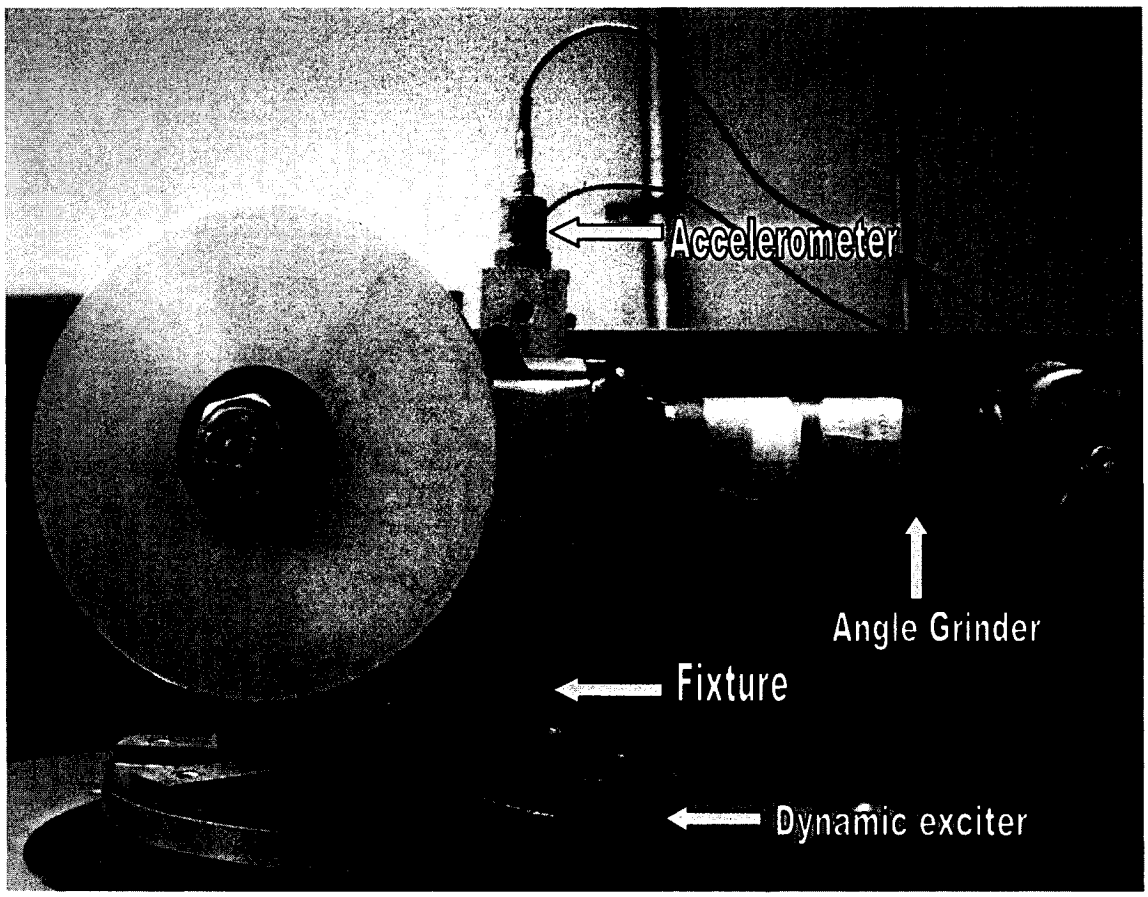

Fig 2.4: Angle grinder mounted on the electro dynamic shaker
along the radial direction(Z-axis)

power amplifier (Model TA250), while controller was programmed to generate broad band random vibration of constant acceleration power spectral density in the 5-2000 Hz frequency range. Figure 2.5 illustrates a pictorial view of the experimental setup. A schematic of the exciter and the measurement apparatus is further shown in Figure 2.6. The grinder was initially mounted to excite the body along a radial direction (Z), as shown in Figure 2.4. The signal from the accelerometer oriented along this axis was conditioned and acquired in the signal analyzer. An additional single axis accelerometer was also installed on the shaker to measure the acceleration due to excitation. The measurements were done on the grinder in non-rotating condition to identify the resonant frequencies and thus the bearing properties. The measured data was analyzed to determine the frequency response characteristics. The analysis was done using a

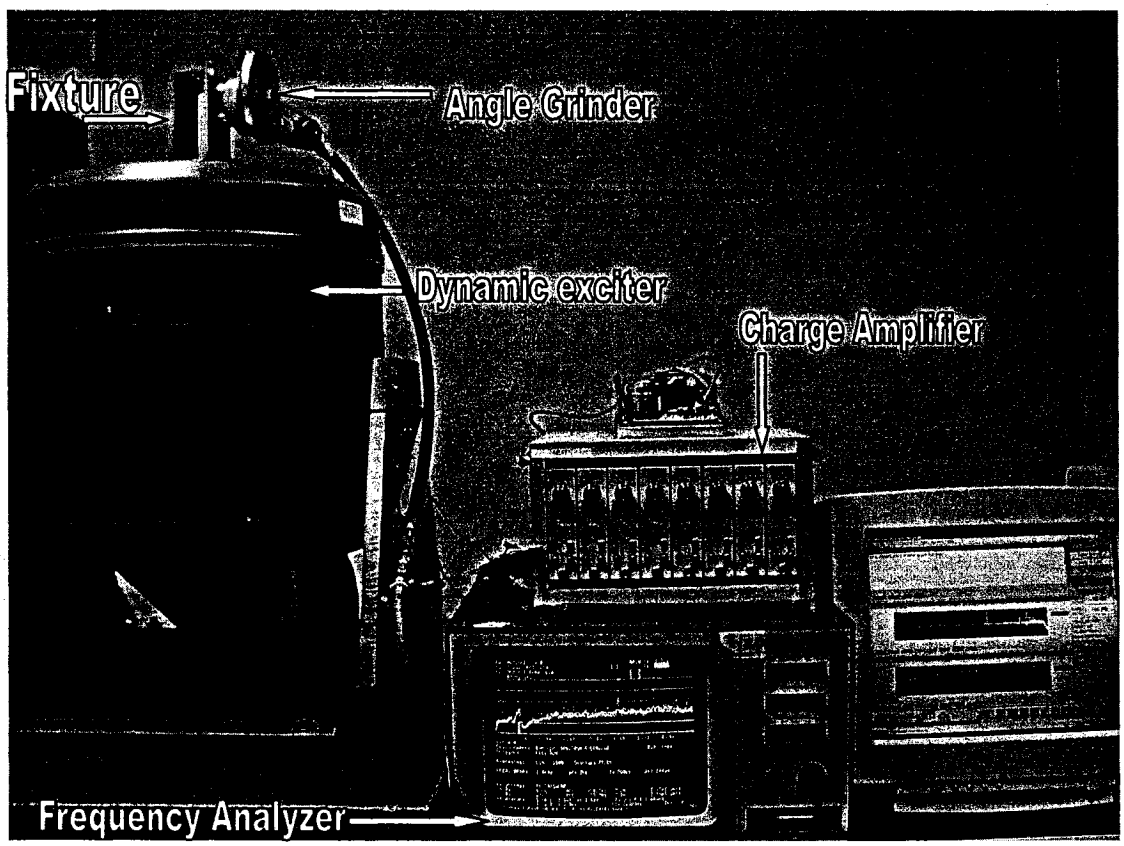

Figure 2.5: Experimental Setup

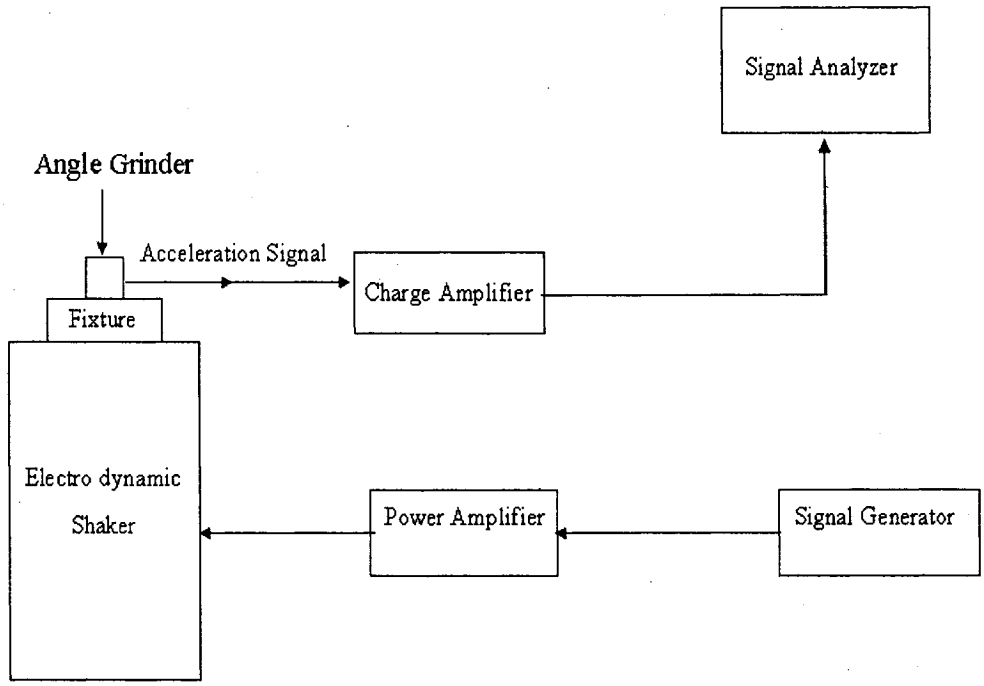

Figure 2.6: Schematic of the excitation and frequency response measurement apparatus

band width of 2000 Hz with a frequency resolution of 2.5 Hz. Figure 2.7 illustrates the frequency response function of the grinder subject to broad band random excitation along the Z-axis. The results show the primary peak in the vicinity of 180 Hz, and several smaller peaks near 120 Hz, 344 Hz, 596 Hz, 726 Hz and 1260 Hz. The experiments were repeated by mounting the grinder horizontally on the dynamic shaker, as shown in Figure 2.8, to subject the grinder to excitation along its X-axis. An accelerometer was placed at the tip of the spindle unit, as shown. The frequency response of the grinder subject to excitation along the axial direction revealed peaks near 170, 410, 590 and 1240 Hz, as evident from the results presented in Figure 2.9.

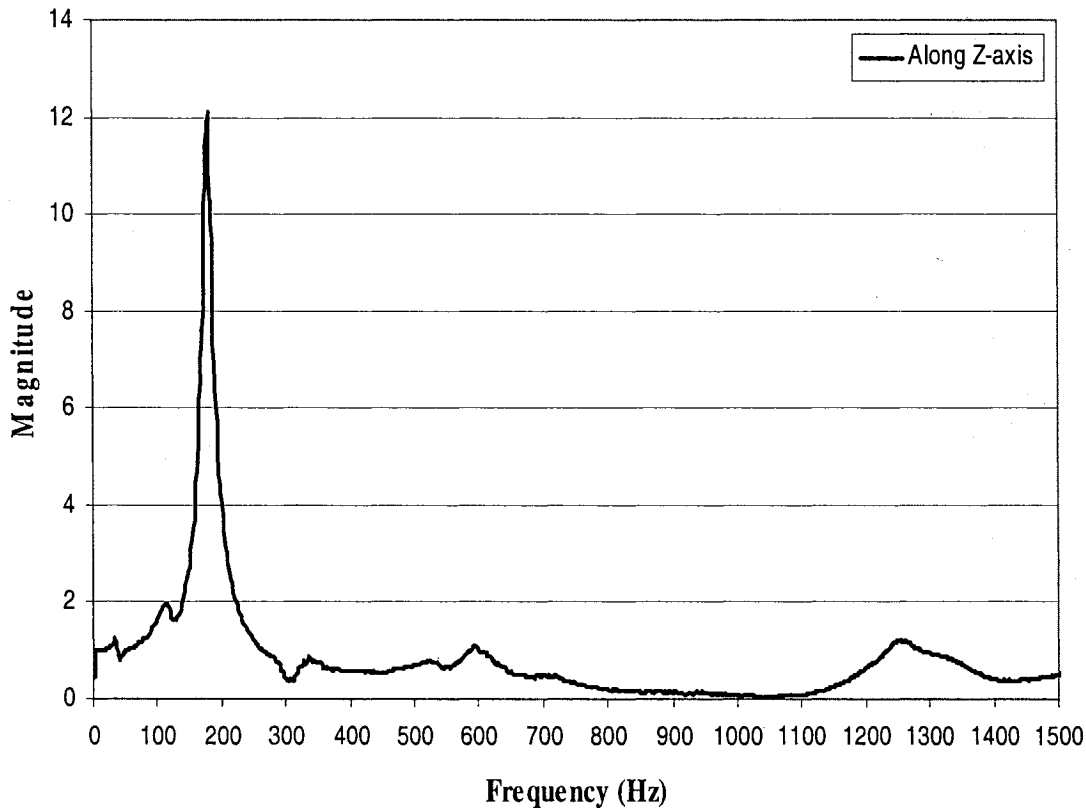

Figure 2.7: Frequency response of the angle grinder along the radial direction (Z-axis)

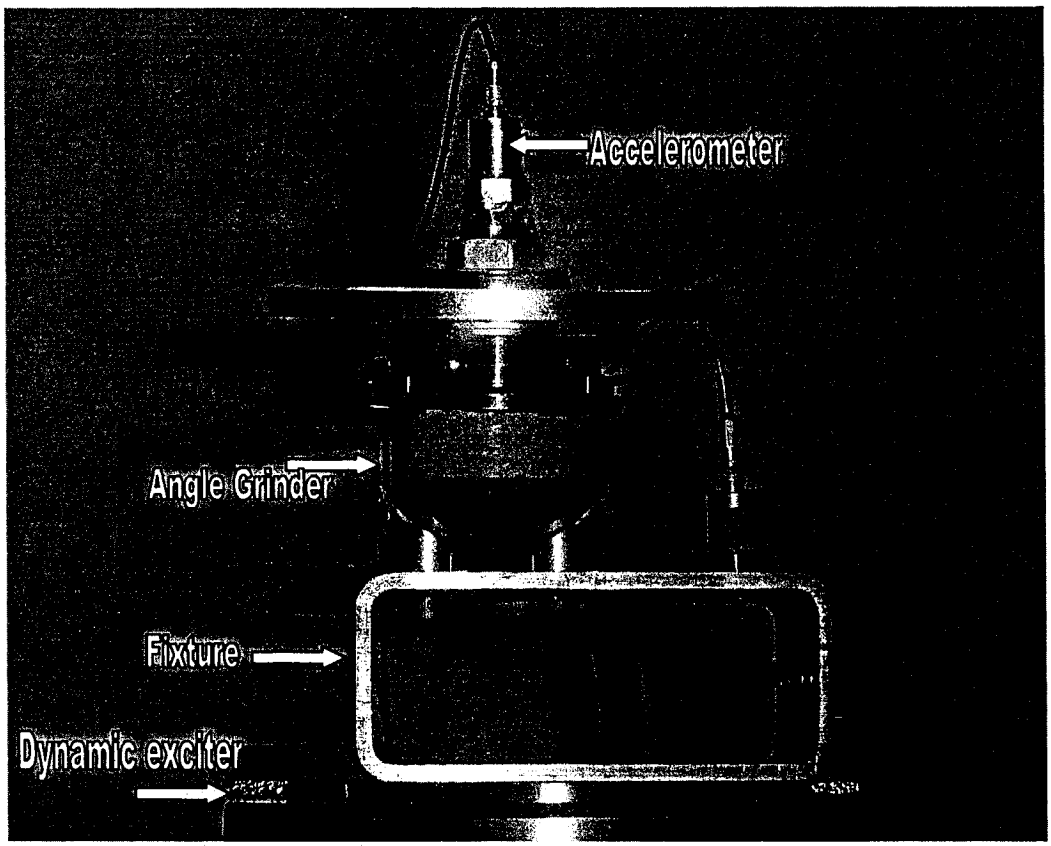

Figure 2.8: Angle grinder mounted on the electro dynamic shaker along the axial direction(X-axis)

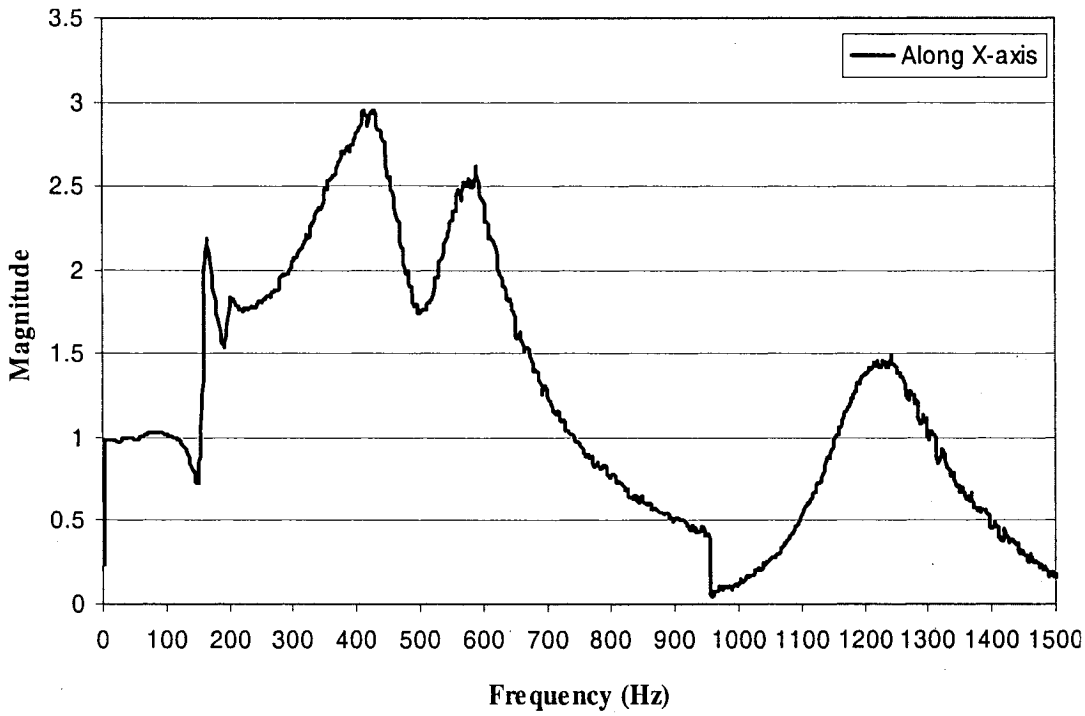

Figure 2.9: Frequency response of the angle grinder along the axial direction (X-axis)

2.6 Eigenvalue Analysis

The stiffness properties of the bearings could be estimated by curve fitting the frequency response of the analytical model to the measured frequency response. An eigenvalue problem is formulated to evaluate the resonant frequencies of the model by considering the coupled motions along z_d and β. The two coupled equations of motion can be expressed in the following matrix form:

$$[\mathrm{M}]\{\ddot{\mathrm{q}}\} + [\mathrm{C}]\{\dot{\mathrm{q}}\} + [\mathrm{K}]\{\mathrm{q}\} = \{\mathrm{p}\} \tag{2.6}$$

where $[\mathrm{M}] = \begin{bmatrix} M & 0 \\ 0 & I_y \end{bmatrix}$;

$[\mathrm{C}] = \begin{bmatrix} 2(C_{bz1} + C_{bz2} + C_0 + C_{sr}) & 2(a_1 C_{bz1} + b_1 C_{bz2} + c_1 C_0 + d_1 C_{sr}) \\ 2(a_1 C_{bz1} + b_1 C_{bz2} + c_1 C_0 + d_1 C_{sr}) & 2(a_1^2 C_{bz1} + b_1^2 C_{bz2} + c_1^2 C_0 + d_1^2 C_{sr}) \end{bmatrix}$; and

$[\mathrm{K}] = \begin{bmatrix} 2(K_{bz1} + K_{bz2} + K_0 + K_{sr}) & 2(a_1 K_{bz1} + b_1 K_{bz2} + c_1 K_0 + d_1 K_{sr}) \\ 2(a_1 K_{bz1} + b_1 K_{bz2} + c_1 K_0 + d_1 K_{sr}) & 2(a_1^2 K_{bz1} + b_1^2 K_{bz2} + c_1^2 K_0 + d_1^2 K_{sr}) \end{bmatrix}$;

$\{\mathrm{q}\} = \begin{bmatrix} z_d \\ \beta \end{bmatrix}$ is the generalized coordinate response vector and $\{\mathrm{p}\} = \begin{Bmatrix} m_u e\omega^2 \sin(\omega t) \\ -a_0 m_u e\omega^2 \sin(\omega t) \end{Bmatrix}$ is the excitation force vector.

Assuming negligible damping due to bearings [80], O-ring and the retainer spring, the homogenous form of equation (2.6) can be written as:

$$[\mathrm{M}]\{\ddot{\mathrm{q}}\} + [\mathrm{K}]\{\mathrm{q}\} = 0 \tag{2.7}$$

The above equation is solved using MATLAB Software to determine the natural frequencies of the grinder. As it is evident from Figure 2.7, the primary peak in the vibration transmissibility along the Z-axis occurs near 180 Hz. Considering that the magnitudes of secondary peaks are significantly smaller, the fundamental natural frequency of the grinding spindle system along the Z-axis may be considered as 180 Hz. The stiffness values of deep groove ball bearings are selected in such a way that the resulting natural frequency of the model is equal to 180 Hz. The measured frequency response along the axial direction (X-axis), as shown in Figure 2.9, revealed several peaks near 170, 410, 590 and 1250 Hz. The frequency of 170 Hz is considered as the fundamental frequency, and the stiffness values of the deep groove ball bearings are selected such that the natural frequency of the model is comparable to 170 Hz. The visco-elastic properties of the deep groove radial ball bearings thus obtained are represented in Table 2.3. Owing to the symmetry along the Y- and Z-axes, the properties along the Y-axis are considered to be identical for the Z-axis. The damping coefficients of the bearings were taken from the literature [80].

Table 2.3 Values of visco-elastic properties of bearing

Parameter	Value	
$K_{bz1} = K_{bz2}$	$1.41*10^5$	N/m
$K_{by1} = K_{by2}$	$1.41*10^5$	N/m
$K_{bx1} = K_{bx2}$	$4.5067*10^5$	N/m
$C_{bz1} = C_{bz2}$	20	Ns/m
$C_{by1} = C_{by2}$	20	Ns/m
$C_{bx1} = C_{bx2}$	30	Ns/m

Bearings play a vital role in the dynamic behavior of a rotor system. They influence the occurrence of critical speeds, the onset of dynamic instability, and the magnitude of vibration in response to external forces. The effective stiffness value of a bearing will depend on many factors, such as cross coupling effect and radial internal clearance. The stiffness values of the bearings identified in this study are compared with those reported in the literature for the comparable bearing model (SKF 6002). These studies have reported the radial stiffness in the order of 10^7 N/m [81, 82], which is significantly higher than the identified value. The difference can be attributed to the estimation method, which can identify the effective stiffness associated with this mode and it accounts for the coupling effects arising from other components, such as the drives, contact stiffness, O-ring, clearances and retainer spring.

A complex eigenvalue analysis is further performed in order to find the damping ratios and the damped frequencies of the shaft-disc system. The natural frequencies and damping ratios obtained along the radial (Z- and Y-axes) and axial (X-axis) directions are summarized in Table 2.4. The results show two natural frequencies along the Z- and Y-axes, which can be associated to rotational and translational motions of the shaft-disc

Table 2.4 Natural Frequencies of the grinder model

Axis	Natural Frequency ω_n (Hz)	Damped Frequency ω_d (Hz)	Damping Ratio ξ
Z	54.816	54.80	0.0245
	180.4	179.85	0.0807
Y	54.816	54.80	0.0245
	180.4	179.85	0.0807
X	170.0	169.89	0.0361

system. The natural frequency along the X-axis corresponds with the translational motion of the system. The damping ratios of the system vary from 0.0245 to 0.0807 for different modes of vibration.

2.7 Simulation Results and Discussion

The coupled second order differential equations of motion, described in section 2.4, are initially solved under mass unbalance excitations without considering the gyroscopic effect. Simulations are performed for different angular speeds up to the recommended maximum speed of 12000 rpm, and the results are analyzed to compute the dynamic forces transmitted to the machine body along all the three directions as a function of the angular speed. It must be noted that the amount of force transmitted through the bearings to the tool body relates to the force transmitted to the hand as the handles are rigidly attached to the machine body. The preliminary analysis is performed under excitation arising from a fixed mass unbalance of 76 gm-mm. The forces transmitted along the Z-, Y- and X-axes are computed from the generalized response coordinates and the properties of the visco-elastic elements, such that:

$$F_{tz} = 2z_d(K_{bz1} + K_{bz2} + K_0 + K_{sr}) + 2\dot{z}_d(C_{bz1} + C_{bz2} + C_0 + C_{sr}) + 2\beta(a_1K_{bz1} + b_1K_{bz2} + c_1K_0 + d_1K_{sr}) + 2\dot{\beta}(a_1C_{bz1} + b_1C_{bz2} + c_1C_0 + d_1C_{sr}) \tag{2.8}$$

$$F_{ty} = 2y_d(K_{by1} + K_{by2} + K_0 + K_{sr}) + 2\dot{y}_d(C_{by1} + C_{by2} + C_0 + C_{sr}) - 2\alpha(a_1K_{by1} + b_1K_{by2} + c_1K_0 + d_1K_{sr}) - 2\dot{\alpha}(a_1C_{by1} + b_1C_{by2} + c_1C_0 + d_1C_{sr}) \tag{2.9}$$

$$F_{tx} = x_d(K_{bx1} + K_{bx2} + K_0 + K_{sr}) + \dot{x}_d(C_{bx1} + C_{bx2} + C_0 + C_{sr})$$

(2.10)

where F_{tz}, F_{ty} and F_{tx} are the forces transmitted to the tool body along the Z-, Y- and X-axes, respectively.

In view of the assumed of symmetric properties along the Y- and Z-axes, the model simulations yield identical force responses along both the axes, as shown in Figures 2.10 and 2.11. The results show the magnitudes of transmitted forces along the two-axes as a function of the operating speed in the 0-12000 rpm range. The magnitude of force transmitted along the axial direction (X-axis) as a function of rotational speed is shown in Figure 2.12. The forces transmitted along the Z- and Y-axes shows two peaks in the magnitude occurring at 3288 rpm and 10820 rpm, which correspond to the natural frequencies of the system namely 54 and 180 Hz. The force response along the axial direction (X-axis) reveals a single peak at 10200 rpm, which correspond to the system natural frequency of 170 Hz. From these results it can be concluded that the amount of force transmitted to the machine body is large along the radial directions (Z- and Y-axes), when compared to that along the axial direction (X-axis).

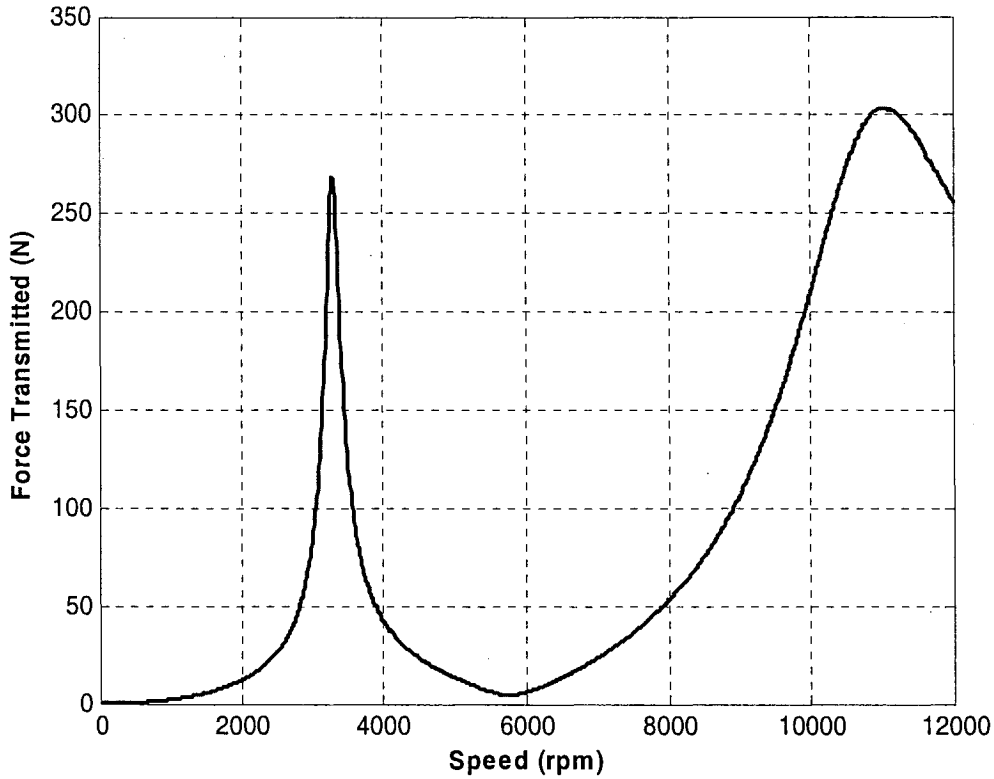

Figure 2.10: Force transmitted along the Z-axis as a function of the operating speed under mass unbalance of 76 gm-mm

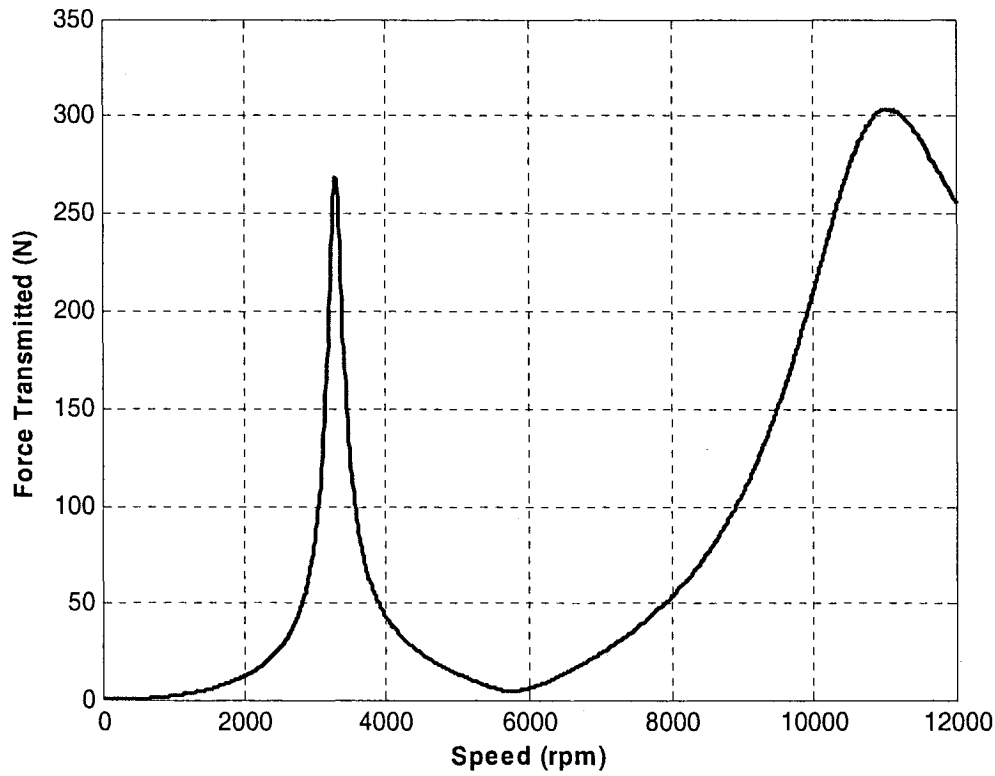

Figure 2.11: Force transmitted along the Y-axis as a function of the operating speed under mass unbalance of 76 gm-mm

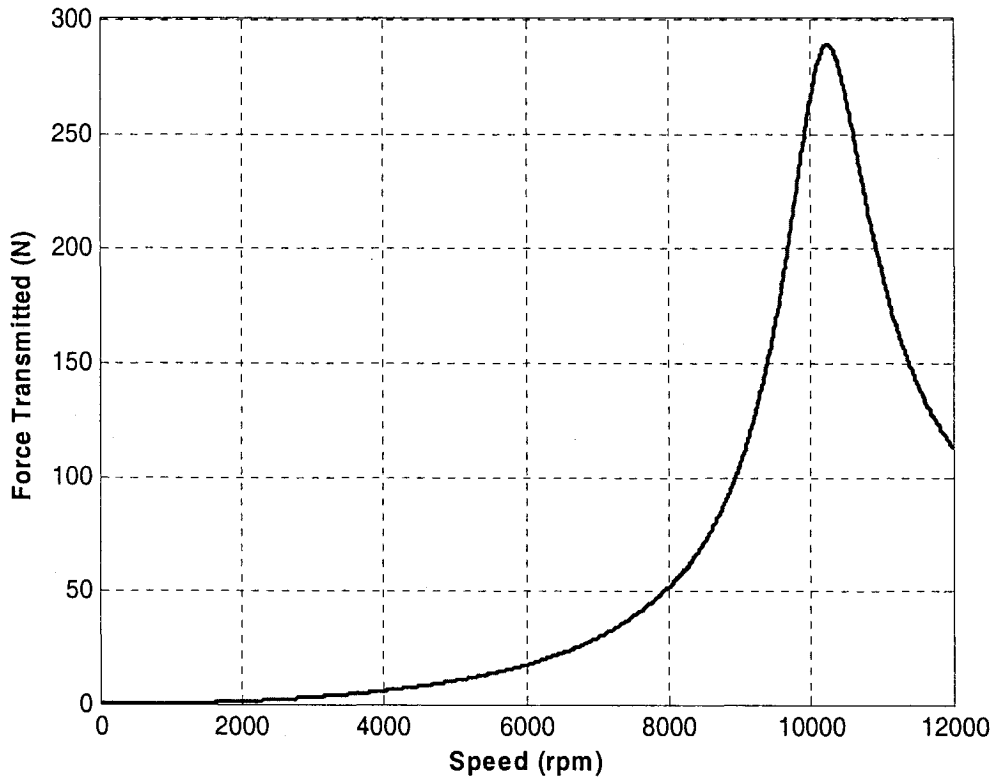

Figure 2.12: Force transmitted along the X-axis as a function of the operating speed under mass unbalance of 76 gm-mm

2.8 Gyroscopic Effect

The shaft-disc assembly described in section 2.3 is also subjected to the gyroscopic couple. By considering the gyroscopic effect in the above 5 DOF grinder model, the force transmitted along the radial direction is calculated for mass unbalance of 76 gm-mm and as a function of the rotational speed upto a maximum of 12000 rpm, as described in section 2.7. Figures 2.13 and 2.14 represent the magnitudes of forces transmission to the machine body, with and without the gyroscopic effect along the Z- and Y-axes, respectively. From these results it is evident that the gyroscopic effect on the force transmission to the machine body is insignificant. As shown in equations (2.2) and (2.4), the terms $I_x\omega\dot{\beta}$ and $I_x\omega\dot{\alpha}$ represent the gyrocouple. As the values of $\dot{\alpha}, \dot{\beta}$ are small, the gyrocouple does not have effect on the force transmission along the Z- and Y-axes.

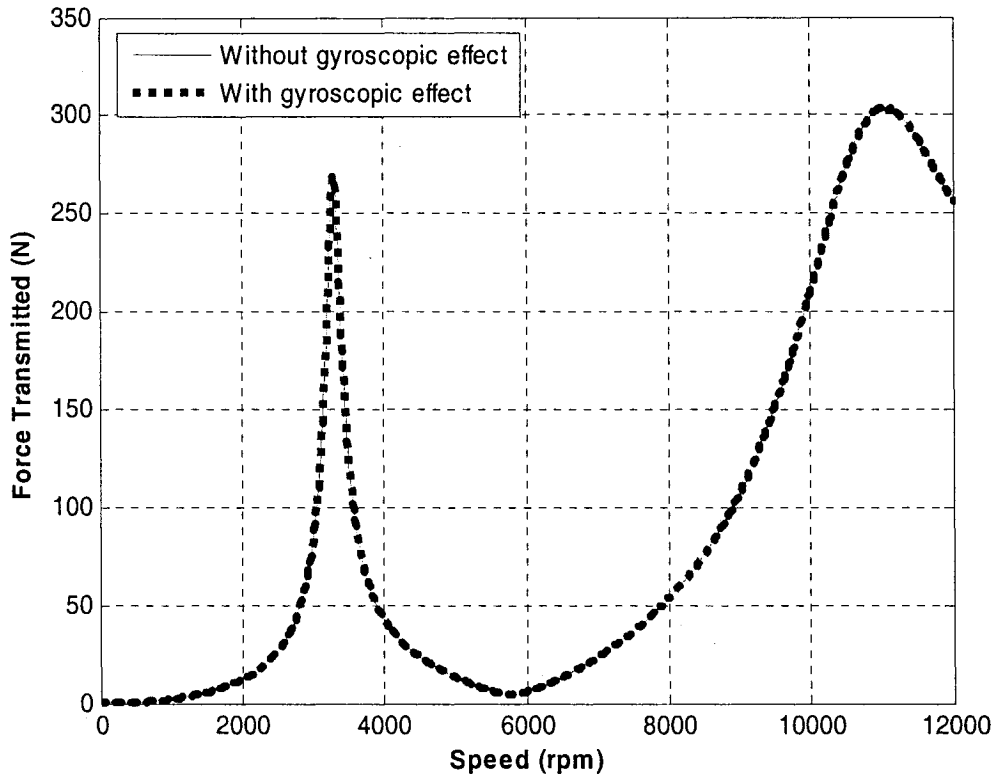

Figure 2.13: Influence of the gyroscopic effect on the force transmission along the Z-axis as a function of the operating speed under mass unbalance of 76 gm-mm

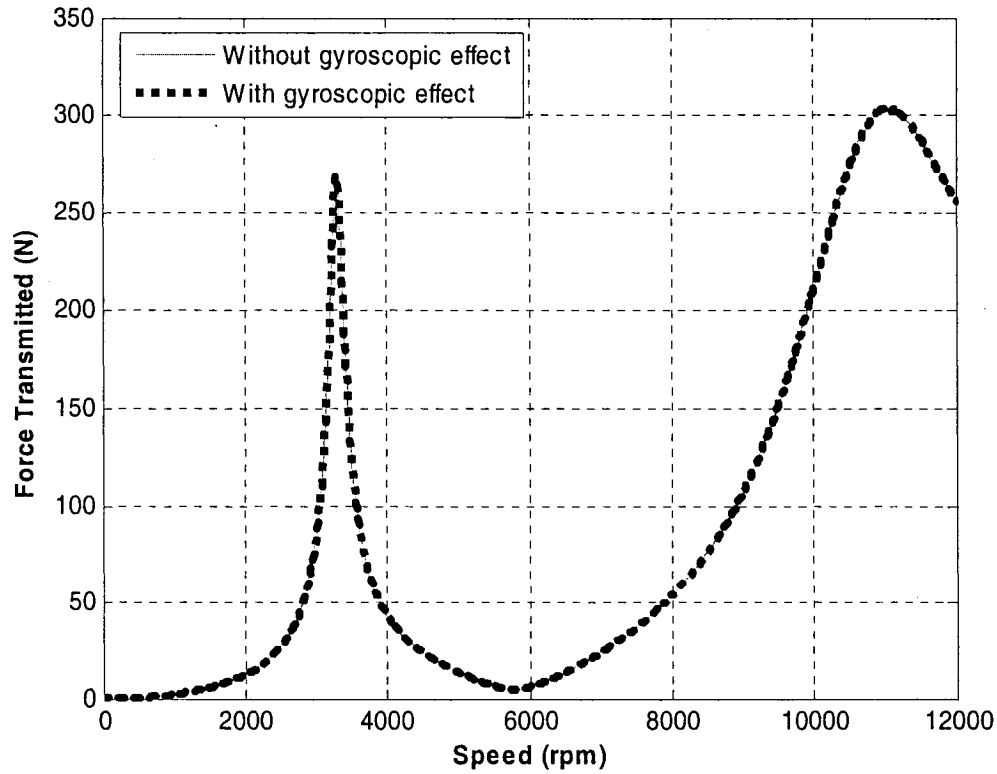

Figure 2.14: Influence of the gyroscopic effect on the force transmission along the Y-axis as a function of the operating speed under mass unbalance of 76 gm-mm

2.9 Summary

A 5 DOF grinder model is developed in this chapter which will be used for formulating the coupled hand-tool system model. The force transmission, because of the rotating mass unbalance, is calculated for different angular speeds. These results suggest that resonance peaks occur at the system natural frequencies. This analysis also reveals that gyroscopic effect is insignificant on the force transmission. The grinder model developed in this chapter is coupled with hand-arm model that will be developed in the next chapter, for development of the coupled hand-tool model.

CHAPTER 3
DEVELOPMENT OF ANALYTICAL HAND-ARM VIBRATION MODEL

3.1 Introduction

The severe health risks posed by prolonged exposure to hand-held power tool vibration, supported by the findings of the epidemiological studies, have prompted a strong desire to enhance a thorough understanding of the vibration response characteristics of the human hand-arm. In the previous chapter the vibration characteristics of the grinder alone was studied. The human hand and arm system is known to absorb considerable amount of vibration energy. A study of power tools vibration transmitted to the human hand-arm system requires the consideration of the coupled hand-tool system. Analytical models of the hand-transmitted vibration may serve as an important tool to design and evaluate vibration isolation mechanisms. A number of studies have been conducted to characterize the dynamic response of the hand-arm system using transmissibility and impedance measurements [55, 63]. The transmissibility measurements, however, have been considered valid for low frequency vibration due to the presence of high noise levels associated with skin-mounted sensors [83]. Driving Point Mechanical Impedance of the hand-arm have been extensively investigated to characterize the biodynamic response, since the driving point impedance is well suited to describe the overall dynamic response. The Impedance may be related to the amount of mechanical energy transferred from power tools [84], and thus occurrence of occupational diseases due to prolonged use of the power tools. In the present chapter the

vibration characteristics of the hand-arm system is studied using the Driving Point Mechanical Impedance information available from past studies.

The vibration transmissibility characteristics of the hand-arm system can be determined through development and analysis of an analytical model. The Driving Point Mechanical Impedance characteristics of the hand-arm system have been employed to enhance the understanding of the biodynamic response of the hand-arm to uncoupled vibration excitations along three orthogonal axes. Driving Point Mechanical Impedance (Z), widely used to describe the dynamic properties of the complex hand-arm system, is defined as the ratio of the driving force (F) to the velocity ($\dot{X}$) measured at the driving-point. Alternatively mechanical compliance (ratio of the driving point displacement to the driving force, X/F) and accelerance (ratio of driving-point acceleration to the driving force, $\ddot{X}/F$) has also been employed to describe the dynamics of the human hand-arm [85].

The Driving Point Mechanical Impedance of the hand-arm system has been characterized by mass-excited, lumped-parameter biodynamic models, where the model parameters are derived from the measured impedance data [67]. Lumped-parameter models, ranging from simple single DOF to many DOF, have been proposed [19, 60-66]. The determination and use of the DPMI response does not involve the internal relationships among the tissues and musculoskeletal structure of the hand and arm. The modulus and phase response, however, fully describe the mass, spring, and damper like behavior of the hand and arm. Although the proposed models provide little insight into the pathological changes caused by hand-transmitted vibration, they serve as useful tools to study vibration amplitudes and power flow in the coupled hand, power tool and work-

piece system [53, 86]. A recent study has presented a comparison of the reported models in view of their applicability for analyses of the coupled hand-tool system [68]. The study concluded that all the models could not be applied due to presence of a low frequency vibration mode that causes excessive deflections of the hand-arm model. The study further concludes that higher order models, with three and four degrees of freedom, in general, yield impedance characteristics within the range of idealized values. The majority of the lower order models yield reasonable magnitudes of static deflections but relatively poor agreement with idealized values of driving point mechanical impedance. The study also states that there is no agreement among the reported models in terms of the natural frequencies of the human hand and arm. Furthermore, the models characterize the uncoupled biodynamic behavior of the hand and arm, neglecting the dynamic coupling effects of the hand and arm.

In this chapter, the Driving Point Mechanical Impedance data derived from the driving point excitation velocity and the resultant forces generated along the three axes, are examined and lumped parameter models of the hand-arm system uncoupled in the different axes are developed for application with the grinder model. A nonlinear programming based optimization technique is employed to identify the model parameters on the basis of the available impedance data.

3.2 Development of the Human Hand-Arm Model to Characterize the Impedance Values

The reported models have been invariably developed on the basis of the measured impedance data under random or sinusoidal displacement, velocity or acceleration excitations [65-67]. The models and formulations generally consider the driving-point

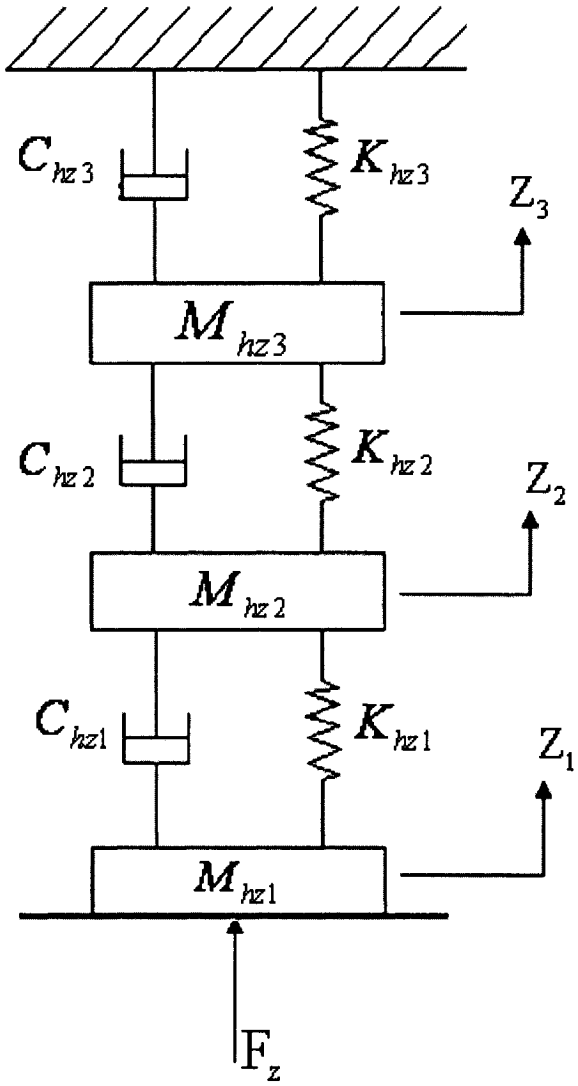

Figure 3.1: Proposed two-degree-of-freedom model of hand –arm biodynamic model

force as the input and velocity as the response to characterize the driving-point mechanical impedance. Moreover, the available data are acquired under excitations applied along a single axis. The data are thus applied to develop models that are considered valid along each individual axis in an uncoupled manner. Figure 3.1 illustrates the model structure outlined in [50, 60, 67]. The same model structure is applied along all

the three orthogonal axes, x_h-, y_h- and z_h-, as defined in the bio-dynamic coordinate system in Figure 1.2. The model is considered as a three degrees-of-freedom system in the published studies, since a force excitation is assumed. Owing to the experimental condition involving motion excitation, the model in this study is considered as a two degrees-of-freedom for each axis of motion. The coupling along the x_h-, y_h-, and z_h-axes, is neglected in this model.

The equations of motion along the z_h-axis of model subject to excitation $z_1(t)$ are written as

$$M_{hz2}\ddot{z}_2 + (K_{hz1} + K_{hz2})z_2 - (K_{hz2})z_3 + (C_{hz1} + C_{hz2})\dot{z}_2 - (C_{hz2})\dot{z}_3 = (K_{hz1})z_1 + (C_{hz1})\dot{z}_1 \tag{3.1}$$

$$M_{hz3}\ddot{z}_3 - (K_{hz2})z_2 + (K_{hz2} + K_{hz3})z_3 - (C_{hz2})\dot{z}_2 + (C_{hz2} + C_{hz3})\dot{z}_3 = 0 \tag{3.2}$$

The equations of motion of the model can be expressed in the following matrix form:

$$[\mathrm{M}]\{\ddot{\mathrm{q}}\} + [\mathrm{C}]\{\dot{\mathrm{q}}\} + [\mathrm{K}]\{\mathrm{q}\} = [K_1]\{z_1\} + [C_1]\{\dot{z}_1\}$$

where [M], [C] and [K] are (2x2) mass, damping and stiffness matrices respectively.{q} is a (2x1) vector of displacement response quantities, $[K_1]$ and $[C_1]$ are (2x1) forcing stiffness and damping vectors, respectively. The dots above the response vectors, "." and ".." designate the first and second order derivatives with respect to time.

Representing equations (3.1) and (3.2) in matrix form

$$\begin{bmatrix} M_{hz2} & 0 \\ 0 & M_{hz3} \end{bmatrix}\begin{Bmatrix} \ddot{z}_2 \\ \ddot{z}_3 \end{Bmatrix}+\begin{bmatrix} C_{hz1}+C_{hz2} & -C_{hz2} \\ -C_{hz2} & C_{hz2}+C_{hz3} \end{bmatrix}\begin{Bmatrix} \dot{z}_2 \\ \dot{z}_3 \end{Bmatrix}$$

$$+\begin{bmatrix} K_{hz1}+K_{hz2} & -K_{hz2} \\ -K_{hz2} & K_{hz2}+K_{hz3} \end{bmatrix}\begin{Bmatrix} z_2 \\ z_3 \end{Bmatrix}=\begin{bmatrix} K_{hz1} & 0 \\ 0 & 0 \end{bmatrix}\begin{Bmatrix} z_1 \\ z_2 \end{Bmatrix}+\begin{bmatrix} C_{hz1} & 0 \\ 0 & 0 \end{bmatrix}\begin{Bmatrix} \dot{z}_1 \\ \dot{z}_2 \end{Bmatrix}$$

The motion transmissibility to M_{h3} and M_{h2} are obtained as:

$$\frac{z_3(s)}{z_1(s)}=\left(\frac{K_{hz2}+sC_{hz2}}{M_{hz3}s^2+(K_{hz2}+K_{hz3})+s(C_{hz2}+C_{hz3})}\right)\left(\frac{K_{hz1}+sC_{hz1}}{\Delta(s)}\right) \tag{3.3}$$

$$\frac{z_2(s)}{z_1(s)}=\left(\frac{K_{hz1}+sC_{hz1}}{\Delta(s)}\right) \tag{3.4}$$

where,

$$\Delta(s)=$$

$$\left\{M_{hz2}s^2+(K_{hz1}+K_{hz2})+s(C_{hz1}+C_{hz2})\right\}-\left\{\frac{(K_{hz2}+sC_{hz2})^2}{M_{hz3}s^2+(K_{hz2}+K_{hz3})+s(C_{hz2}+C_{hz3})}\right\}$$

The Driving Point Mechanical Impedance (DPMI) is derived from the driving point excitation velocity $\dot{z}_1$ and the resultant force at mass M_{hz1}. The resultant force F_z at the lower mass can be computed from the equation of motion for mass M_{hz1}:

$$M_{hz1}\ddot{z}_1 + K_{hz1}(z_1 - z_2) + C_{hz1}(\dot{z}_1 - \dot{z}_2) = F_z \tag{3.5}$$

where F_z is the force developed at the driving-point along the z_h-axis.

The DPMI response of the model can then be derived as follows:

$$\text{z(s)}=\frac{F_z(s)}{sz_1(s)} = M_{hz1}s + \left(\frac{K_{hz1}}{s} + C_{hz1}\right)\left(1 - \frac{z_2(s)}{z_1(s)}\right) \tag{3.6}$$

Similarly the equations of motion along the y_h- and x_h-axes of the hand-arm system are written as:

$\underline{y_h - axis:}$

$$M_{hy2}\ddot{y}_2 + (K_{hy1} + K_{hy2})y_2 - (K_{hy2})y_3 + (C_{hy1} + C_{hy2})\dot{y}_2 - (C_{hy2})\dot{y}_3 = (K_{hy1})y_1 + (C_{hy1})\dot{y}_1 \tag{3.7}$$

$$M_{hy3}\ddot{y}_3 - (K_{hy2})y_2 + (K_{hy2} + K_{hy3})y_3 - (C_{hy2})\dot{y}_2 + (C_{hy2} + C_{hy3})\dot{y}_3 = 0 \tag{3.8}$$

$\underline{x_h - axis:}$

$$M_{hx2}\ddot{x}_2 + (K_{hx1} + K_{hx2})x_2 - (K_{hx2})x_3 + (C_{hx1} + C_{hx2})\dot{x}_2 - (C_{hx2})\dot{x}_3 = (K_{hx1})x_1 + (C_{hx1})\dot{x}_1 \tag{3.9}$$

$$M_{hx3}\ddot{x}_3 - (K_{hx2})x_2 + (K_{hx2} + K_{hx3})x_3 - (C_{hx2})\dot{x}_2 + (C_{hx2} + C_{hx3})\dot{x}_3 = 0 \tag{3.10}$$

The Driving Point Mechanical Impedance of the hand-arm along the y_h- and x_h-axes are also derived in the same manner, as described in Equations (3.3) to (3.6).

3.3 Estimation of Model Parameters

A nonlinear programming based optimization technique, involving the use of a constrained optimization algorithm is effectively employed to determine the model parameters [59]. An objective function is formulated to minimize the sum of squares of the errors between the magnitudes and phase of measured and model driving point impedance characteristics as a function of the excitation frequency in the range from 10 to 1000 Hz. The measured Driving Point Mechanical Impedance responses along the z_h-and x_h-axes, are obtained from [87] and along the y_h-axis from [50]. These are shown in Figures 3.2 to 3.4. In order to extract the relevant model parameters, a curve fitting exercise is carried out. The experimental DPMI is fitted with least square error curves where the error is specified as:

$$E(\bar{\lambda}) = \left[\sum_{k}^{n} \left\{ |Z(\omega_k)| - |Z_m(\omega_k)| \right\}^2 + \sum_{k}^{n} \left\{ \phi(\omega_k) - \phi_m(\omega_k) \right\}^2 \right] \tag{3.11}$$

The squared error $E(\bar{\lambda})$ is the objective function with $\bar{\lambda}$ as a vector of model parameters given by:

$$\bar{\lambda} = \{m_1, m_2, m_3, c_1, c_2, c_3, k_1, k_2, k_3\}^T$$

In equation (3.11), 'T' designates the transpose. $|Z(\omega_k)|$ and $\phi(\omega_k)$ are the magnitude and phase of driving-point impedance derived from the lumped-parameter model at an excitation frequency ω_k and $|Z_m(\omega_k)|$ and $\phi_m(\omega_k)$ are the corresponding measured magnitude and phase of the driving-point impedance derived from the synthesis of

measured values, n is the number of discrete frequencies selected in the frequency range of interest.

The above objective function is subject to following parametric constraints:

$$m_1 > 0; m_2 > 0; m_3 > 0;$$
$$c_1 > 0; c_2 > 0; c_3 > 0;$$
$$k_1 > 0; k_2 > 0; k_3 > 0;$$

$$3.50 \leq \sum_{1}^{3} m_i \geq 6.00 \tag{3.12}$$

The constrained optimization problem, defined in equations (3.11 to 3.12) is solved using MATLAB software package. The optimization algorithm attempts to minimize the sum of squares of the errors in both impedance magnitude and phase computed for the frequencies in the range 10 to 1000 Hz. The solutions were obtained for different starting values of the parameter vector $\overline{\lambda}$ and the resulting model parameters were examined to obtain optimum values and the minimum error of the objective function. Different optimization runs corresponding to different starting values converged to similar values of the model parameter and the error function.

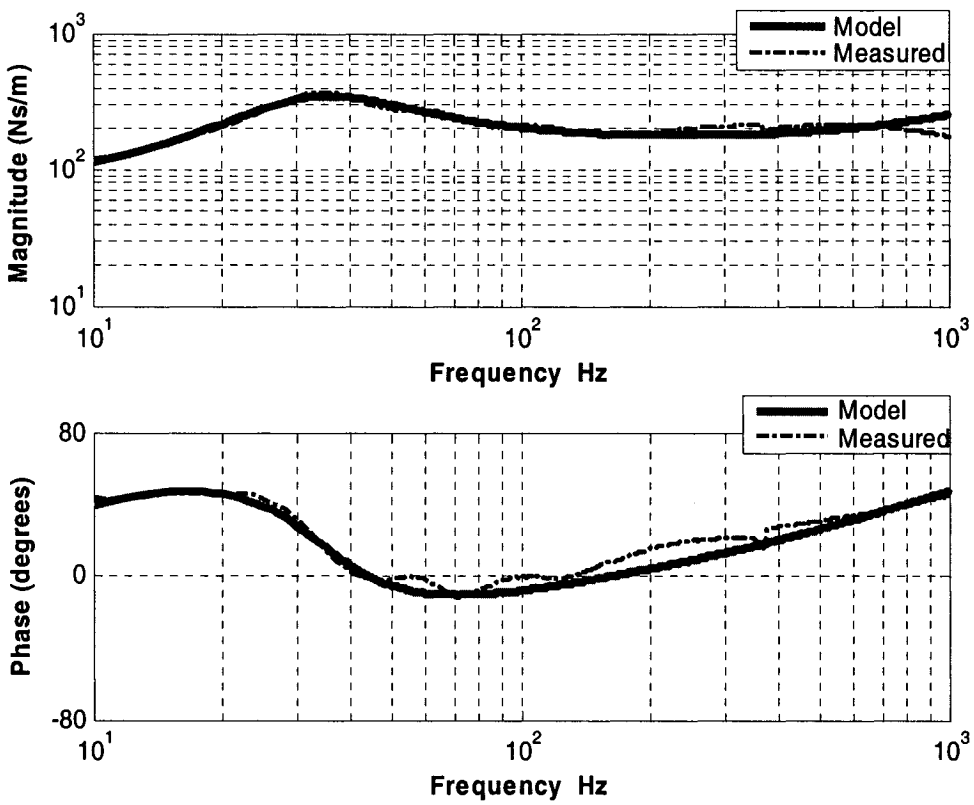

Figure 3.2: Comparisons of measured and model magnitude and phase responses (z_h -axis)

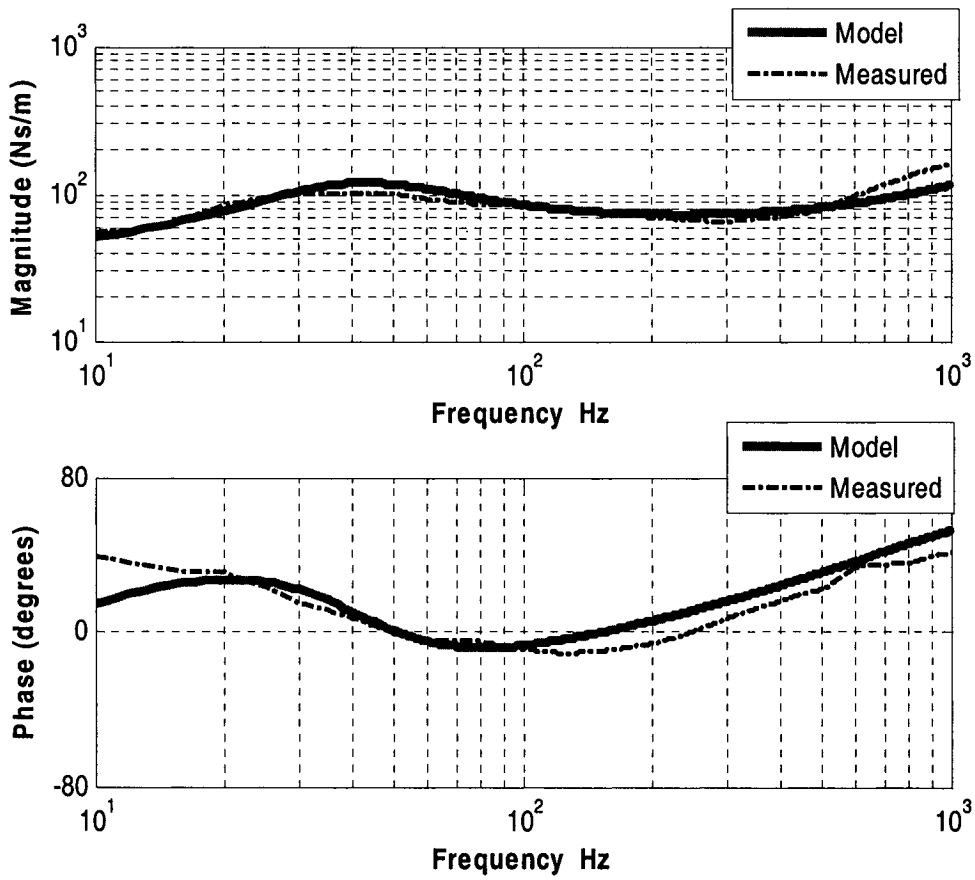

Figure 3.3: Comparisons of measured and model magnitude and phase responses (y_h -axis)

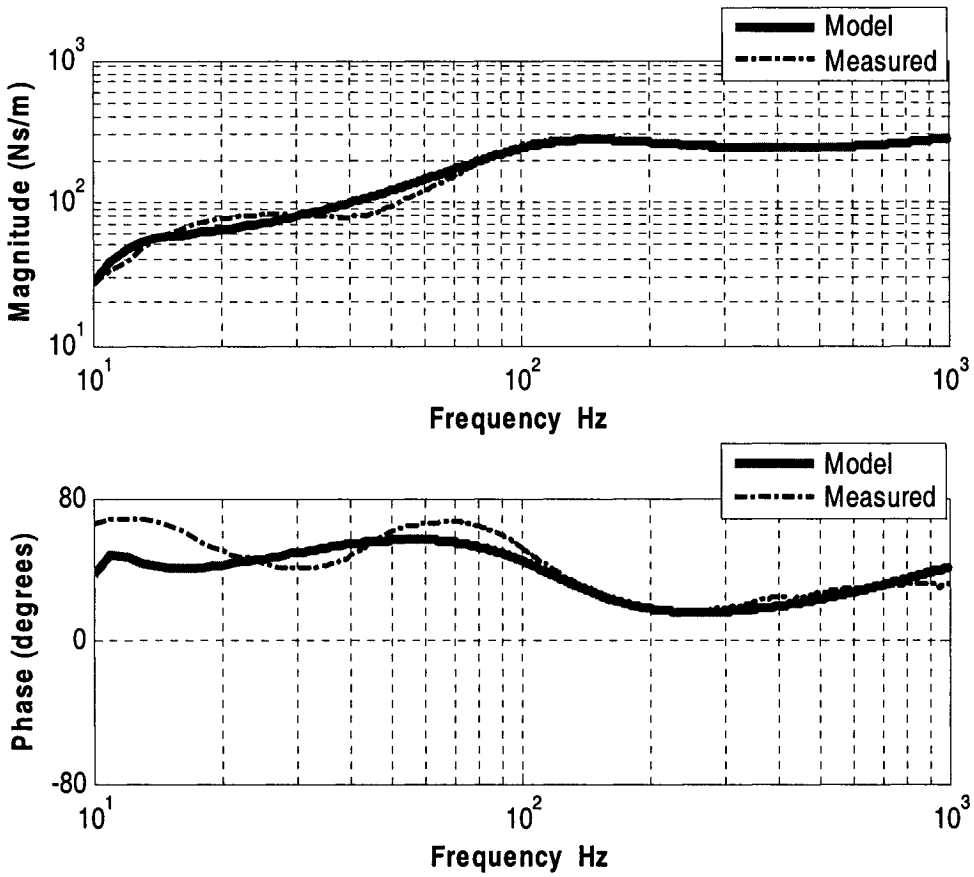

Figure 3.4: Comparisons of measured and model magnitude and phase responses (x_h -axis)

3.3.1 Model Parameter Values

The model parameters for the hand-arm model that best fit the impedance values, both in magnitude and phase are thus summarized in Table 3.1. The total mass of the model is constrained within a range of average values for the human male hand-arm system, which is approximately 8% of the total body mass [88]. The model parameters

Table 3.1 Model parameter values for the hand-arm model

Model Parameters	z_h-axis	y_h-axis	x_h-axis
M_{h1} (kg)	0.03	0.03	0.03
M_{h2} (kg)	1.2039	0.4	0.2532
M_{h3} (kg)	2.4067	3.25	3.5
K_{h1} (N/m)	56873	27100	165390
K_{h2} (N/m)	800	800	300
K_{h3} (N/m)	12000	8000	10000
C_{h1} (Ns/m)	171.63	70	200
C_{h2} (Ns/m)	87.786	53.962	30.429
C_{h3} (Ns/m)	500	325	375

presented in Table 3.1 reveal that the sum of the three hand masses are 3.61, 3.68 and 3.75 kg in the z_h-, y_h- and x_h- directions, respectively. From the above analysis, it is evident that the model mass is concentrated near the fixed base of the hand-arm (i.e. M_{h3}). The mass M_{h2} is observed to be the second largest in all the three directions. The mass M_{h1}, which is directly in contact with the handle and is subjected to excitations, is the smallest in magnitude, irrespective of the direction of excitation. For the x_h-axis impedance model the spring constant K_{h1} is large in comparison with the remaining

visco-elastic elements of the model, as evident in Table 3.1, suggesting a strong coupling between masses M_{h1} and M_{h2}. The mass M_{h2} is coupled to mass M_{h3} by a relatively weak spring K_{h2}, and the mass M_{h3} is coupled to the base by a comparatively stiff spring K_{h3} and a strong damping element C_{h3}. Along the y_h- and z_h-axes, the mass M_{h2} is coupled to mass M_{h3} by a relatively weak spring K_{h2} while the mass M_{h3} is coupled to the base by a comparatively stiff spring K_{h3} and a strong damping element C_{h3}.

From Table 3.1, it is seen that mass M_{h1} is same along all the three axes, z_h-, y_h- and x_h-, however, masses M_{h2} and M_{h3} have different curve fitted values along different directions. This may be the result of neglecting the coupling along the three axes, which makes it impossible to arrive at single value for these masses along the three directions satisfying the experimental measurements. The curve fitted values are retained for subsequent calculations.

Equation (3.6) is solved to compute the driving-point impedance and phase response using the identified model parameters. Figures 3.2-3.4 illustrate comparisons of the model responses along the z_h-, y_h- and x_h-axes, respectively, with the reported mean synthesized data [50, 87]. The comparison of the model response and measured impedance characteristics reveal that the proposed lumped parameter model, presented in Figure 3.1, can predict the measured impedance responses accurately in the entire frequency range in all the three directions. The magnitudes of the impedance responses of the proposed models generally correlate very well with the measured impedance magnitudes in the entire frequency range, while some deviations can be observed in the phase responses. The deviations in the model and measured impedance phase responses

occur in almost entire frequency range for the z_h- and y_h-axes, while the deviations in the x_h-axis response mostly occur at frequencies below 100 Hz. These deviations can be attributed to the broad range of test conditions, such as various grip forces and hand-arm postures, dynamic coupling coefficients, that are not considered in the synthesized data.

3.4 Natural Frequencies of the Hand-Arm Model

From the above impedance curves (Figures 3.2 -3.4) it can be concluded that the peaks occur in the 30-40 Hz bands in the z_h-direction, 30-45 Hz bands in the y_h-direction and 100-150 Hz bands in the x_h-direction. The proposed hand-arm models are analyzed to derive their natural frequencies. As the hand-arm system is a highly damped system, a complex modal analysis is performed [89, 90]. The eigenvalues obtained from the modal analysis provide the range of frequencies at which responses could be significant. The equations of motion of the hand-arm model can be expressed in the following matrix form:

$$[M]\{\ddot{q}\} + [C]\{\dot{q}\} + [K]\{q\} = \{p\} \tag{3.13}$$

where $\{p\}$ is a (2x1) excitation force vector

Equation (3.13) can be expressed as a system of first order differential equations,

$$[\mu]\{\dot{\zeta}\} + [\kappa]\{\zeta\} = \{F\} \tag{3.14}$$

where,

$$[\mu] = \begin{bmatrix} 0 & M \\ M & C \end{bmatrix}_{4x4};$$

$$[\kappa] = \begin{bmatrix} -M & 0 \\ 0 & K \end{bmatrix}_{4x4};$$

$$\zeta = \begin{bmatrix} \{\dot{z}\} \\ \{z\} \end{bmatrix}_{4x1};$$

$$F = \begin{bmatrix} \{0\} \\ \{p\} \end{bmatrix}_{4x1};$$

In order to obtain the eigenvalues and eigenvectors of the system, the homogenous form of equation is solved initially using MATLAB Software. Undamped natural frequencies and damping factors from the damped analysis are computed from the Eigen values. For an underdamped mode, the eigenvalue λ_i can be expressed as:

$$\lambda_i = \xi_i \omega_{ni} \pm j\omega_{ni}\sqrt{(1-\xi_i^2)} \tag{3.15}$$

where

$\omega_{ni} = \sqrt{A_i^2 + B_i^2}$ = natural frequency.

$\omega_{di} = B_i$ =damped frequency of resonant oscillations

$\xi_i = \sqrt{(1-(\frac{\omega_{di}}{\omega_{ni}})^2)}$ =damping ratio for each mode

For an overdamped mode, the real eigenvalues λ_i can be related to ω_{ni} and ξ_i in the following manner

$$\lambda_i = C_i = \xi_i \omega_{ni} + \omega_{ni}\sqrt{\xi_i^2 - 1}$$

$$\lambda_i^* = C_i^* = \xi_i \omega_{ni} - \omega_{ni}\sqrt{\xi_i^2 - 1}$$

$$\xi_i = \frac{(C_i + C_i^*)}{\sqrt{(C_i + C_i^*)^2 - (C_i - C_i^*)^2}} = \text{damping ratio for the overdamped mode} \tag{3.16}$$

$$\omega_{ni} = \frac{(C_i + C_i^*)}{2\xi_i} = \text{natural frequency}$$

3.5 Eigenvalue Analysis of HAV Model

The eigenvalue problems for the models are solved for each axis of motion, and the natural frequencies and damping ratios are computed from the above analysis. The natural frequencies together with the damping ratios of the proposed hand-arm model along the z_h-, y_h- and x_h-axes are summarized in Table 3.2. The results suggest the

Table 3.2 Natural Frequencies of the hand-arm model

Axis	Natural Frequency ω_n (Hz)	Damped Frequency ω_d (Hz)	Damping Ratio ξ
z_h	11.601	-	1.7136
	34.836	30.1	0.5164
y_h	8.270	-	1.1350
	42.035	33.0930	0.6166
x_h	8.630	-	1.0684
	128.734	106.31	0.5639

presence of a single over damped mode in each axis, which corresponds to a relatively low frequency. The damped natural frequencies of the model along the y_h- and z_h-axes occur as 33.1 Hz and 30.1 Hz, respectively, which correspond well with the primary peaks in the measured impedance responses, shown in Figures 3.2 and 3.3. These modes also reveal relatively high damping ratios in the 0.5-0.6 range. The results suggest the

presence of a damped natural frequency of 106.31 Hz of the x_h-axis model, which also corresponds well with the resonant peak of the measured impedance response curve shown in Figure 3.4. The damping ratio corresponding to this mode (0.5639) is also comparable to those observed for the y_h and z_h-axes, models. The damping ratios of the hand-arm model from the above eigenvalue analysis clearly shows that the proposed hand-arm system model is heavily damped.

3.6 Summary

This chapter describes a methodology to identify the parameters of the hand arm vibration (HAV) models using mechanical impedance data and nonlinear programming based optimization technique. Two degrees-of-freedom (DOF) linear models are formulated to yield impedance characteristics in the 10-1000 Hz frequency range along the three axes of vibration. In this chapter the Driving Point Mechanical Impedance is derived from the driving point excitation velocity and the resultant force generated. The analytical model parameters are derived to fit the measured data for all the three orthogonal directions of vibrations. The complex eigenvalue analysis is performed on the developed hand-arm model and damped natural frequencies are identified. These natural frequencies correlate well with the biodynamic response characteristics. The hand arm model developed in this chapter is used in the next chapter for the coupled hand-tool analysis.

CHAPTER 4
MODELING AND VALIDATION OF COUPLED HAND-TOOL SYSTEM

4.1 Introduction

Assessment of power tool vibration necessitates an estimation of the hand-transmitted vibration and a thorough understanding of the vibration transmission characteristics of the coupled hand-tool system. Owing to the severe health effects of prolonged exposure to hand-transmitted vibration from operation of power tools, it is essential to characterize and assess the vibration from different tools in an efficient manner, and to develop efficient analytical models for designing and assessing vibration attenuation mechanisms. The characteristics of hand-transmitted vibration are mainly dependant on the type of power tool and nature of task performed by the operators. The current standards on HAV (hand-arm vibration) provide guidelines pertaining to the measurement and assessment of the severity of vibration generated in the immediate vicinity of the hand [22, 41, 42]. The standard, ISO-5349 (2001) [42] recommends the use of vector sum or the root-sum-of-square of the acceleration components. It is thus believed that the hand-transmitted vibration is equally important in all the three directions. The frequencies of hand-transmitted vibration caused by the operation of hand-held power tools are known to vary over a wide range, depending upon the type of tool, operation, and hand-tool orientation. Moreover, the vibration transmission characteristics of the hand-arm system are strongly related to the magnitude and dominant directions of vibration [56]. The vibration characteristics of various power tools, measured at the handle, have been reported in the literature [20, 91] and the

reported data show that the handle vibration characteristics of different tools are considerably different.

The workers in the welding and foundry industry are subjected to high risk of vibration injuries due to high vibration levels transmitted to the hands. Grinding machines are one of the primary tools used in the industry, and the residual unbalance in the grinding wheel is one of the primary causes of high levels of vibration. This imbalance depends on the quality of the wheel and its precise fit on the tool spindle. Another source of vibration is the work process, i.e., the interaction between the machine and the material it works on. The coupling that exists between the tool and hands of the operator in the form of grip force exerted by the hand around the tool, static force exerted by the hand on the tool, size of vibrating surface in contact with the hand, can also influence the transmission of vibration energy produced by vibrating tools. The response of the power tool and the human hand-arm will vary as a result of the coupling in human hand and power tool. The coupled hand-tool analysis could yield significant insight into many desirable design features and vibration isolation mechanisms. In this study, the grinder and hand-arm models, developed in the previous chapters, are integrated to develop the coupled hand-tool model. The available measured data are used to demonstrate the validity of the coupled system model. The response of the coupled hand-tool model is studied as a function of mass unbalance of the grinding wheel. A parametric study is also conducted to study the influence of machine casing weight and bearing damping on the hand-transmitted vibration. The effect of hand-handle interface properties have also been studied by introducing visco-elastic properties representing an anti-vibration glove.

4.2 Development of Coupled Hand-Tool Model

Figures 4.1 and 4.2 present the coupled hand-tool model along the radial directions (Z- and Y-axes). Figure 4.3 presents the same along the axial direction (X-axis). The mass due to shaft-disc assembly is represented by m_d, and I_z and I_y represent the mass moments of inertia about the Z- and Y-axes, respectively. The shaft and the disc are supported by a pair of deep groove radial ball bearings located at points p and q along the shaft, and an O-ring and a retainer spring located at points r and s. The grinding wheel is mounted at the end of the shaft, as shown. The distances between the centre of gravity (cg) of the shaft-disc assembly and the bearing-1, bearing-2 (located at p and q, respectively), the O-ring and the retainer spring are represented by a_1, b_1, c_1 and d_1, respectively. The distance between the centre of the grinding wheel (w) and the centre of gravity of the shaft-disc (cg) is represented by a_0. Let m_u be the mass unbalance acting at an eccentricity e. K_{b1} and C_{b1} are the constant spring rate and damping coefficient of bearing-1 located at p. Similarly K_{b2} and C_{b2} represent the spring rate and damping coefficient for bearing-2 located at q. The properties of these two bearings are assumed to be same, such that $K_{b1} = K_{b2}$ and $C_{b1} = C_{b2}$ along both the axes. K_0, C_0, K_{sr} and C_{sr} represent the visco-elastic properties of the O-ring and the retainer spring, respectively, whose values are obtained from the literature [54]. The mass of the machine casing together with the handles is considered as M_b. M_{h1}, M_{h2} and M_{h3} represent the hand-arm masses, where the mass M_{h1} is rigidly attached to the machine casing mass M_b and the response of the hand mass M_{h1} is the same as the response of the tool body mass M_b. K_{h1}, K_{h2}, K_{h3} represent the stiffness properties and C_{h1}, C_{h2} and C_{h3}

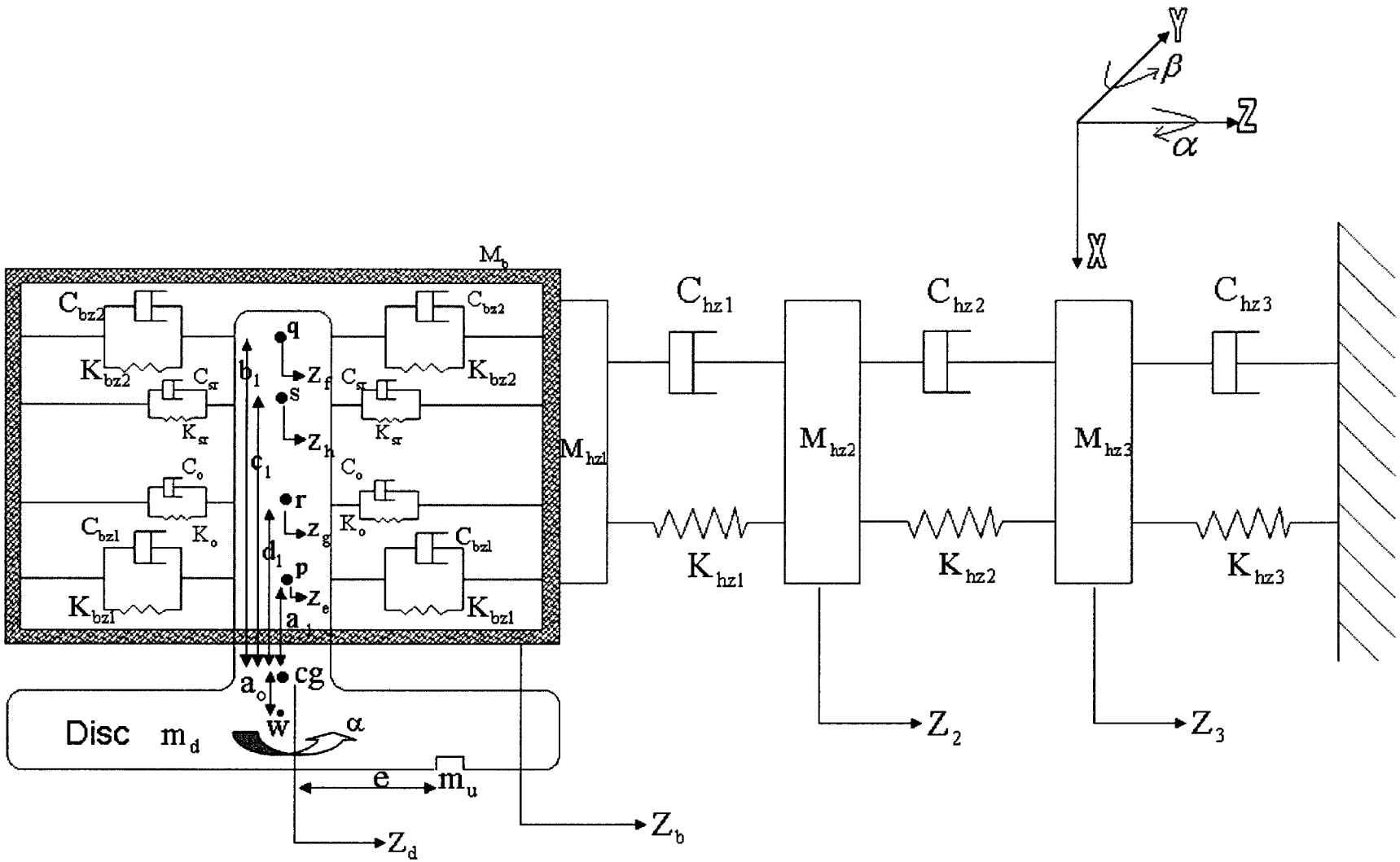

Figure 4.1: Analytical model representation of the coupled human hand and the grinder along the Z-axis

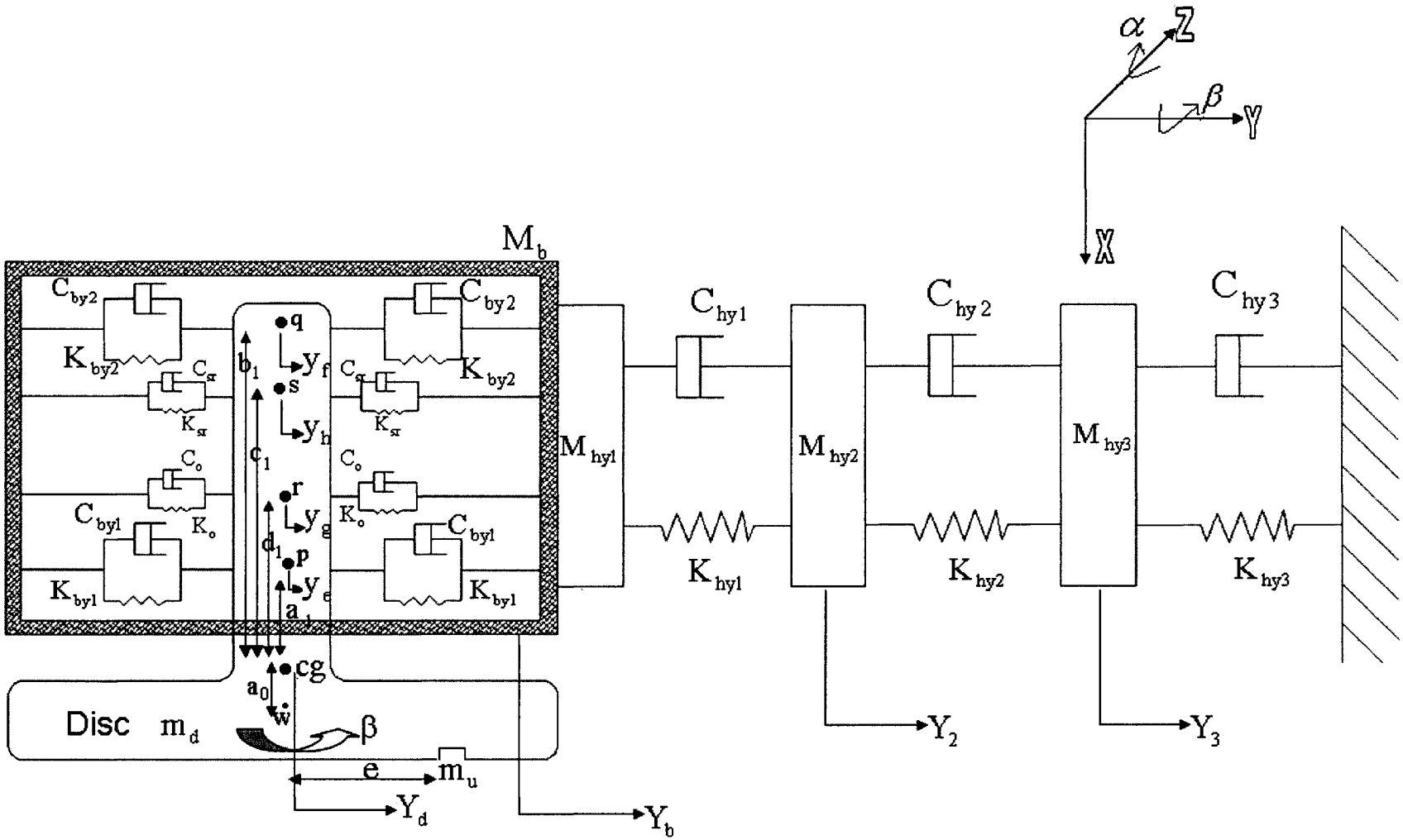

Figure 4.2: Analytical model representation of the coupled human hand and the grinder along the Y-axis

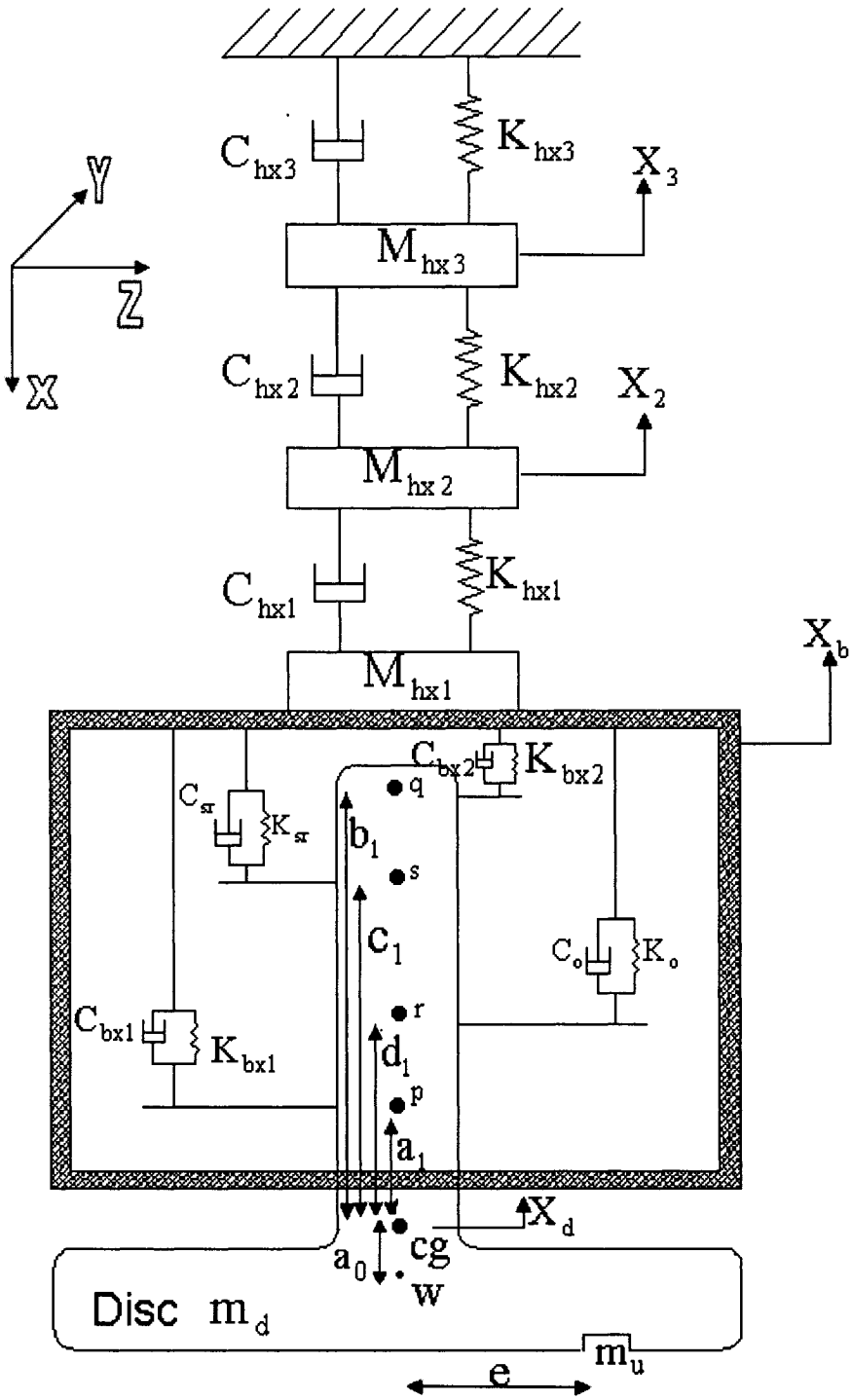

Figure 4.3: Analytical model representation of the coupled human hand and the grinder along the X-axis

represent the damping properties of the hand-arm model along the Z-, Y- and X-axes. he contributions due to the flexibility of the disc and the shaft are neglected in the model. The forces and motions caused by the gear drive and the pneumatic system are ignored. The bearings are assumed to possess constant properties, while the clearance effects are assumed to be negligible. The effect of cross coupling in Z-, Y- and X-axes is also neglected. The visco-elastic properties of the O-ring and the retainer spring are assumed to be equal along all the three axes (X-, Y- and Z-). The tool body together with the support and trigger handles, is considered as a rigid body with three degrees-of-freedom along the X-, Y- and Z-axes. The effect of grip force and push force at the hand -handle interface is also neglected. The grinding wheels exhibit mass unbalance due to non-uniform wear, uneven weight distribution, etc. Such unbalance yields poor quality of the work piece. The cutting forces are generated because of the interactions of the tool with the work piece and the variations in the cutting forces can cause the system to excite dynamically. Owing to extreme complexities associated with characterization of cutting forces, the role of rotating mass unbalance on the nature of the HTV alone is considered in this study. As it is evident from Chapter 2, that gyroscopic effect is insignificant on the hand-transmitted vibration, hence it is not considered in the coupled hand-tool analysis.

4.3 Equations of Motion

The equations of motion of the coupled hand-tool system are derived considering 14 degrees-of-freedom i.e., 5 degrees-of-freedom along the Z-axis, 5 degrees-of-freedom along the Y-axis and 4 degrees-of-freedom along the X-axis. These include the translational motion of the shaft-disc system (z_d, y_d, x_d), rotational motions of the shaft-

disc system (α about the Z-axis and β about the Y-axis), motion of the tool body $M_b(z_b, y_b, x_b)$, motions of the hand-arm masses $M_{h2}(z_2, y_{2,} x_2)$ and $M_{h3}(z_3, y_3, x_3)$. The equations of motion for the coupled-hand tool model along the radial (Z- and Y-) and axial (X) directions are derived under the presence of a rotating mass unbalance excitation along the radial direction. The axial motions of the shaft can be attributed mostly to the lumped effect of cross coupling, vibration of the gear and pneumatic drive. The effects of the cross coupling and the motions due to gear and pneumatic drives on the axial motion are considered by introducing an additional excitation component arising from disc unbalance. Due to the lack of appropriate data, it is assumed that 15% of the mass unbalance would account for the axial excitation component.

Equations of Motion along the Z-axis:

The centroidal motion of the shaft-disc assembly along the Z-axis can be related to the motion of the shaft in the vicinity of the bearing supports (z_e, z_h), O-ring (z_f), retainer spring (z_g) and to its rotation β about the Y-axis. Assuming rigid shaft and disc assembly, these motion coordinates can be related as described in section 2.4. Let m_u represents the mass unbalance of the grinding wheel with an eccentricity e, such that the total mass of the shaft-disc assembly is $M = m_d + m_u$. The equations of motion for the coupled hand-tool model along the Z-axis are written as:

$$M\ddot{z}_d + 2(K_{bz1} + K_{bz2} + K_0 + K_{sr})z_d + 2(C_{bz1} + C_{bz2} + C_0 + C_{sr})\dot{z}_d + 2(a_1K_{bz1} + b_1K_{bz2} + c_1K_0 + d_1K_{sr})\beta + 2(a_1C_{bz1} + b_1C_{bz2} + c_1C_0 + d_1C_{sr})\dot{\beta} - 2(K_{bz1} + K_{bz2} + K_0 + K_{sr})\dot{z}_b - 2(C_{bz1} + C_{bz2} + C_0 + C_{sr})\dot{z}_b = m_u e\omega^2 \sin(\omega t) \tag{4.1}$$

$$I_y\ddot{\beta} + 2(a_1K_{bz1} + b_1K_{bz2} + c_1K_0 + d_1K_{sr})z_d + 2(a_1C_{bz1} + b_1C_{bz2} + c_1C_0 + d_1C_{sr})\dot{z}_d + 2(a_1^2K_{bz1} + b_1^2K_{bz2} + c_1^2K_0 + d_1^2K_{sr})\beta + 2(a_1^2C_{bz1} + b_1^2C_{bz2} + c_1^2C_0 + d_1^2C_{sr})\dot{\beta} - 2(a_1K_{bz1} + b_1K_{bz2} + c_1K_0 + d_1K_{sr})z_b - 2(a_1C_{bz1} + b_1C_{bz2} + c_1C_0 + d_1C_{sr})\dot{z}_b = -a_0m_ue\omega^2\sin(\omega t)$$

(4.2)

$$M_b\ddot{z}_b - 2(K_{bz1} + K_{bz2} + K_0 + K_{sr})z_d - 2(C_{bz1} + C_{bz2} + C_0 + C_{sr})\dot{z}_d - 2(a_1K_{bz1} + b_1K_{bz2} + c_1K_0 + d_1K_{sr})\beta - 2(a_1K_{bz1} + b_1K_{bz2} + c_1K_0 + d_1K_{sr})\dot{\beta} + (2(K_{bz1} + K_{bz2} + K_0 + K_{sr}) + K_{hz1})z_b + (2(C_{bz1} + C_{bz2} + C_0 + C_{sr}) + C_{hz1})\dot{z}_b - (K_{hz1})z_2 - (C_{hz1})\dot{z}_2 = 0$$

(4.3)

$$M_{hz2}\ddot{z}_2 - (K_{hz1})z_b - (C_{hz1})\dot{z}_b + (K_{hz1} + K_{hz2})z_2 + (C_{hz1} + C_{hz2})\dot{z}_2 - (K_{hz2})z_3 - (C_{hz2})\dot{z}_3 = 0$$

(4.4)

$$M_{hz3}\ddot{z}_3 - (K_{hz2})z_2 - (C_{hz2})\dot{z}_2 + (K_{hz2} + K_{hz3})z_3 + (C_{hz2} + C_{hz3})\dot{z}_3 = 0$$

(4.5)

where M_{hz2}, M_{hz3} represent the hand-arm masses, while K_{hz1}, K_{hz2}, K_{hz3} and C_{hz1}, C_{hz2}, C_{hz3}, represent the stiffness and damping coefficients, of the hand-arm model along the Z-axis.

Equations of Motion along the Y-axis:

The centroidal motion of the shaft-disc assembly along the Y-axis in a similar manner can be related to the motion of the shaft in the vicinity of the bearing supports (y_e, y_h), O-ring (y_f), retainer spring (y_g) and to its rotation α about the Z-axis. The equations of motion for the coupled hand-tool model along the Y-axis are thus derived as:

$$M\ddot{y}_d + 2(K_{by1} + K_{by2} + K_0 + K_{sr})y_d + 2(C_{by1} + C_{by2} + C_0 + C_{sr})\dot{y}_d - 2(a_1K_{by1} + b_1K_{by2} + c_1K_0 + d_1K_{sr})\alpha - 2(a_1C_{by1} + b_1C_{by2} + c_1C_0 + d_1C_{sr})\dot{\alpha} - 2(K_{by1} + K_{by2} + K_0 + K_{sr})y_b - 2(C_{by1} + C_{by2} + C_0 + C_{sr})\dot{y}_b = m_u e\omega^2 \cos(\omega t) \quad (4.6)$$

$$I_z\ddot{\alpha} - 2(a_1K_{by1} + b_1K_{by2} + c_1K_0 + d_1K_{sr})y_d - 2(a_1C_{by1} + b_1C_{by2} + c_1C_0 + d_1C_{sr})\dot{y}_d + 2(a_1^2K_{by1} + b_1^2K_{by2} + c_1^2K_0 + d_1^2K_{sr})\alpha + 2(a_1^2C_{by1} + b_1^2C_{by2} + c_1^2C_0 + d_1^2C_{sr})\dot{\alpha} + 2(a_1K_{by1} + b_1K_{by2} + c_1K_0 + d_1K_{sr})y_b + 2(a_1C_{by1} + b_1C_{by2} + c_1C_0 + d_1C_{sr})\dot{y}_b = a_0m_u e\omega^2 \cos(\omega t) \quad (4.7)$$

$$M_b\ddot{y}_b - 2(K_{by1} + K_{by2} + K_0 + K_{sr})y_d - 2(C_{by1} + C_{by2} + C_0 + C_{sr})\dot{y}_d + 2(a_1K_{by1} + b_1K_{by2} + c_1K_0 + d_1K_{sr})\alpha + 2(a_1K_{by1} + b_1K_{by2} + c_1K_0 + d_1K_{sr})\dot{\alpha} + (2(K_{by1} + K_{by2} + K_0 + K_{sr}) + K_{hy1})y_b + (2(C_{by1} + C_{by2} + C_0 + C_{sr}) + C_{hy1})\dot{y}_b - (K_{hy1})y_2 - (C_{hy1})\dot{y}_2 = 0 \quad (4.8)$$

$$M_{hy2}\ddot{y}_2 - (K_{hy1})y_b - (C_{hy1})\dot{y}_b + (K_{hy1} + K_{hy2})y_2 + (C_{hy1} + C_{hy2})\dot{y}_2 - (K_{hy2})y_3 - (C_{hy2})\dot{y}_3 = 0 \quad (4.9)$$

$$M_{hy3}\ddot{y}_3 - (K_{hy2})y_2 - (C_{hy2})\dot{y}_2 + (K_{hy2} + K_{hy3})y_3 + (C_{hy2} + C_{hy3})\dot{y}_3 = 0 \quad (4.10)$$

where M_{hy2}, M_{hy3} represent the hand-arm masses, while K_{hy1}, K_{hy2}, K_{hy3} and C_{hy1}, C_{hy2}, C_{hy3}, represent the stiffness and damping coefficients, of the hand-arm model along the Y-axis.

Equations of Motion along the X-axis:

The cross coupling effect and the effect of vibration of the gear and the pneumatic drive is represented as a function of mass unbalance as described earlier. An equivalent

excitation of $(0.15m_u e\omega^2)$ is considered along the X-axis. The equations of motion of the coupled hand-tool model along the X-axis are written as:

$$M\ddot{x}_d + (K_{bx1} + K_{bx2} + K_0 + K_{sr})x_d + (C_{bx1} + C_{bx2} + C_0 + C_{sr})\dot{x}_d - (K_{bx1} + K_{bx2} + K_0 + K_{sr})x_b - (C_{bx1} + C_{bx2} + C_0 + C_{sr})\dot{x}_b = (0.15m_u e\omega^2)\sin(\omega t) \tag{4.11}$$

$$M_b\ddot{x}_b - (K_{bx1} + K_{bx2} + K_0 + K_{sr})x_d - (C_{bx1} + C_{bx2} + C_0 + C_{sr})\dot{x}_d + (K_{bx1} + K_{bx2} + K_0 + K_{sr} + K_{hx1})x_b + (C_{bx1} + C_{bx2} + C_0 + C_{sr} + C_{hx1})\dot{x}_b - (K_{hx1})x_2 - (C_{hx1})\dot{x}_2 = 0 \tag{4.12}$$

$$M_{hx2}\ddot{x}_2 - (K_{hx1})x_b - (C_{hx1})\dot{x}_b + (K_{hx1} + K_{hx2})x_2 + (C_{hx1} + C_{hx2})\dot{x}_2 - (K_{hx2})x_3 - (C_{hx2})\dot{x}_3 = 0 \tag{4.13}$$

$$M_{hx3}\ddot{x}_3 - (K_{hx2})x_2 - (C_{hx2})\dot{x}_2 + (K_{hx2} + K_{hx3})x_3 + (C_{hx2} + C_{hx3})\dot{x}_3 = 0 \tag{4.14}$$

where M_{hx2}, M_{hx3} represent the hand-arm masses, while K_{hx1}, K_{hx2}, K_{hx3} and C_{hx1}, C_{hx2}, C_{hx3}, represent the stiffness and damping coefficients, of the hand-arm model along the X-axis.

4.4 Eigenvalue Analysis

Eigenvalue problem is formulated and solved to identify the natural frequencies and damping ratios of the coupled hand-tool model along all the three axes. The parameters of the grinder model, described in Chapter 2, and those of the hand-arm model, identified in Chapter 3, are used for the analysis. In order to obtain the eigenvalues and eigenvectors of the system, the homogenous form of equations (4.1-4.14) are solved using MATLAB software and the results are summarized in Tables 4.1-4.3.

Table 4.1 Natural Frequencies of the coupled hand-tool model along the Z-axis

	Natural Frequency ω_n (Hz)	Damped Frequency ω_d (Hz)	Damping Ratio ξ	Dominant deflection modes (From eigenvectors)
1	1.921	1.55	0.5907	z_b
2	11.614	-	1.7778	z_3
3	39.495	34.1	0.5046	z_2
4	56.559	56.19	0.1140	β, z_d
5	185.695	184.4305	0.1165	z_d, β

Table 4.2 Natural Frequencies of the coupled hand-tool model along the Y-axis

	Natural Frequency ω_n (Hz)	Damped Frequency ω_d (Hz)	Damping Ratio ξ	Dominant deflection modes (From eigenvectors)
1	2.041	1.89	0.3785	y_b
2	8.298	-	1.1567	y_3
3	43.865	34.85	0.6073	y_2
4	56.429	56.20	0.0901	α, y_d
5	185.662	184.44	0.1145	y_d, α

Table 4.3 Natural Frequencies of the coupled hand-tool model along the X-axis

	Natural Frequency ω_n (Hz)	Damped Frequency ω_d (Hz)	Damping Ratio ξ	Dominant deflection modes (From eigenvectors)
1	1.332	1.22	0.4015	x_b
2	8.636	-	1.0764	x_3
3	132.293	109.07	0.5659	x_2
4	180.086	178.92	0.1136	x_d

The eigenvector associated with a particular eigenvalue represents the relative amplitudes of oscillations of the model masses at that natural frequency. The numerical values of the eigenvectors of the coupled hand-tool model along all the three axes are represented in Appendix B. The natural frequencies together with the damping ratios and the corresponding dominant deflection modes of the coupled-hand tool model, along the Z-axis are summarized in Table 4.1. The two highest natural frequencies 185.695 Hz and 56.559 Hz, correspond with the tool motions (z_d, β), while the corresponding damping ratios are relatively small, 0.1165 and 0.1140. The two natural frequencies 39.495 Hz and 11.614 Hz, relate to dominant hand-arm motions (z_2 and z_3), while the damping ratios associated with these modes are relatively high, 0.5046 and 1.7778. The lowest natural frequency, 1.921 Hz represents the case when the tool-body translational motion (z_b) is dominant.

Similarly, the natural frequencies together with the damping ratios and the corresponding dominant deflection modes of the coupled-hand tool model, along the Y-axis are summarized in Table 4.2. The two highest natural frequencies 185.662 Hz and 56.429 Hz, correspond with the tool motions (y_d, α) with relatively low damping ratios, as observed for the Z-axis. The remaining two natural frequencies 43.865 Hz and 8.298 Hz , correspond with the deflections of the hand-arm system (y_2 and y_3), with relatively high damping ratios due to the biological system. The lowest natural frequency, 2.041 Hz represents the case when the tool-body translational motion (y_b) is dominant. The natural frequencies together with the damping ratios and the corresponding dominant deflection modes of the coupled-hand tool model, along the X-axis (Table 4.3) suggest the tool

mode near the highest natural frequency of 180.086 Hz, (x_d). The remaining natural frequencies of 132.293 Hz, 8.636 Hz and 1.33 Hz correspond with the hand-arm motions (x_2 and x_3), and the tool body motion (x_b) of the coupled system.

4.5 Simulation Results and Discussion

The mathematical formulations described in section 4.3 yield coupled second order differential equations of motion for the coupled hand-grinder model. These equations for the 14-DOF system model are solved using the ode45 function available within the MATLAB software package, under varying levels of mass unbalance excitations. Simulations are performed for different angular speeds up to the recommend maximum speed of 12000 rpm. Four different values of mass unbalance 76, 295, 402 and 510 gm-mm are considered for the analyses. The assessment method outlined in ISO 5349 [42] suggests the use of rms accelerations due to vibration transmitted in the vicinity of the hand. The time-histories of the responses of the tool body and the hand masses are thus analyzed to determine the rms accelerations.

$$\ddot{q}_{rms} = \sqrt{\frac{1}{T}\int_0^T \ddot{q}^2(t)\,dt}$$

where $\ddot{q}(t)$ is the instantaneous acceleration, $\ddot{q}_{rms}$ is the rms acceleration and T is the period of exposure.

It must be noted that, the hand mass M_{h1} is rigidly attached to the machine tool body M_b, as shown in Figure 4.1. The rms acceleration response of the machine tool body M_b would thus represent vibration exposure of the human hand-arm and the response of

the hand mass M_{h1}. The rms acceleration responses of the tool body M_b, along all the three axes (Z-,Y- and X-), are obtained for different values of mass unbalance and as a function of the rotational speed, as shown in Figures 4.4-4.6, respectively. The results clearly show that as the amount of mass unbalance increases, the rms acceleration response of the machine tool body increases in the entire speed range, irrespective of the axes of motion. The results further show that the responses along the Y- and Z- axes differ, particularly near 3300 rpm, even though the grinder model and its parameters are considered to be identical along the two-axes. These deviations are mostly caused by the differences in the hand-arm model and the coupling effects. The rms acceleration responses of the tool body along the Z- and Y-axes, shown in Figures 4.4 and 4.5, show two significant peaks occurring around 3370 rpm and 11065 rpm, which correspond to tool natural frequencies of the coupled hand-tool model, near 56.2 and 184.43 Hz. The responses corresponding to remaining modes are not evident due to relatively high damping ratios for the modes associated with the hand-arm system. These responses can be observed, when the results are presented in log-log scale, as shown in Figure 4.4a. Moreover, the natural modes of the hand-arm systems generally occur at lower frequencies, where the magnitudes of unbalance excitations are lower. The tool body response or the rms accelerations due to vibration occurring at the hand-tool interface along the X-axis, shown in Figure 4.6, also increases with increase in the mass unbalance in the entire range of operating speed. The peak in the rms acceleration response occurs around 10735 rpm, which corresponds with the primary natural frequency of 178.92 Hz associated with the tool.

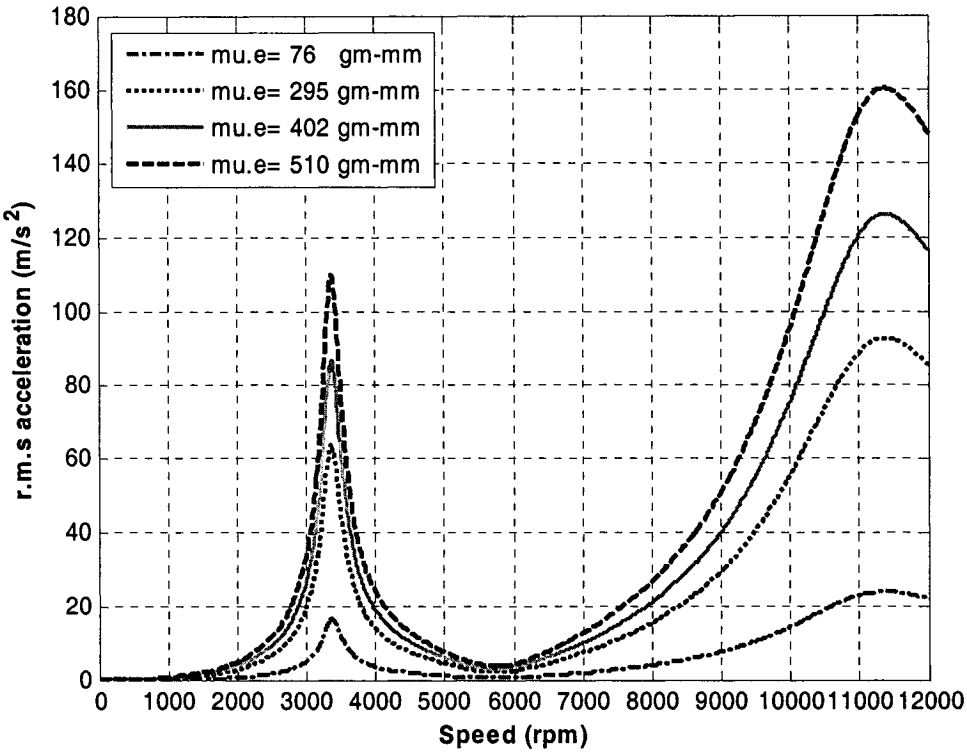

Figure 4.4: Influence of mass unbalance on the rms acceleration response of the tool body mass along the Z-axis

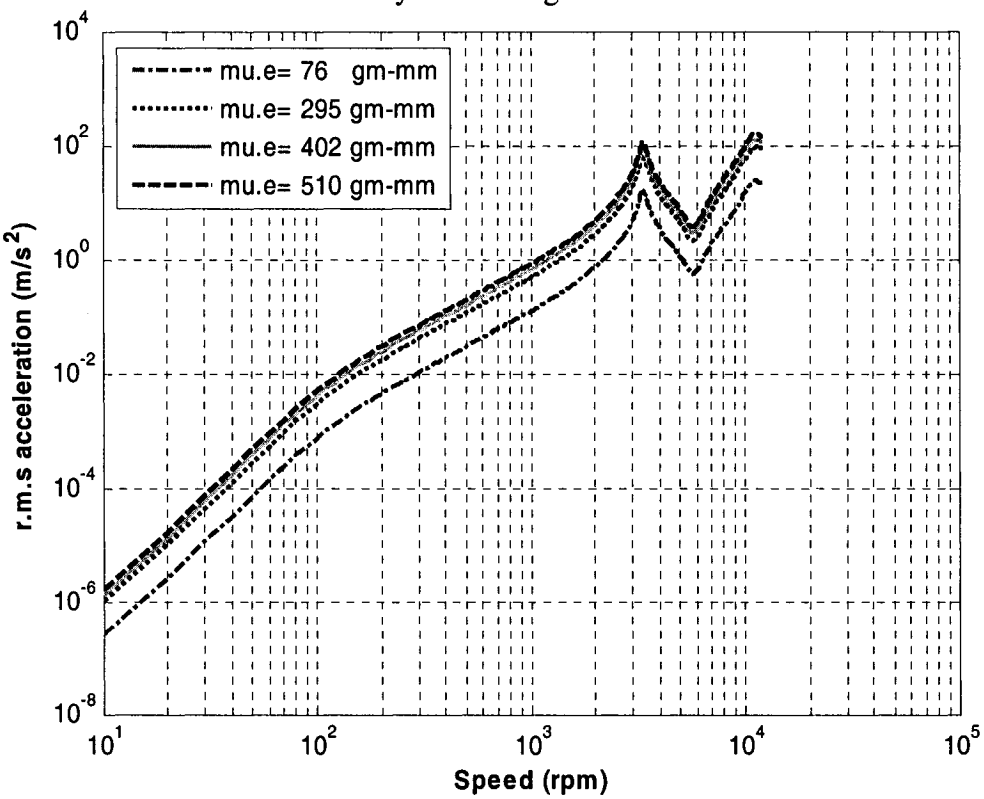

Figure 4.4a: Representation of the influence of mass unbalance on the rms acceleration response of the tool body mass along the Z-axis in log-log scale

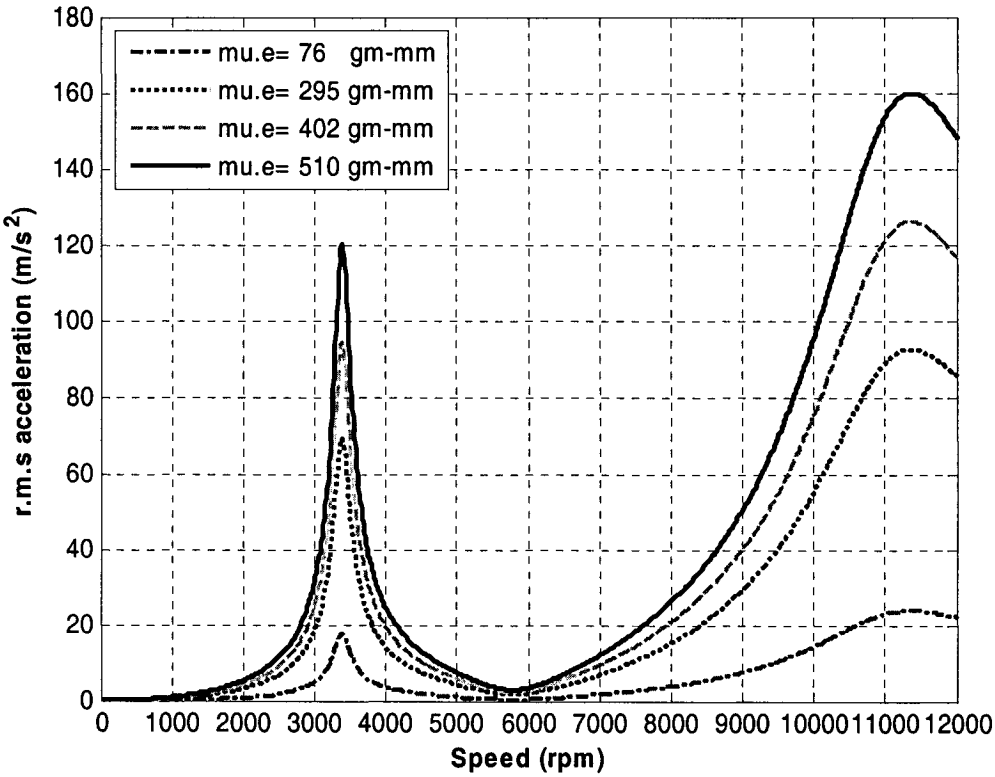

Figure 4.5: Influence of mass unbalance on the rms acceleration response of the tool body mass along the Y-axis

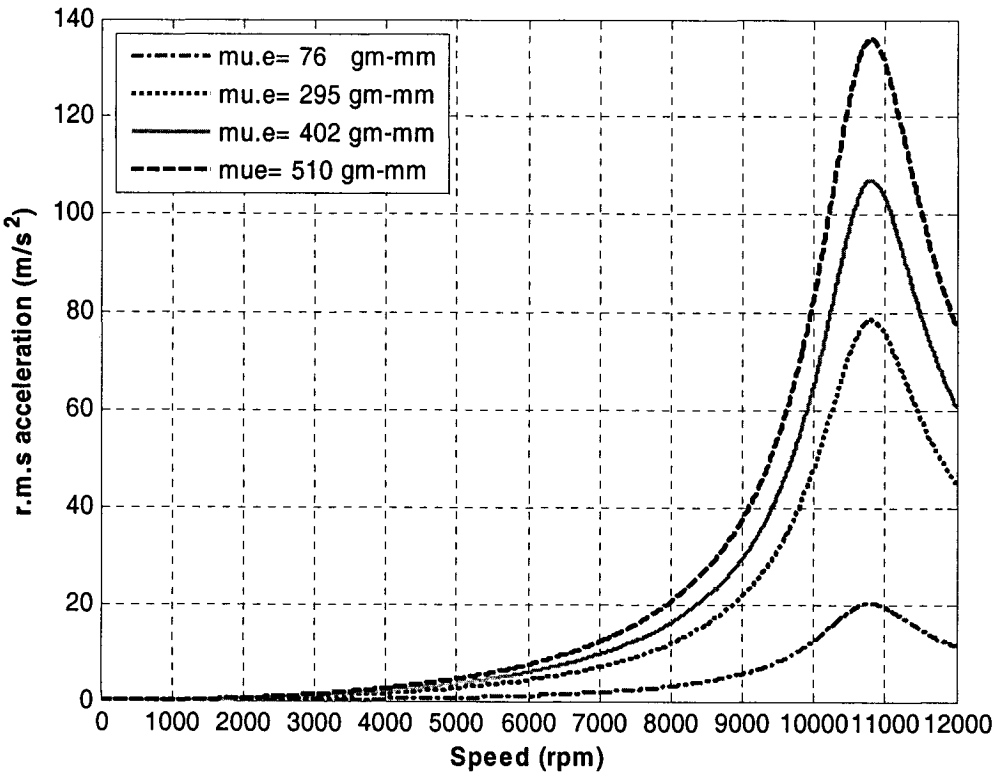

Figure 4.6: Influence of mass unbalance on the rms acceleration response of the tool body mass along the X-axis

The responses are also obtained for the hand masses M_{h2} and M_{h3}, as a function of the rotational speed and for different values of the mass unbalance along all the three axes (Z-,Y- and X-), as shown in Figures 4.7-4.12. The response characteristics of all the hand-arm model masses increase with increase in the mass unbalance, irrespective of the axis of vibration considered, as observed with the tool body responses. The human hand and arm, however, yields considerable attenuation of the tool body vibrations transmitted to different masses of the hand-arm model. The rms acceleration responses of the hand mass M_{h2} along the Z- and Y-axes (Figures 4.7 and 4.8) are considerably lower than those of the tool body mass response. The hand-arm system yields most significant attenuation of high-frequency vibration, as it is evident from peak responses near 11000 rpm. The degree of attenuation of vibration along the X-axis, however, is considerably smaller, as evident in Figure 4.9. This is attributed to relatively higher natural frequency of the hand-arm system along the X-axis (132 Hz) and high damping ratio. The magnitudes of vibration transmitted to the hand mass M_{h3} closer to the support are most significantly attenuated along all the three axes and in the entire speed range, as shown in Figures 4.10-4.12. This is attributed to considerably lower natural frequency associated with deflections of this mass (11.6 Hz along the Z-axis, 8.3 Hz along the Y-axis and 8.6 Hz along the X-axis).

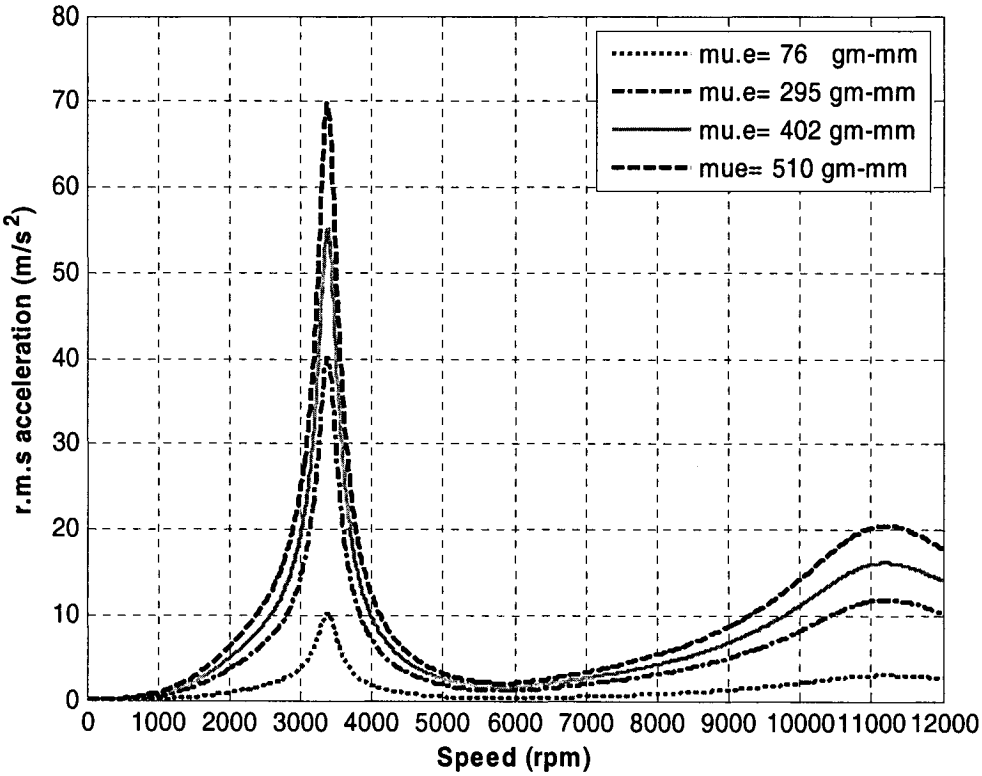

Figure 4.7: Influence of mass unbalance on the rms acceleration response of the hand mass M_{hz2} along the Z-axis

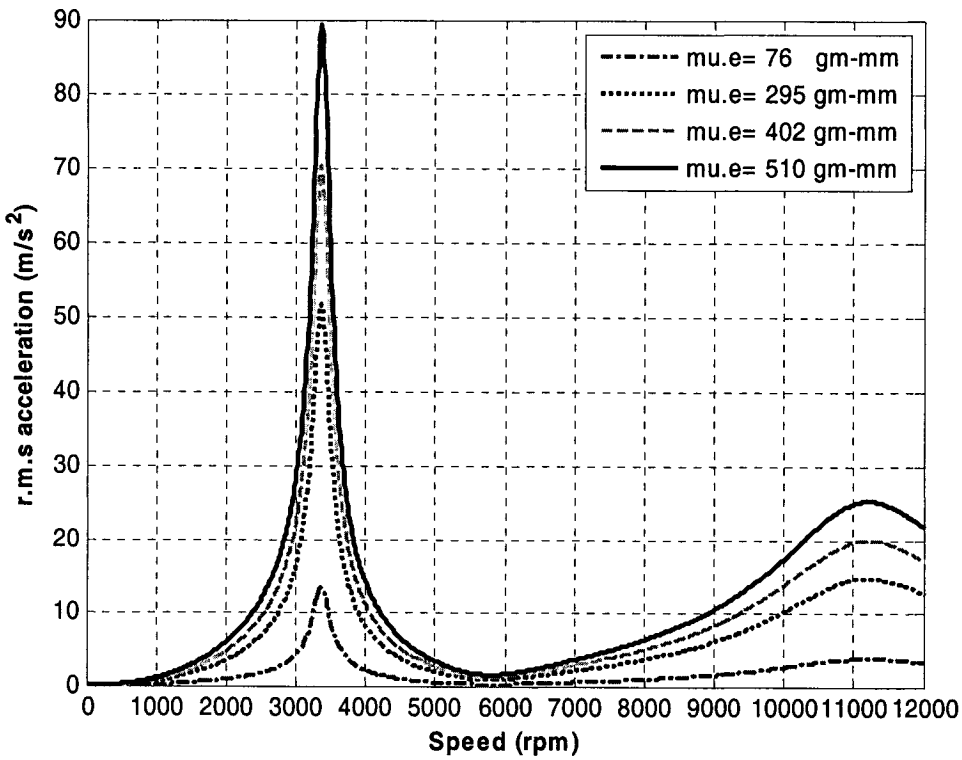

Figure 4.8: Influence of mass unbalance on the rms acceleration response of the hand mass M_{hy2} along the Y-axis

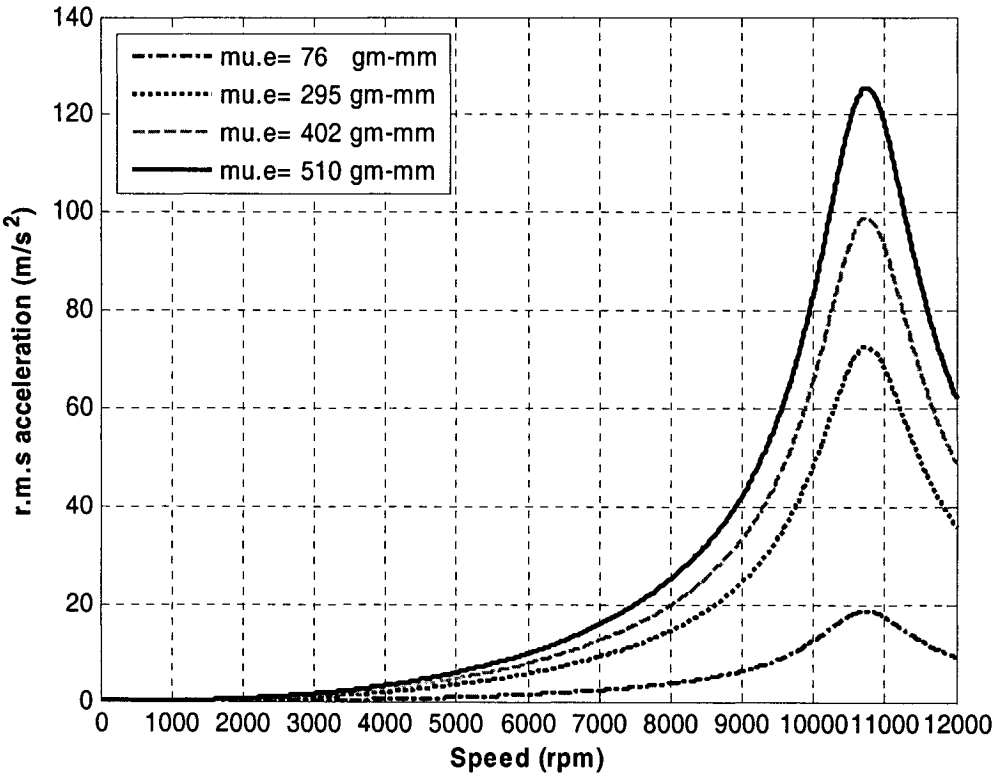

Figure 4.9: Influence of mass unbalance on the rms acceleration response of the hand mass M_{hx2} along the X-axis

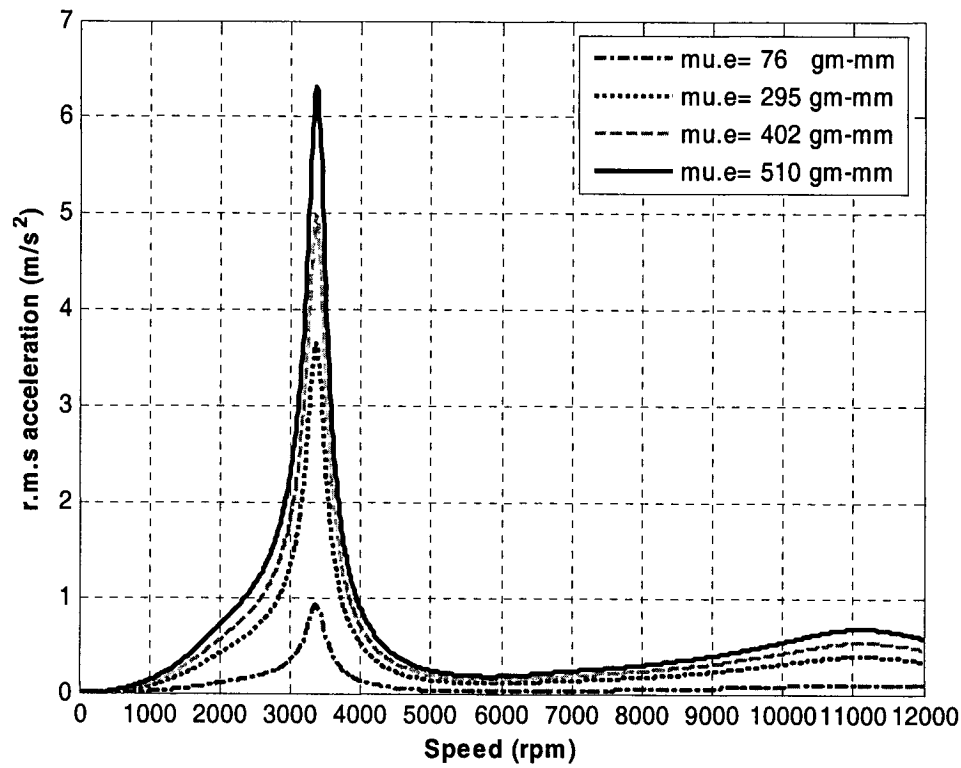

Figure 4.10: Influence of mass unbalance on the rms acceleration response of the hand mass M_{hz3} along the Z-axis

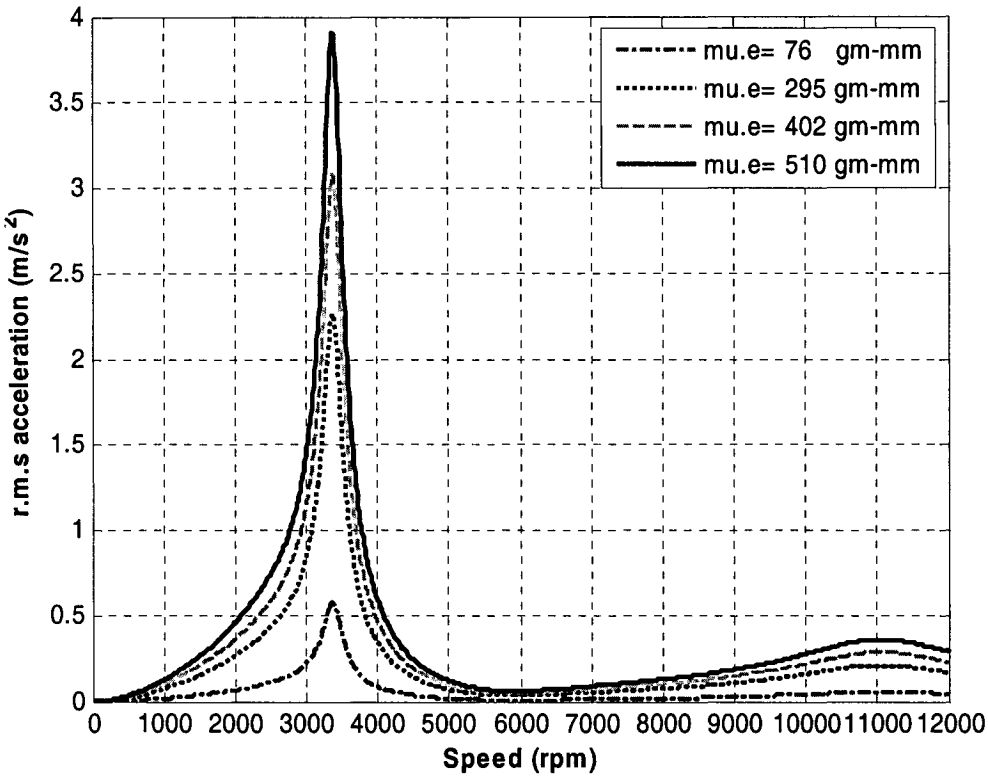

Figure 4.11: Influence of mass unbalance on the rms acceleration response of the hand mass M_{hy3} along the Y-axis

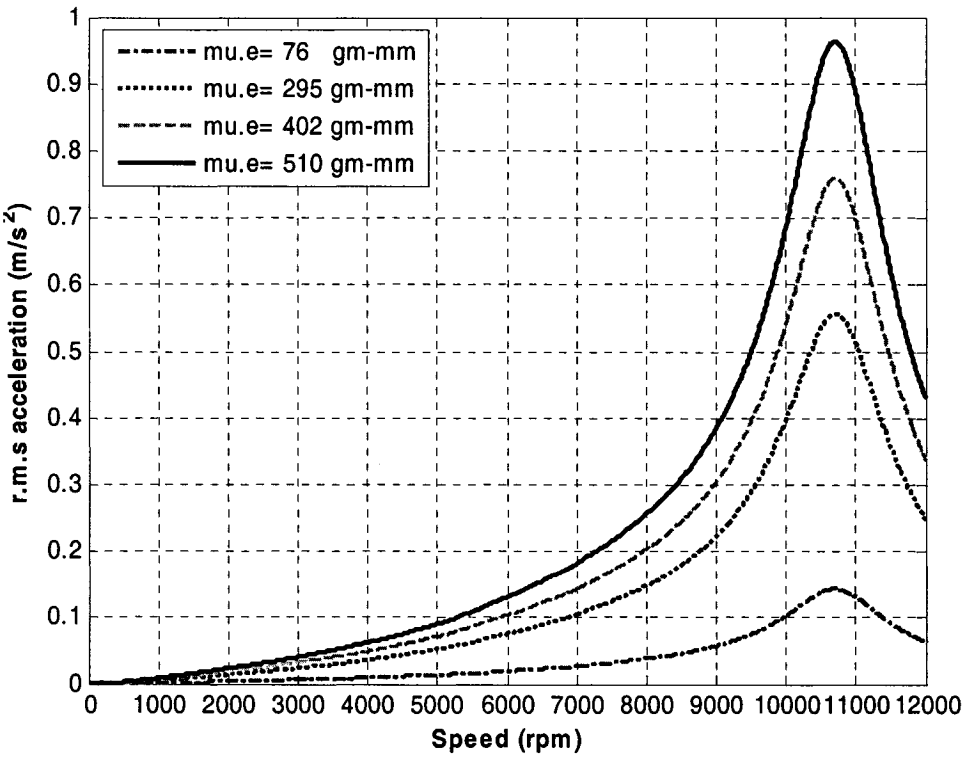

Figure 4.12: Influence of mass unbalance on the rms acceleration response of the hand mass M_{hx3} along the X-axis

Figures 4.13 to 4.15 further show comparisons of rms acceleration responses of the tool body mass M_b, and the the hand masses M_{h2} and M_{h3}, along the Z-, Y- and X-axes, respectively, under excitations arising from a mass unbalance of 76 gm-mm. The figures show the responses as a function of rotational speed upto a maximum of 12000 rpm. The results clearly show that the magnitudes of vibrations transmitted to the hand-arm structure are considerably smaller than those of the tool body mass. The attenuation is far more pronounced for the M_{h3} located close to the shoulder. This conforms with the observations reported in many studies that the vibration become confined to the hand alone at frequencies above 150 Hz [56, 57, 92]. The vibration response of the M_{h2} along the X-axis, however, tends to be higher at higher rpm as shown in Figure 4.15. This is because of the larger coupling stiffness value present between M_{h2} and M_b along this axis.

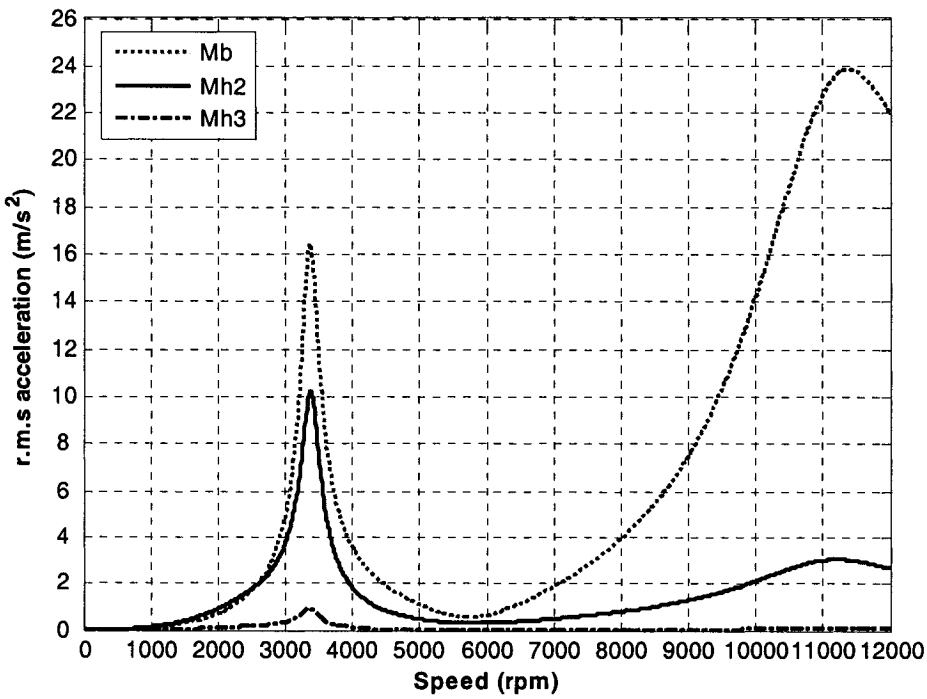

Figure 4.13: rms acceleration response of the coupled hand-tool model along the Z-axis for mass unbalance of 76gm-mm

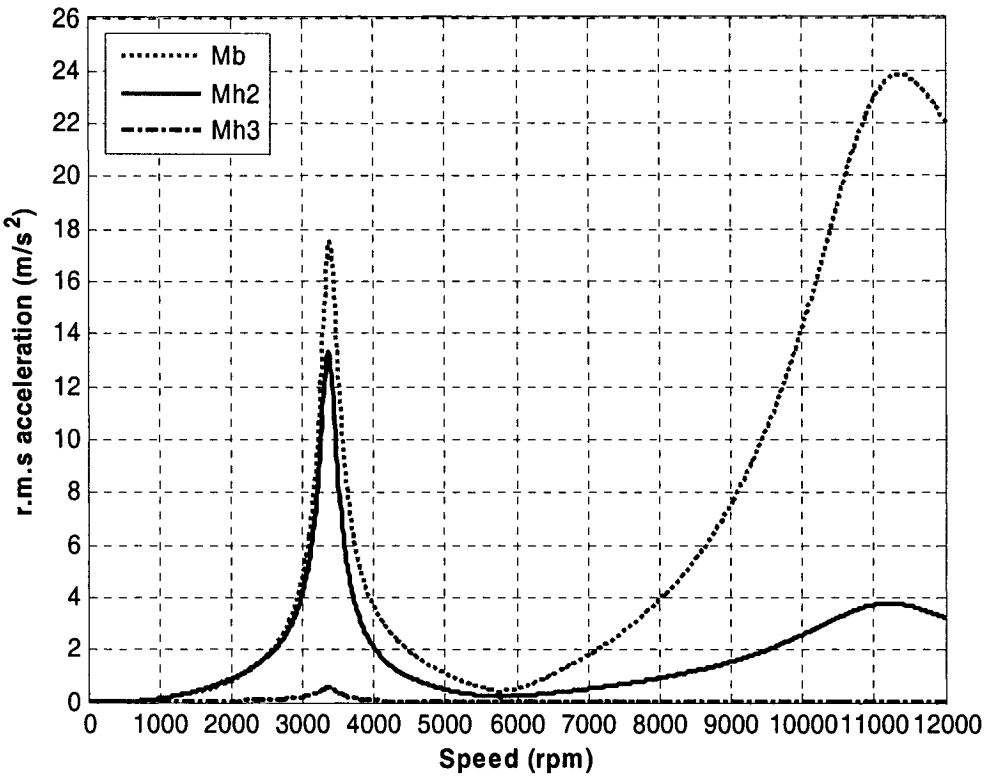

Figure 4.14: rms acceleration response of the coupled hand-tool model along the Y-axis for mass unbalance of 76 gm-mm

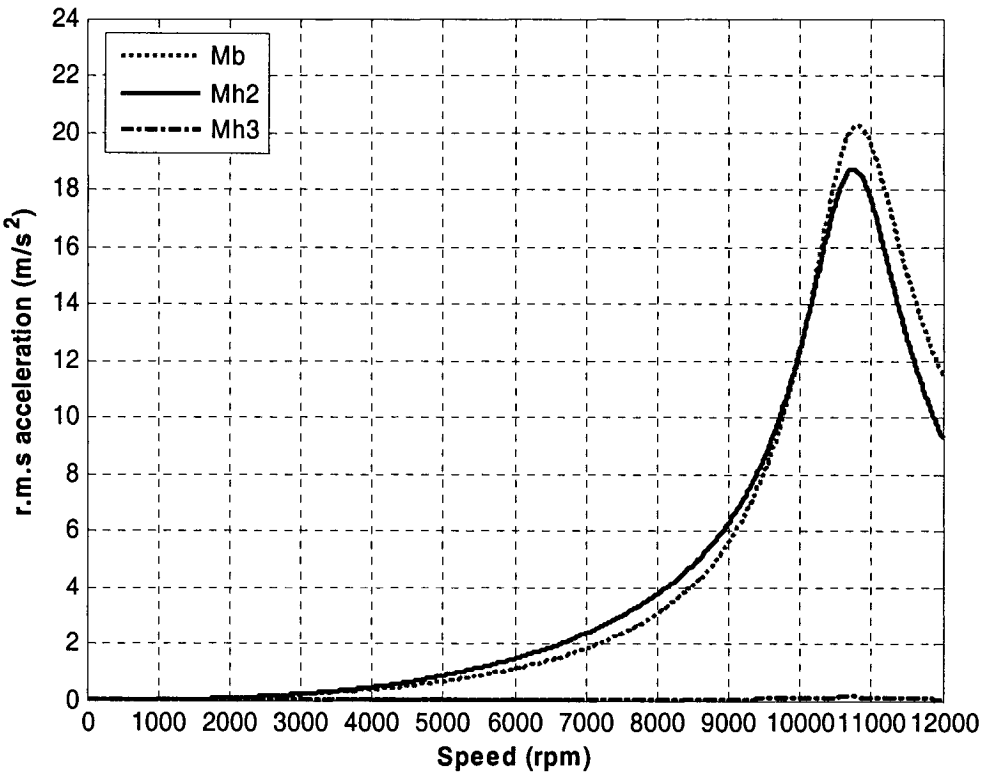

Figure 4.15: rms acceleration response of the coupled hand-tool model along the X-axis for mass unbalance of 76 gm-mm

4.6 Comparisons of the Coupled Hand-Tool Model Responses with the Measured Data

The computed response characteristics of the hand-tool model are compared to the experimental results presented in [93], to demonstrate the validity of the proposed coupled hand-tool model. The experiments were conducted by considering different amounts of mass unbalance and the rms acceleration response of the machine tool body was measured along all the three axes (X-, Y- and Z-). The reported results were obtained in the absence of autobalancer, while the effect of feed force was judged to be insignificant, since it was uncompensated in the experiment. Figure 4.16 presents the mean acceleration values of the machine tool body measured along the X-, Y- and Z-axes, as a function of the mass unbalance. The magnitudes of mass unbalance are indicated as 'U1', 'U2', 'U3', 'U4', respectively, representing mass unbalances of 76 gm-mm, 295 gm-mm, 402 gm-mm and 510 gm-mm. As shown in Figure 4.16, these results show that, as the mass unbalance increases, the rms acceleration responses of the tool body generally increase, irrespective of the axis of vibration. The responses along all the three directions exhibit peaks around the frequency band of 170 Hz, which corresponds to the operating speed of the grinder used in the experimental study. The rms acceleration response of the machine tool body, however, is lower along the Y-axis, when compared to those along the Z- and X-axis. This phenomena is observed for all the values of mass unbalance considered in the study. The rms acceleration responses of the tool body along the Z- and X-axis around the frequency band of 170 Hz vary from approximately 20 m/s^2 to100m/s^2 for different values of mass unbalance (76 gm-mm, 295 gm-mm, 402 gm-mm and 510 gm-mm). Along the Y-axis, the rms acceleration

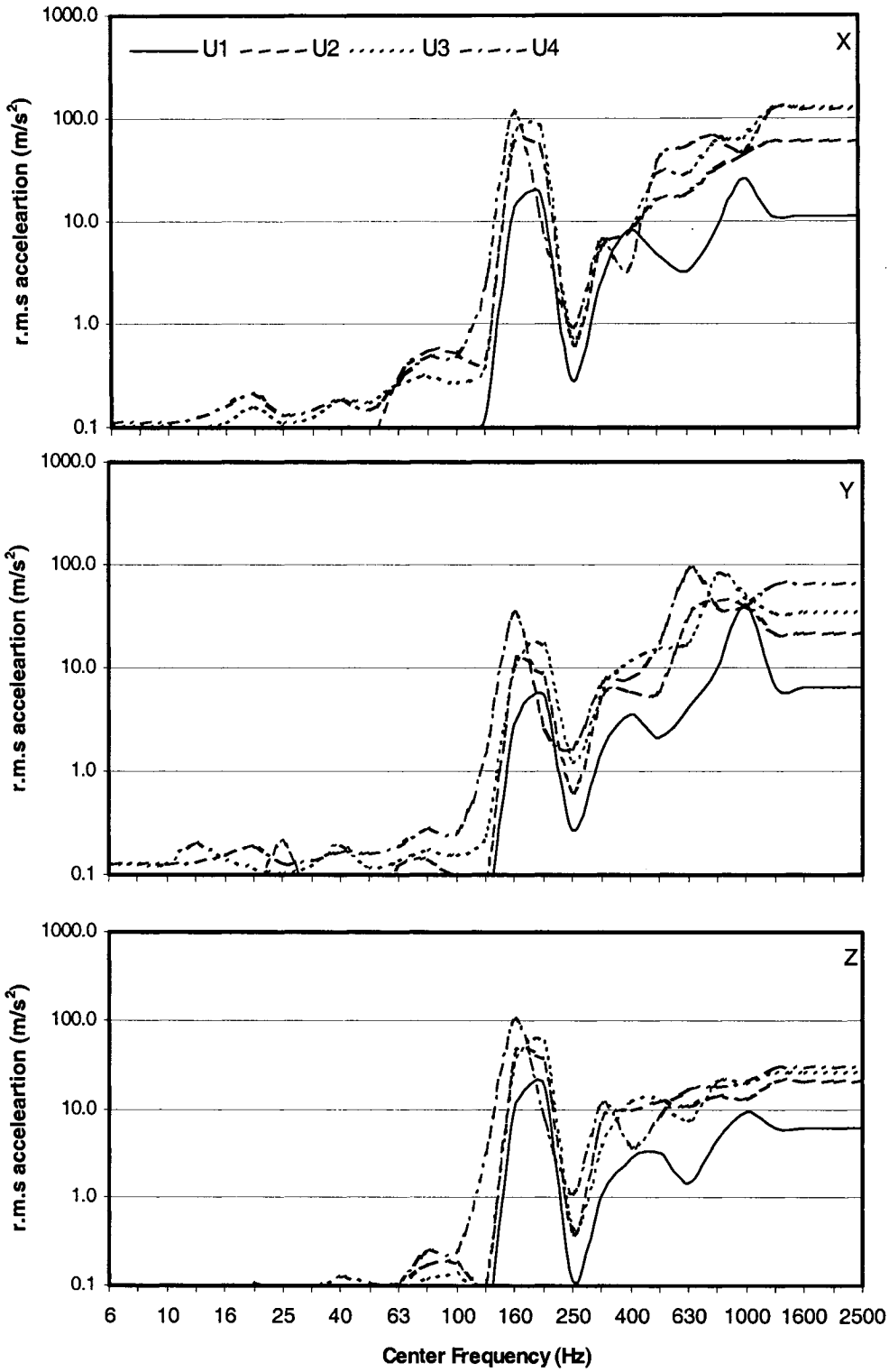

Figure 4.16: mean rms acceleration response as a function of the mass unbalance (U1=76 gm-mm,U2=295 gm-mm,U3=402 gm-mm,U4=510 gm-mm) [93]

values vary from $5\,m/s^2$ to $40\,m/s^2$ with increase in the mass unbalance. Response peaks however show variations in the corresponding frequency, although clustered around 170 Hz. Variations in the frequency corresponding to the peak response is attributed to changes in the operating speed caused by varying supply pressure.

The rms accelerations of the machine tool body at a frequency of 170 Hz are further computed, which corresponds to the approximate speed at which experiments were conducted. The computed values are compared with the measured data, corresponding to 170 Hz, as shown in Figure 4.17 to 4.19. The comparisons show for the Z-axis (Figure 4.17) show reasonably good correlation with the measured data for the entire range of mass unbalance considered. The peak deviation between the measured and computed values is in the order of 12.5%, which occurs under the mass unbalance of 402 gm-mm. The model response along the Y-axis, however, is significantly higher than the measured data, as illustrated in Figure 4.18. The computed values are approximately twice the measured values for the entire range of mass unbalance considered. The model response along the X-axis on the other hand, tends to be lower than the measured data, as illustrated in Figure 4.19. The peak deviation is in the order of 27.5%, which occurs at the mass unbalance of 295 gm-mm. The deviations between the model and measured responses could be attributed to many factors. These include the lack of consideration nonlinear properties, bearing clearances, flexibility of the grinding disc and the spindle, coupling effects and the interactions of the pneumatic and gear drives. Moreover, the orientations of the hand-arm model used in the coupled system formulation does not truly represent the operating conditions of the grinder. As it is evident from the grinder design presented in Chapter 2, the two handles are placed 90^o apart. The operator generally

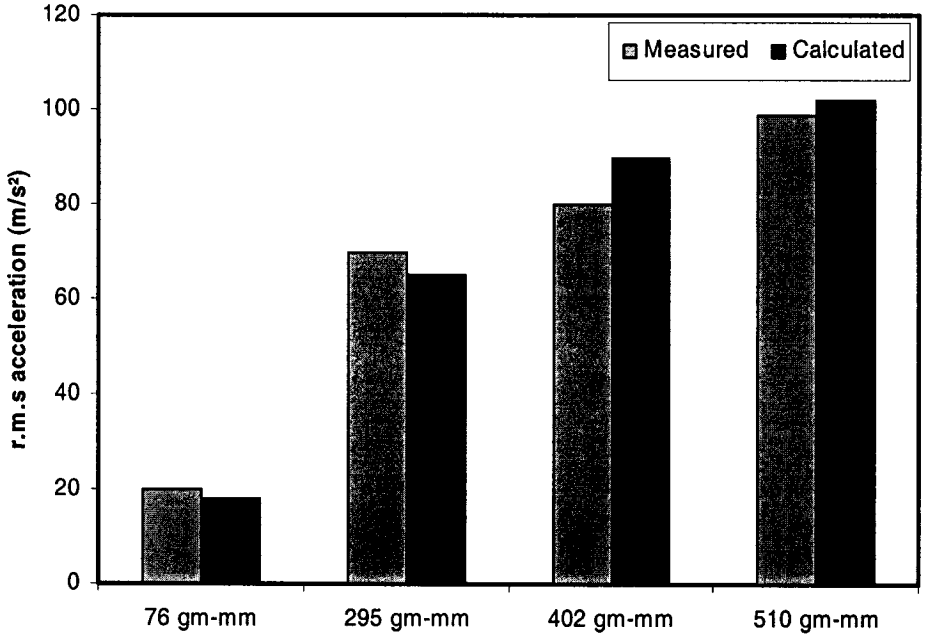

Figure 4.17: Comparisons of measured and calculated rms acceleration values for the tool body mass M_b for different mass unbalance (Z-axis)

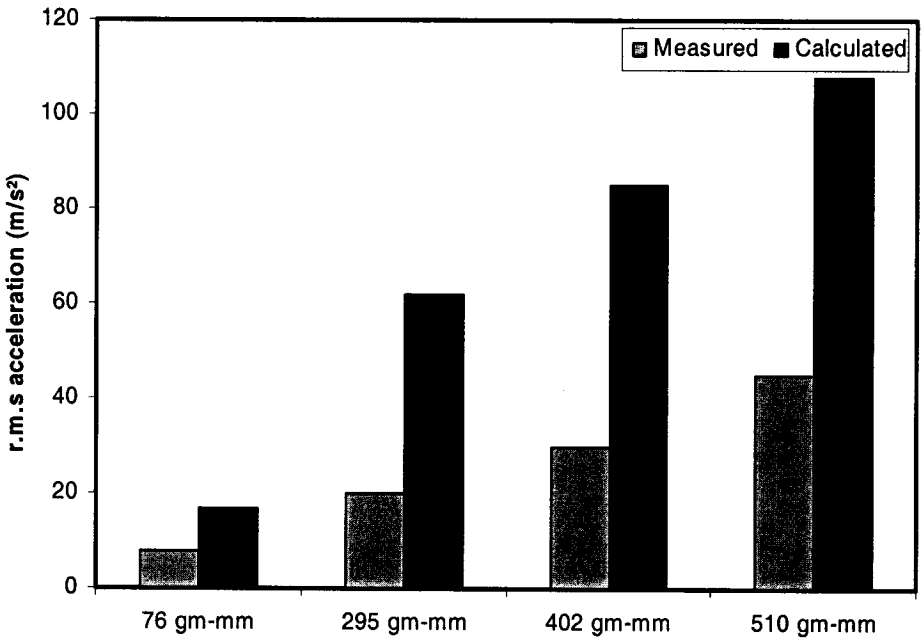

Figure 4.18: Comparisons of measured and calculated rms acceleration values For the tool body mass M_b for different mass unbalance (Y-axis)

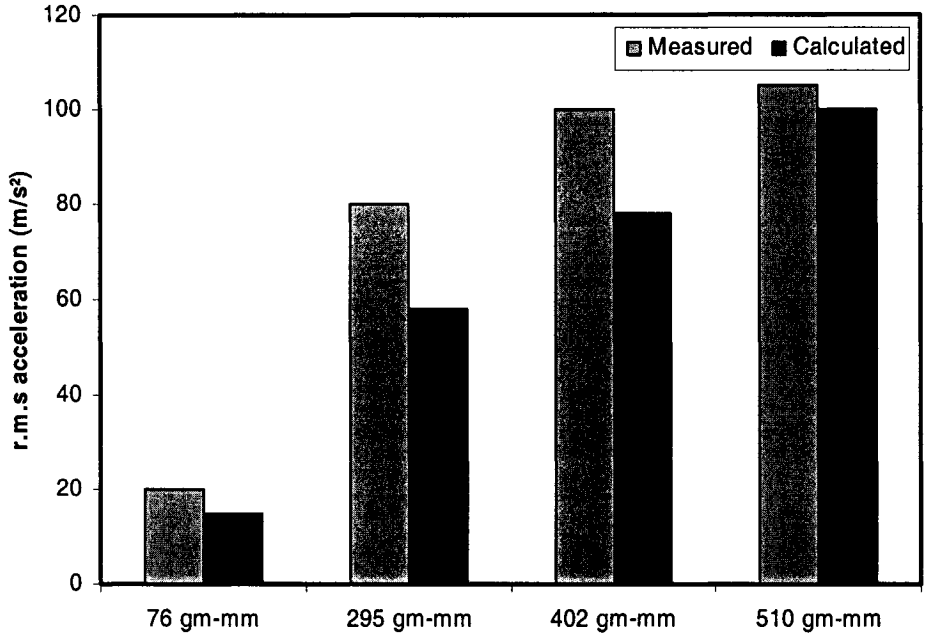

Figure 4.19: Comparisons of measured and calculated rms acceleration values for the tool body mass M_b for different mass unbalance (X-axis).

guides the tool by orienting one arm along the Z-axis, and other closer to the Y-axis. Additional efforts are thus needed to characterize the driving-point mechanical impedances of the two hand-arms exposed to Z- and Y-axes vibration, respectively.

4.7 Effects of Variation in Machine Casing Weight

The vibrations caused by the operations of a hand-held grinder depends upon many design and operating factors. The operating parameters may include the cutting forces, operating speed, grip and feed forces and state of the tool. Apart from these, the design factors related to mass of the tool, spindle, bearing properties, drive, O-ring, etc., would also affect the vibration responses of the tool. In this study, the role of tool body mass, damping due to bearing, and an elastic hand-handle interface (such as glove material) in

the vibration transmission performance is investigated. The weight of a hand-held tool is a typical external load to which the operator is subjected. The risk of a tool causing work-related musculoskeletal disorders varies according to the amplitude of the load as well as the duration of the task performed. There are no simple recommendations specifying tool weight limits for all situations. As an external load, the weight should be limited according to the working conditions, and the frequency, speed and duration of the operation to be performed [22]. The influence of inertial properties of the tool body on the magnitudes of hand transmitted vibration is investigated by varying the machine casing weight. Further, no attempt has been made in varying the inertial properties of the shaft-disc assembly, such as, mass moments of inertia I_x, I_y and I_z. The machine casing weight M_b is varied in steps of 0.5 kg. The acceleration responses of the tool body along the Z-, Y-, and X-axes are derived for mass unbalance of 76 gm-mm and different values of rotational speed, are expressed in terms of the rms accelerations in Figures 4.20-4.22, respectively. The results show that the peak acceleration responses along all the three axes can be reduced by increasing the tool body mass. The reduction is more pronounced at the higher resonant frequency, where the tool is mostly expected to operate. While this trend is observed along all the three axes (Z-, Y- and X-), a heavier tool would be undesirable.

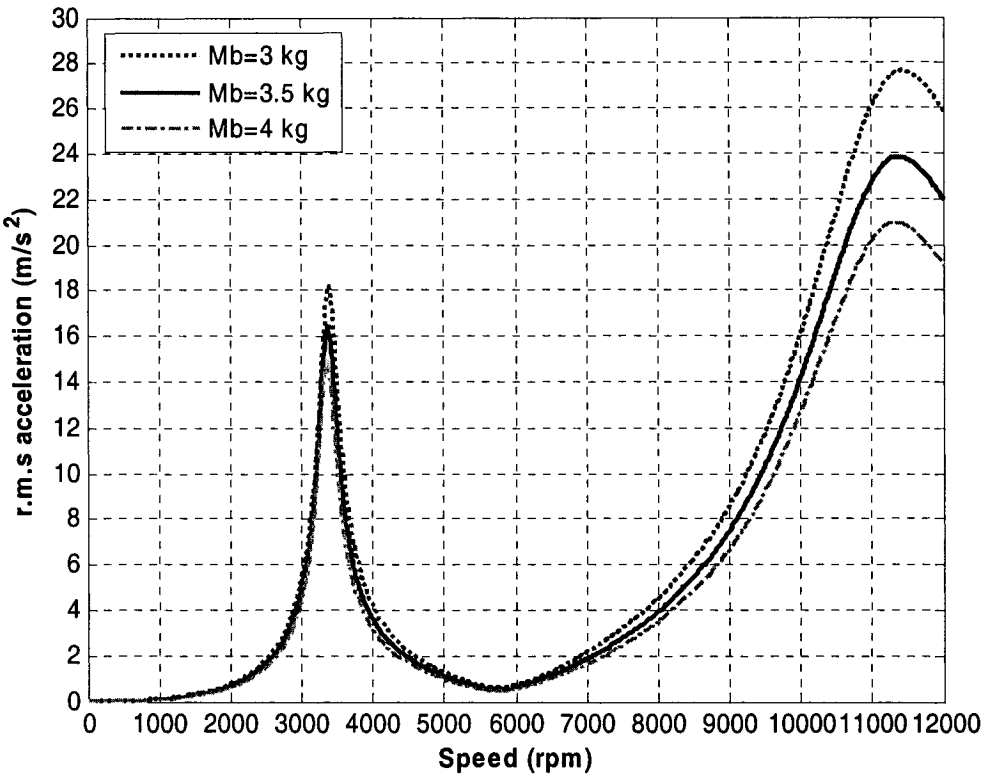

Figure 4.20: Influence of the machine casing weight on the rms acceleration response of the tool body mass along the Z-axis for mass unbalance of 76gm-mm

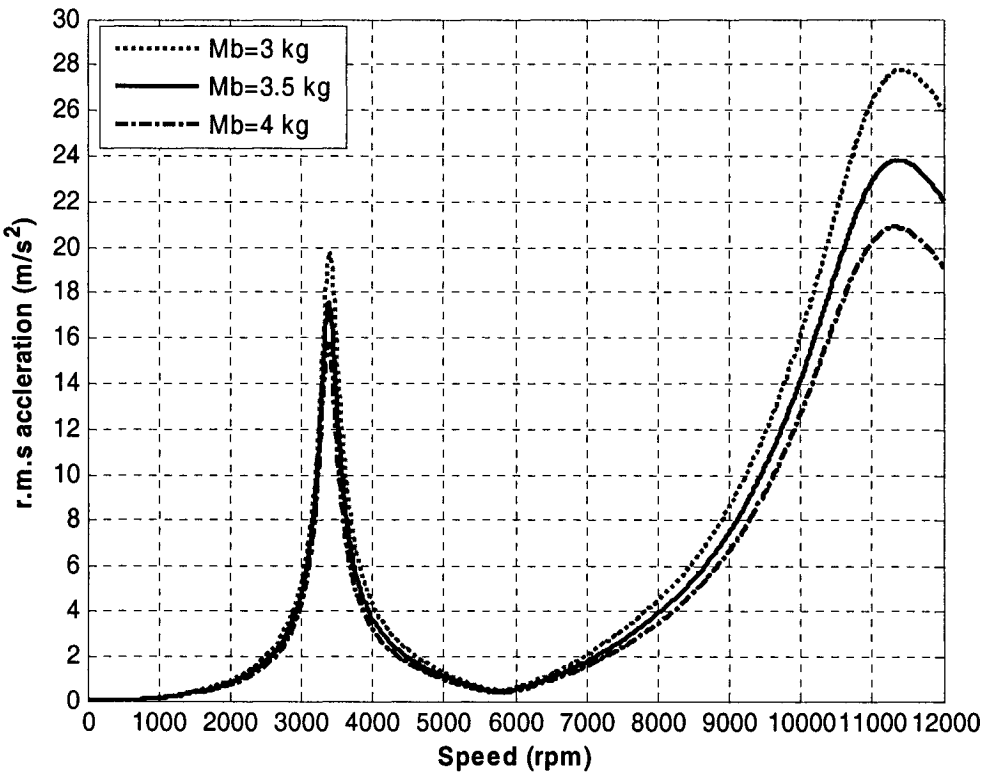

Figure 4.21: Influence of the machine casing weight on the rms acceleration response of the tool body mass along the Y-axis for mass unbalance of 76gm-mm

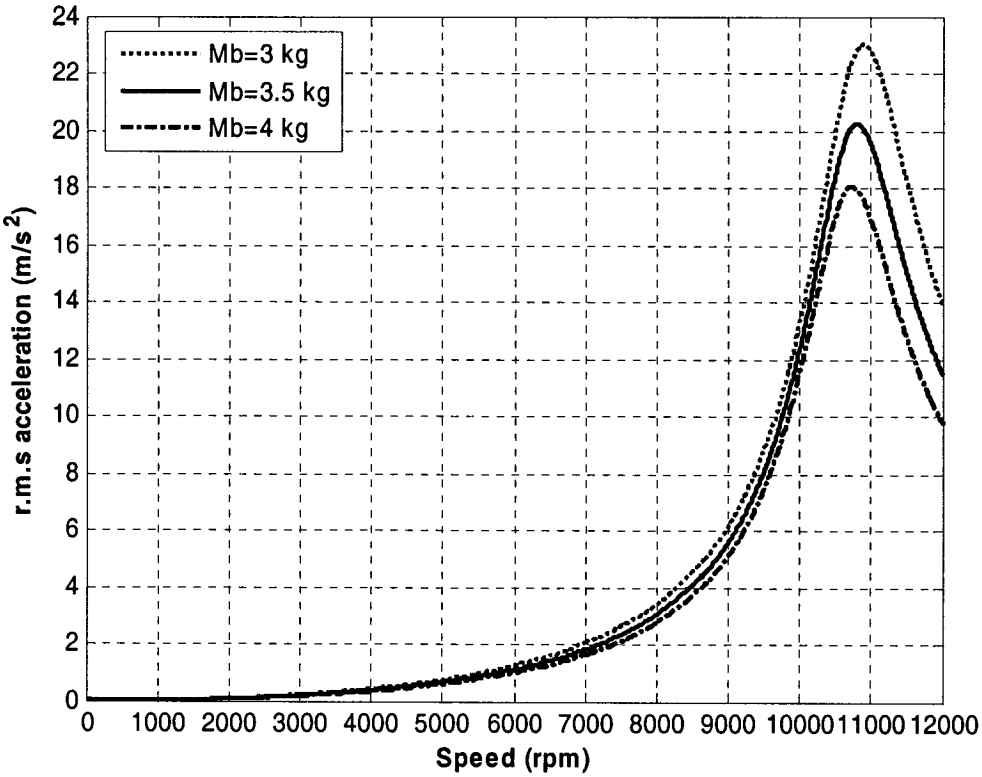

Figure 4.22: Influence of the machine casing weight on the rms acceleration response of the tool body mass along the X-axis for mass unbalance of 76gm-mm

4.8 Effects of Variation in Bearing Damping

The influence of damping properties of the bearings on the magnitudes of transmitted vibration is investigated by varying the viscous damping coefficients of both the bearings. The bearing damping coefficients are varied by increasing and decreasing the nominal value by 20%. The acceleration responses of the tool body along the Z-, Y- and X-axes are evaluated for mass unbalance of 76 gm-mm and different values of the bearing damping. The responses in terms of rms accelerations are compared as a function of rotational speed in Figures 4.23 to 4.25, for the Z- ,Y- and X-axes, respectively. These results clearly indicate that the damping has a considerable effect only at the resonant responses. At the resonant frequencies, as the bearing damping increases the hand

transmitted vibration decreases. A 20% increase in bearing damping could help reduce the peak rms accelerations by 15%.

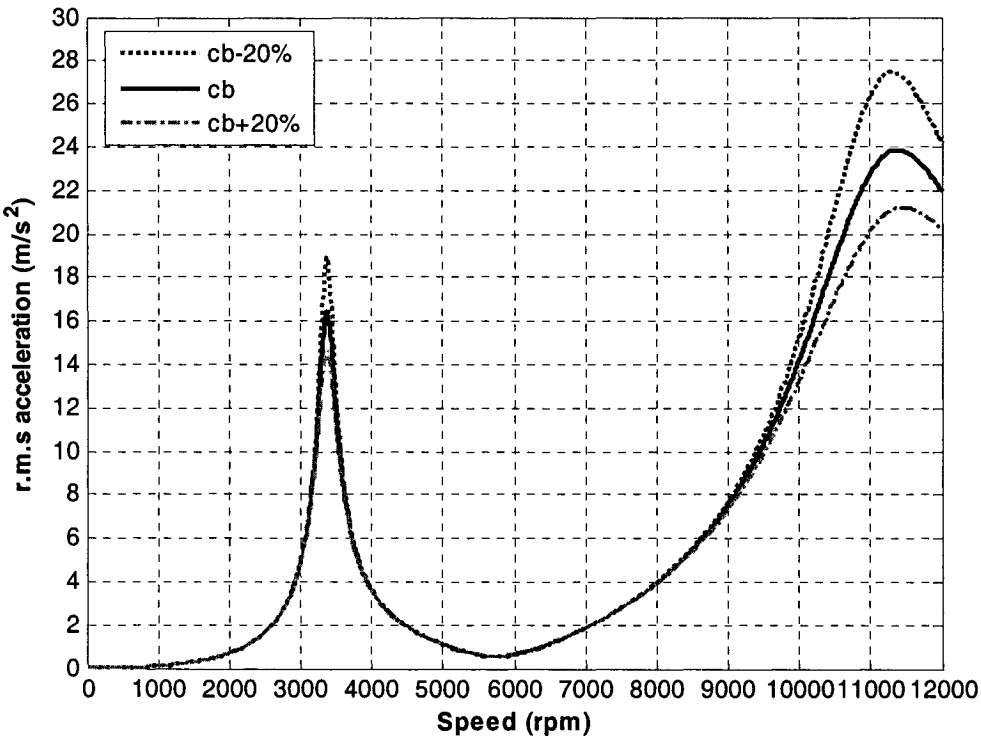

Figure 4.23: Influence of the bearing damping on the rms acceleration response of the tool body mass along the Z-axis for mass unbalance of 76 gm-mm

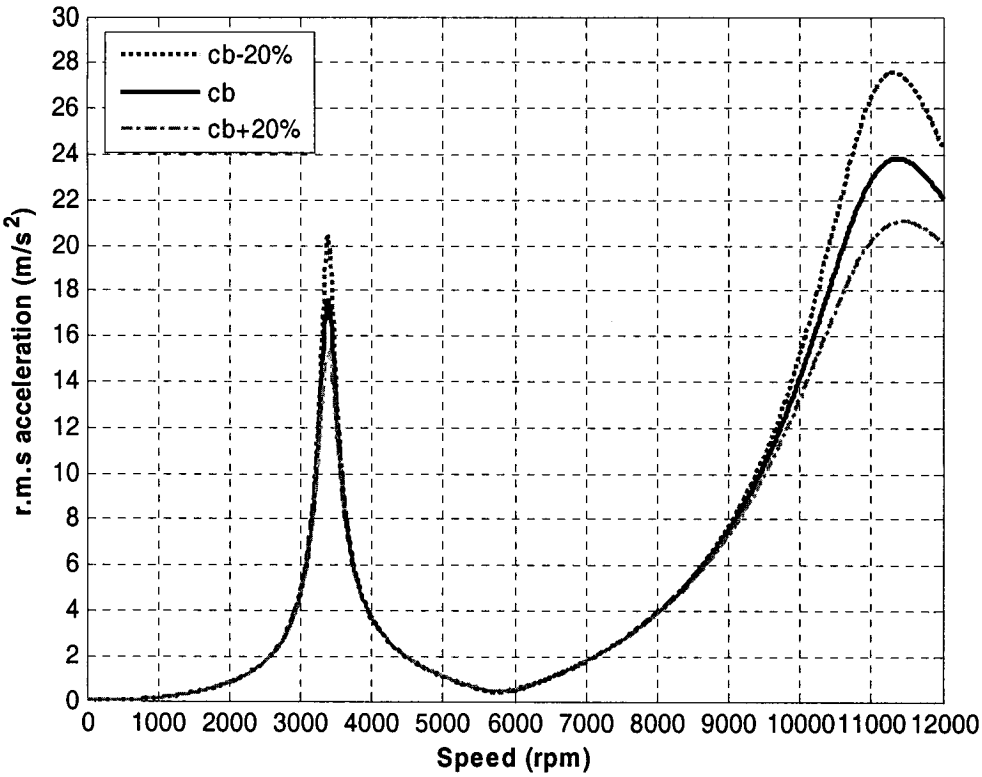

Figure 4.24: Influence of the bearing damping on the rms acceleration response of the tool body mass along the Y-axis for mass unbalance of 76 gm-mm

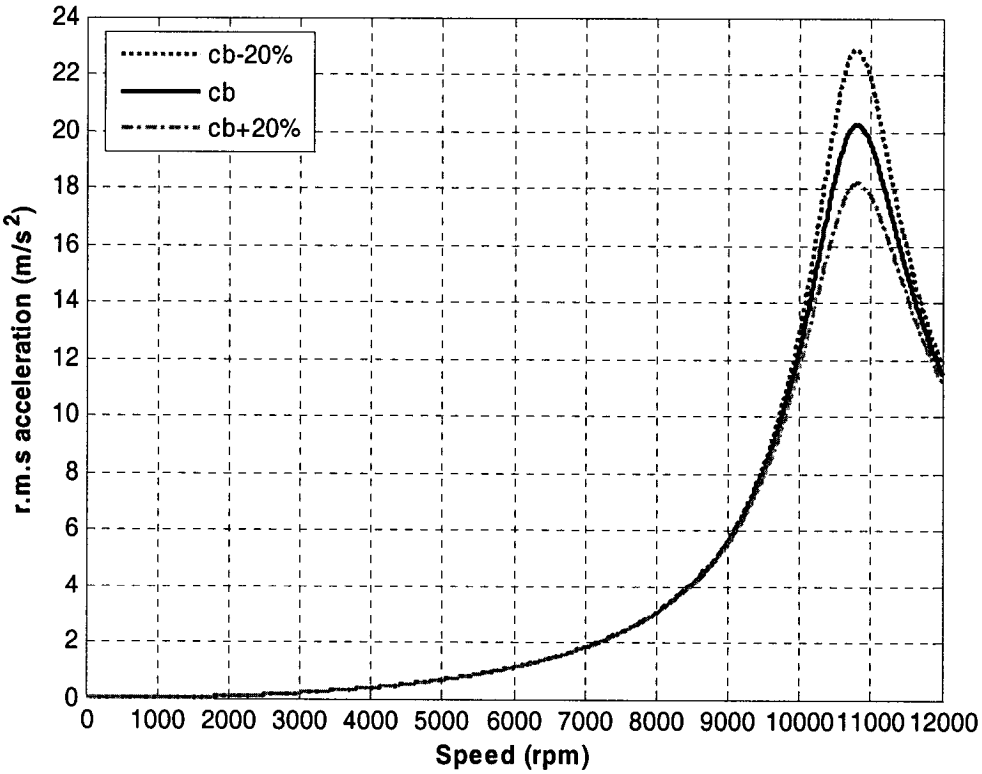

Figure 4.25: Influence of the bearing damping on the rms acceleration response of the tool body mass along the X-axis for mass unbalance of 76 gm-mm

4.9 Influence of Hand-Handle Interface Properties

High levels of hand-transmitted vibration, and the associated health and safety risks have prompted numerous studies on design of effective tools and vibration isolators. The general methods used in these studies can be classified under three broad categories.

i. Dynamic balancing of the rotating components of power tools [94].

ii. Implementing vibration isolators within the tool [95].

iii. Using anti-vibration gloves [6, 96, 97].

In most of the rotary hand-held power tools, the residual rotor unbalance causes vibration which can be reduced by properly balancing the rotor [94]. The term "automatic balancing" refers to a general balancing methodology, where the centrifugal forces developed by the masses moving freely in a concentric circular path around the shaft center are used to balance the rotor. The use of vibration isolators to reduce the hand-transmitted vibration has been demonstrated for some tools. Even though some degree of vibration reduction has been achieved, their general implementation has been limited due to excessive design complexities [95]. The effectiveness of various anti-vibration hand gloves in reducing the vibration intensity at the hand have been thoroughly investigated [6, 96]. A few studies reported in the literature have established that the vibration transmissibility characteristics of these gloves are strongly related to the highly complex visco-elastic properties of the coupled hand-glove system [97]. Physically, gloves or glovelike materials introduce a third component in the hand-machine interface and form a more complex viscoelastic system that may alter the characteristics of hand-transmitted vibration (HTV) and the vibration transmissibility of the hand-arm system. Depending on

the glove materials and tool-operating conditions, this may have either positive or negative effects.

A few investigators have also attempted to study the vibration transmissibility characteristics of anti-vibration gloves. It has been established that the vibration-attenuation performance of the gloves can be enhanced only at the expense of high dexterity loss [12, 98]. The International Standard Organization (ISO) has defined a standardized laboratory method to measure and evaluate the vibration attenuation performance of the gloves [99]. Although the basic methodology of the standard has been generally accepted, several fundamental deficiencies and technical problems have been identified. While a few lumped parameter models have been developed characterizing the hand and coupled glove-hand system, no attempt has been made to characterize the coupled hand-glove-tool model. The hand-tool model developed in this study is modified to incorporate the visco-elastic properties of gloves or glove-like materials at the hand-tool interface in order to study the effects of such materials.

4.9.1 Equations of Motion

The equations of motion of the coupled hand-tool system with anti-vibration gloves are derived considering 17 degrees-of-freedom i.e., 6 degrees-of-freedom along the Z-axis, 6 degrees-of-freedom along the Y-axis and 5 degrees-of-freedom along the X-axis. These include the translational motion of the disc (z_d, y_d, x_d), rotational motions of the disc (α about Z-axis and β about Y-axis), motion of the tool body $M_b(z_b, y_b, x_b)$, motions of hand masses $M_{h1}(z_1, y_1, x_1)$, $M_{h2}(z_2, y_2, x_2)$ and $M_{h3}(z_3, y_3, x_3)$. The glove mass M_g is assumed to be in contact with the hand mass M_{h1}. Hence, M_{h1} represents

the total of the hand mass and the glove mass. Figures 4.26 and 4.27 present the coupled hand-tool model with anti-vibration gloves along the radial directions (Z- and Y-axes), and Figure 4.28 presents the same along the axial direction (X-axis). This coupled hand-glove-tool model is developed based on the assumptions outlined section 4.2, and K_{hg} and C_{hg} represent constant stiffness and viscous damping coefficients of the anti-vibration glove material. These visco-elastic properties of the anti-vibration gloves are assumed to be identical along all the three axes (X-, Y- and Z-).

Equations of Motion along the Z-axis:

The equations of motion of the coupled hand-tool model with anti-vibration gloves are derived along the Z-axis by considering mass unbalance excitation as input to the system. Let m_u represents the mass unbalance of the grinding wheel with an eccentricity e, such that the total mass of the shaft disc assembly is $M = m_d + m_u$. The equations of motion for the coupled hand-tool model along the Z-axis with anti-vibration gloves are written as:

$$M\ddot{z}_d + 2(K_{bz1} + K_{bz2} + K_0 + K_{sr})z_d + 2(C_{bz1} + C_{bz2} + C_0 + C_{sr})\dot{z}_d + 2(a_1K_{bz1} + b_1K_{bz2} + c_1K_0 + d_1K_{sr})\beta + 2(a_1C_{bz1} + b_1C_{bz2} + c_1C_0 + d_1C_{sr})\dot{\beta} - 2(K_{bz1} + K_{bz2} + K_0 + K_{sr})z_b - 2(C_{bz1} + C_{bz2} + C_0 + C_{sr})\dot{z}_b = m_u e\omega^2 \sin(\omega t) \tag{4.15}$$

$$I_y\ddot{\beta} + 2(a_1K_{bz1} + b_1K_{bz2} + c_1K_0 + d_1K_{sr})z_d + 2(a_1C_{bz1} + b_1C_{bz2} + c_1C_0 + d_1C_{sr})\dot{z}_d + 2(a_1^2K_{bz1} + b_1^2K_{bz2} + c_1^2K_0 + d_1^2K_{sr})\beta + 2(a_1^2C_{bz1} + b_1^2C_{bz2} + c_1^2C_0 + d_1^2C_{sr})\dot{\beta} - 2(a_1K_{bz1} + b_1K_{bz2} + c_1K_0 + d_1K_{sr})z_b - 2(a_1C_{bz1} + b_1C_{bz2} + c_1C_0 + d_1C_{sr})\dot{z}_b = -a_0m_u e\omega^2 \sin(\omega t) \tag{4.16}$$

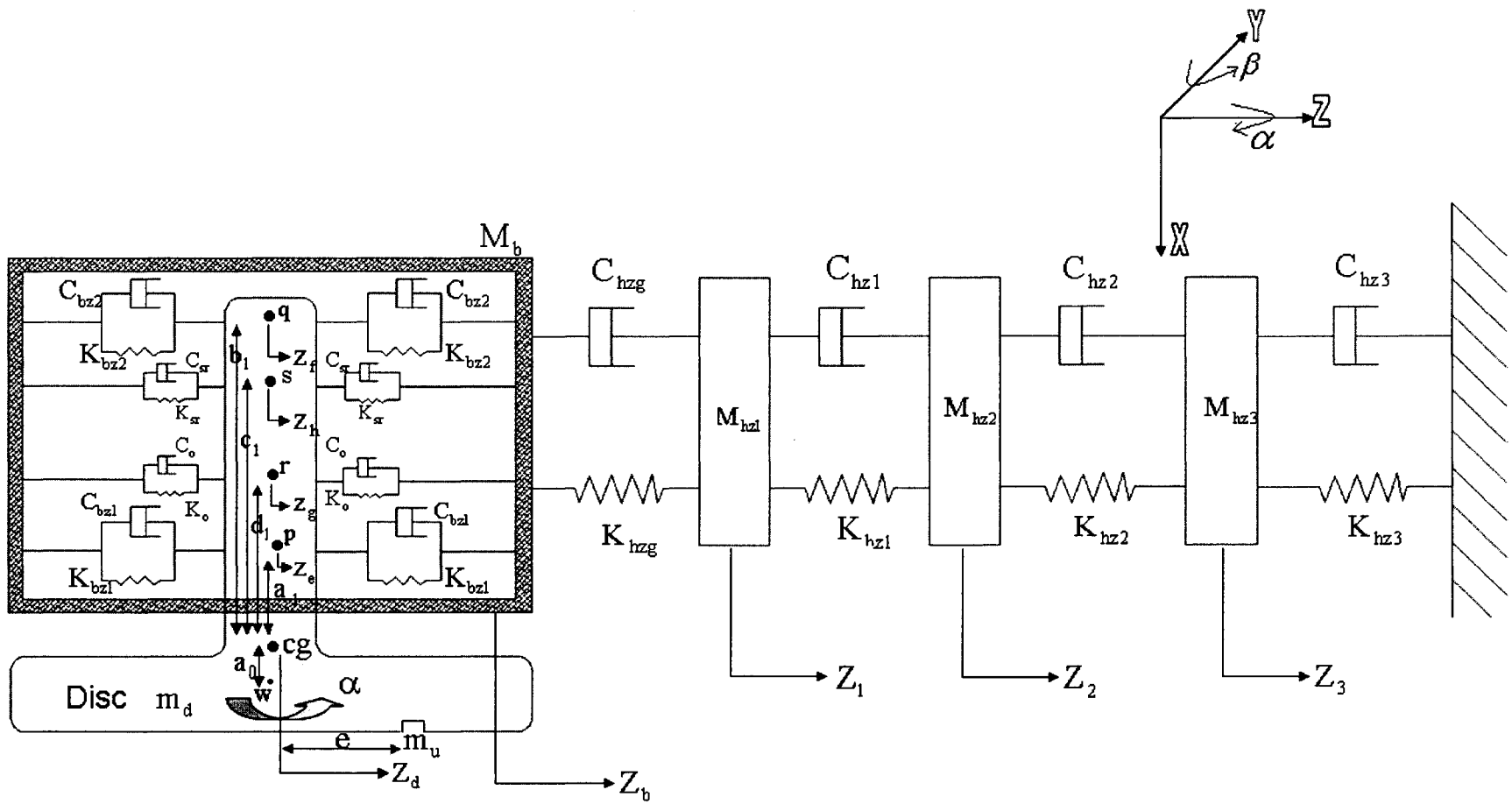

Figure 4.26: Analytical model representation of the coupled human hand and the grinder along the Z-axis with anti-vibration gloves

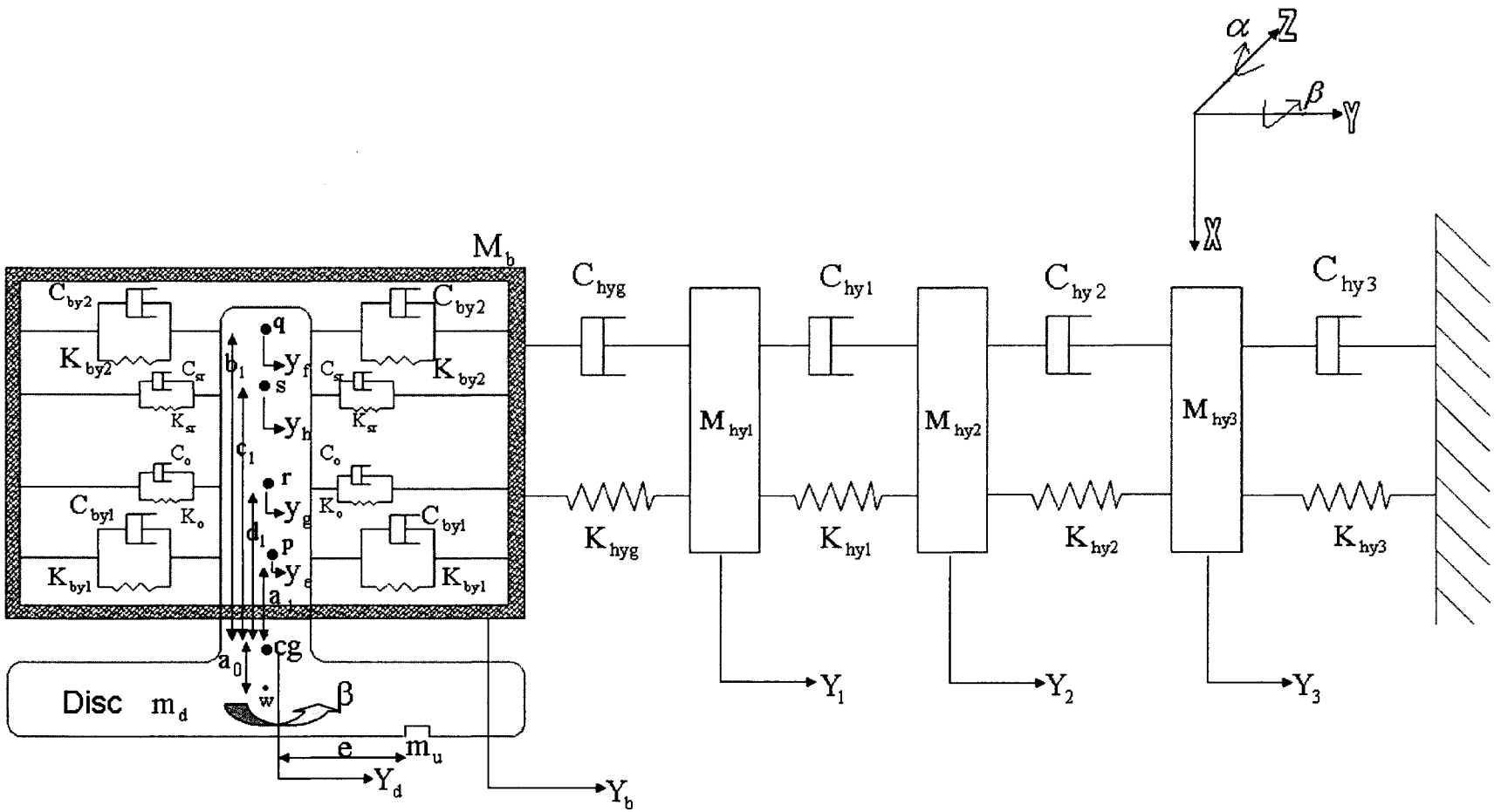

Figure 4.27: Analytical model representation of the coupled human hand and the grinder along the Y-axis with anti-vibration gloves

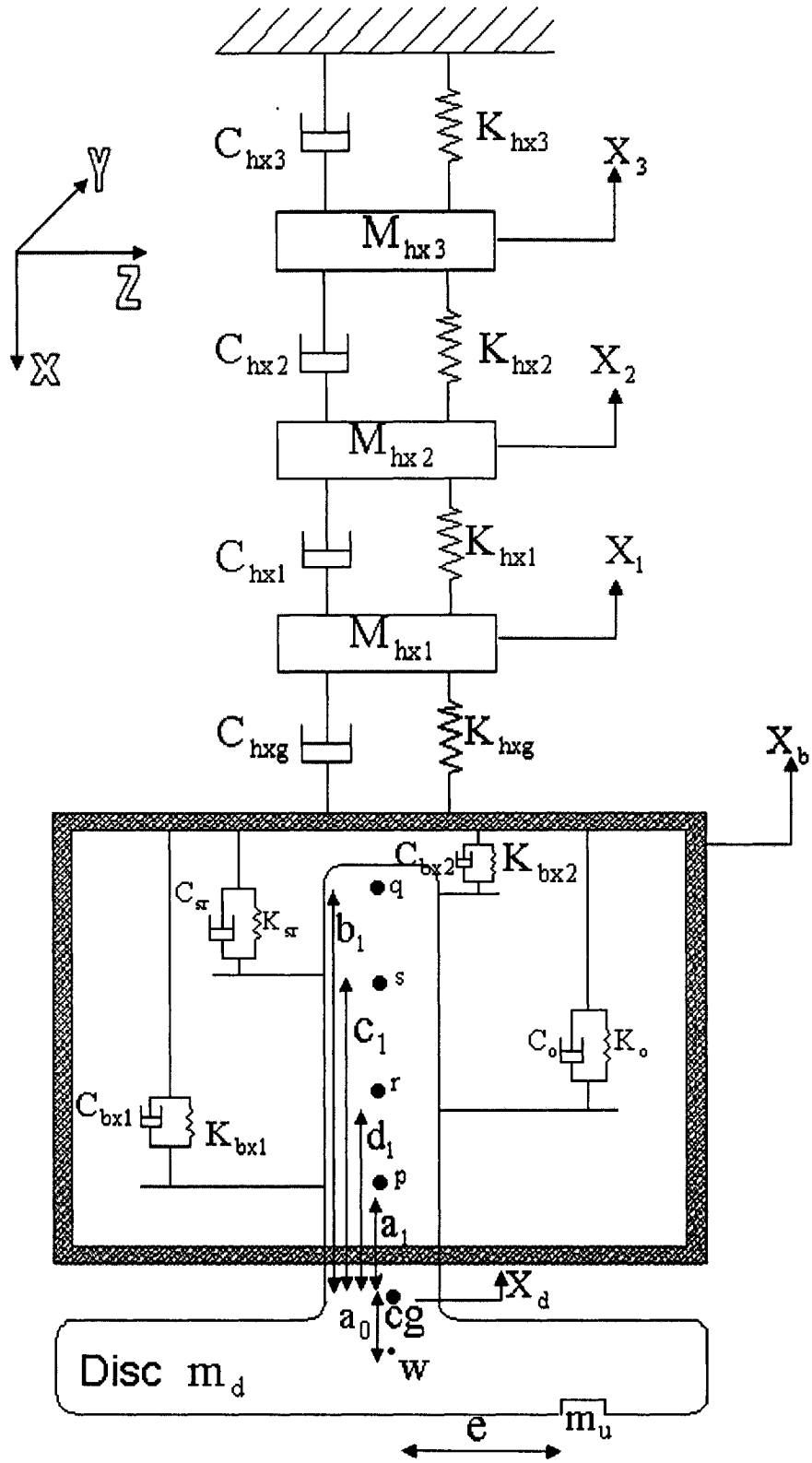

Figure 4.28: Analytical model representation of the coupled human hand and the grinder along the X-axis with anti-vibration gloves

$$M_b\ddot{z}_b - 2(K_{bz1} + K_{bz2} + K_0 + K_{sr})z_d - 2(C_{bz1} + C_{bz2} + C_0 + C_{sr})\dot{z}_d - 2(a_1K_{bz1} + b_1K_{bz2} + c_1K_0 + d_1K_{sr})\beta - 2(a_1C_{bz1} + b_1C_{bz2} + c_1C_0 + d_1C_{sr})\dot{\beta} + (2(K_{bz1} + K_{bz2} + K_0 + K_{sr}) + K_{hzg})z_b + (2(C_{bz1} + C_{bz2} + C_0 + C_{sr}) + C_{hzg})\dot{z}_b - (K_{hzg})z_1 - (C_{hzg})\dot{z}_1 = 0$$

(4.17)

$$M_{hz1}\ddot{z}_1 - (K_{hzg})z_b - (C_{hzg})\dot{z}_b + (K_{hzg} + K_{hz1})z_1 + (C_{hzg} + C_{hz1})\dot{z}_1 - (K_{hz1})z_2 - (C_{hz1})\dot{z}_2 = 0$$

(4.18)

$$M_{hz2}\ddot{z}_2 - (K_{hz1})z_1 - (C_{hz1})\dot{z}_1 + (K_{hz1} + K_{hz2})z_2 + (C_{hz1} + C_{hz2})\dot{z}_2 - (K_{hz2})z_3 - (C_{hz2})\dot{z}_3 = 0$$

(4.19)

$$M_{hz3}\ddot{z}_3 - (K_{hz2})z_2 - (C_{hz2})\dot{z}_2 + (K_{hz2} + K_{hz3})z_3 + (C_{hz2} + C_{hz3})\dot{z}_3 = 0$$

(4.20)

Equations of Motion along the Y-axis:

The equations of motion of the coupled hand-tool model with anti-vibration gloves are derived along the Y-axis by considering mass unbalance excitation as input to the system. The equations of motion for the coupled hand-tool model along the Y-axis with anti-vibration gloves are written as:

$$M\ddot{y}_d + 2(K_{by1} + K_{by2} + K_0 + K_{sr})y_d + 2(C_{by1} + C_{by2} + C_0 + C_{sr})\dot{y}_d - 2(a_1K_{by1} + b_1K_{by2} + c_1K_0 + d_1K_{sr})\alpha - 2(a_1C_{by1} + b_1C_{by2} + c_1C_0 + d_1C_{sr})\dot{\alpha} - 2(K_{by1} + K_{by2} + K_0 + K_{sr})y_b - 2(C_{by1} + C_{by2} + C_0 + C_{sr})\dot{y}_b = m_u e\omega^2 \cos(\omega t)$$

(4.21)

$$I_z\ddot{\alpha} - 2(a_1K_{by1} + b_1K_{by2} + c_1K_0 + d_1K_{sr})y_d - 2(a_1K_{by1} + b_1K_{by2} + c_1K_0 + d_1K_{sr})\dot{y}_d + 2(a_1^2K_{by1} + b_1^2K_{by2} + c_1^2K_0 + d_1^2K_{sr})\alpha + 2(a_1^2C_{by1} + b_1^2C_{by2} + c_1^2C_0 + d_1^2C_{sr})\dot{\alpha} + 2(a_1K_{by1} + b_1K_{by2} + c_1K_0 + d_1K_{sr})y_b + 2(a_1C_{by1} + b_1C_{by2} + c_1C_0 + d_1C_{sr})\dot{y}_b = a_0m_u e\omega^2 \cos(\omega t)$$

(4.22)

$$M_b\ddot{y}_b - 2(K_{by1} + K_{by2} + K_0 + K_{sr})y_d - 2(C_{by1} + C_{by2} + C_0 + C_{sr})\dot{y}_d + 2(a_1K_{by1} + b_1K_{by2} + c_1K_0 + d_1K_{sr})\alpha + 2(a_1C_{by1} + b_1C_{by2} + c_1C_0 + d_1C_{sr})\dot{\alpha} + (2(K_{by1} + K_{by2} + K_0 + K_{sr}) + K_{hyg})y_b + (2(C_{by1} + C_{by2} + C_0 + C_{sr}) + C_{hyg})\dot{y}_b - (K_{hyg})y_1 - (C_{hyg})\dot{y}_1 = 0 \quad (4.23)$$

$$M_{hy1}\ddot{y}_1 - (K_{hyg})y_b - (C_{hyg})\dot{y}_b + (K_{hyg} + K_{hy1})y_1 + (C_{hyg} + C_{hy1})\dot{y}_1 - (K_{hy1})y_2 - (C_{hy1})\dot{y}_2 = 0 \quad (4.24)$$

$$M_{hy2}\ddot{y}_2 - (K_{hy1})y_1 - (C_{hy1})\dot{y}_1 + (K_{hy1} + K_{hy2})y_2 + (C_{hy1} + C_{hy2})\dot{y}_2 - (K_{hy2})y_3 - (C_{hy2})\dot{y}_3 = 0 \quad (4.25)$$

$$M_{hy3}\ddot{y}_3 - (K_{hy2})y_2 - (C_{hy2})\dot{y}_2 + (K_{hy2} + K_{hy3})y_3 + (C_{hy2} + C_{hy3})\dot{y}_3 = 0 \quad (4.26)$$

Equations of Motion along the X-axis:

As described in section 4.3, the cross coupling effect and the effect of vibration of the gear and the pneumatic drive is represented as a function of mass unbalance by considering an equivalent excitation of $(0.15m_ue\omega^2)$ along the X-axis. The equations of motion of the coupled hand-tool model along the X-axis are written as:

$$M\ddot{x}_d + (K_{bx1} + K_{bx2} + K_0 + K_{sr})x_d + (C_{bx1} + C_{bx2} + C_0 + C_{sr})\dot{x}_d - (K_{bx1} + K_{bx2} + K_0 + K_{sr})x_b - (C_{bx1} + C_{bx2} + C_0 + C_{sr})\dot{x}_b = (0.15m_ue\omega^2)\sin(\omega t) \quad (4.27)$$

$$M_b\ddot{x}_b - (K_{bx1} + K_{bx2} + K_0 + K_{sr})x_d - (C_{bx1} + C_{bx2} + C_0 + C_{sr})\dot{x}_d + (K_{bx1} + K_{bx2} + K_0 + K_{sr} + K_{hxg})x_b + (C_{bx1} + C_{bx2} + C_0 + C_{sr} + C_{hxg})\dot{x}_b - (K_{hxg})x_1 - (C_{hxg})\dot{x}_1 = 0 \quad (4.28)$$

$$M_{hx1}\ddot{x}_1 - (K_{hxg})x_b - (C_{hxg})\dot{x}_b + (K_{hxg} + K_{hx1})x_1 + (C_{hxg} + C_{hx1})\dot{x}_1 - (K_{hx1})x_2 - (C_{hx1})\dot{x}_2 = 0 \quad (4.29)$$

$$M_{hx2}\ddot{x}_2 - (K_{hx1})x_1 - (C_{hx1})\dot{x}_1 + (K_{hx1} + K_{hx2})x_2 + (C_{hx1} + C_{hx2})\dot{x}_2 - (K_{hx2})x_3 - (C_{hx2})\dot{x}_3 = 0 \quad (4.30)$$

$$M_{hx3}\ddot{x}_3 - (K_{hx2})x_2 - (C_{hx2})\dot{x}_2 + (K_{hx2} + K_{hx3})x_3 + (C_{hx2} + C_{hx3})\dot{x}_3 = 0 \quad (4.31)$$

4.9.2 Eigenvalue Analysis

A large number of anti-vibration gloves comprising natural rubber, neoprene, sorobothane, plastic foam, air-filled alveolar, etc., have been commercially developed to isolate the hand from the vibrating handle [49, 100, 101]. The model parameters for anti-vibration glove that is considered in this study are obtained from [13] and summarized in the Table 4.4. All the other model parameters relevant to the tool and handle models are same as those used in the earlier sections.

Table 4.4 Parameters of anti-vibration glove [13]

Glove Parameters	Values
Mass M_g	0.125 kg
Stiffness K_g	$1.5*10^4$ N/m
Damping C_g	48.7 Ns/m

An eigenvalue problem is formulated and solved to identify the natural frequencies and damping ratios of the coupled hand-tool model with anti-vibration gloves along all the three axes (Z-, Y- and X-). Tables 4.5 to 4.7 summarize the natural frequencies, damped frequency, damping ratio and associated dominant deflection modes of the model along the Z-, Y- and X-axes, respectively. The numerical values of the eigenvectors of

Table 4.5 Natural Frequencies of the coupled hand-tool model along the Z-axis with anti-vibration gloves

	Natural Frequency ω_n (Hz)	Damped Frequency ω_d (Hz)	Damping Ratio ξ	Dominant deflection modes (From eigen vectors)
1	1.867	1.57	0.5415	z_b
2	11.594	-	1.7901	z_3
3	18.150	16.18	0.4531	z_2
4	56.265	56.23	0.0354	β, z_d
5	113.101	-	1.0864	z_1
6	185.649	184.4302	0.1144	z_d, β

Table 4.6 Natural Frequencies of the coupled hand-tool model along the Y-axis with anti-vibration gloves

	Natural Frequency ω_n (Hz)	Damped Frequency ω_d (Hz)	Damping Ratio ξ	Dominant deflection modes (From eigen vectors)
1	1.971	1.86	0.3318	y_b
2	8.279	-	1.1861	y_3
3	25.355	19.58	0.6353	y_2
4	56.260	56.22	0.0379	α, y_d
5	90.367	54.53	0.7974	y_1
6	185.649	184.42	0.1149	y_d, α

Table 4.7 Natural Frequencies of the coupled hand-tool model along the X-axis with anti-vibration gloves

	Natural Frequency ω_n (Hz)	Damped Frequency ω_d (Hz)	Damping Ratio ξ	Dominant deflection modes (From eigen vectors)
1	1.297	-	4.1402	x_b
2	8.634	-	1.0019	x_3
3	32.181	27.69	0.5096	x_2
4	179.375	179.09	0.0564	x_d
5	212.558	104.3	0.8713	x_1

the coupled hand-tool model with anti-vibration gloves along all the three axes are represented in Appendix D.

The results show the presence of an additional modes at 113.1 Hz in Z-axis, 90.4 Hz in Y-axis and 212.6 Hz in X-axis, which are associated with the glove material. Furthermore, the primary tool frequencies tend to be similar to those obtained for the model without the glove. The results attained for the Z-axis model reveal two natural frequencies of 185.649 Hz and 56.265 Hz corresponding to the tool modes (z_d, β), which are lightly damped (damping ratios= 0.1144 and 0.0354). These frequencies are almost identical to those attained for the model without the gloves. The frequency associated with hand mass modes, however, decrease considerably due to visco-elastic coupling at the hand-handle interface. The hand mass mode frequency decreases from 39.5 Hz to 18.1 Hz in the Z-axis, from 43.9 Hz to 25.4 Hz in Y-axis, and 132.3 Hz to 32.3 Hz in the X-axis, respectively.

4.9.3 Simulation Results

The mathematical formulations of the coupled hand-tool model with anti-vibration gloves, are solved to determine the rms acceleration values due to vibration transmitted to the hand mass M_{h1}. The analyses are performed for different angular speeds up to a maximum speed of 12000 rpm, while the excitations arising from a fixed mass unbalance of 76 gm-mm alone are considered. The responses of the hand masses M_{h1}, M_{h2} and M_{h3} are obtained along all the three axes (Z-, Y- and X-) with and without the anti-vibration gloves. Figures 4.29 to 4.31 illustrate the comparisons of vibration responses of the hand mass M_{h1}, derived from the models with and without the anti-vibration glove,

along the Z-, Y- and X-axes, respectively. The results clearly indicate that the anti-vibration gloves can be effectively applied to help reduce the severity of the vibration exposure. In the Z-axis, the glove material yields slight amplification of vibration around 1000 rpm, which is attributed to the system natural frequency of 16.18 Hz. However, the response at this speed is quite negligible in comparison with the resonant responses. Similar results are also found along the Y-axis, as shown in Figure 4.30. Along the X-axis, as shown in Figure 4.31, the vibration exposure is reduced for speeds above 1600 rpm and below this speed the vibration exposure is amplified, because of the presence of the lower natural frequency of 27.69 Hz.

Similarly, the vibration exposure of hand mass M_{h2} is also reduced along the three axes (Z-, Y- and X-) as shown in Figures 4.32 to 4.34, respectively. The reduction is much pronounced at higher speeds, while the responses at lower speeds are slightly amplified. Similar results are also obtained for hand mass M_{h3} along all the three axes (Z-, Y- and X-) and are shown in Figures 4.35-37, respectively. The results of the above study reveal that anti-vibration gloves will yield effective attenuation of vibration.

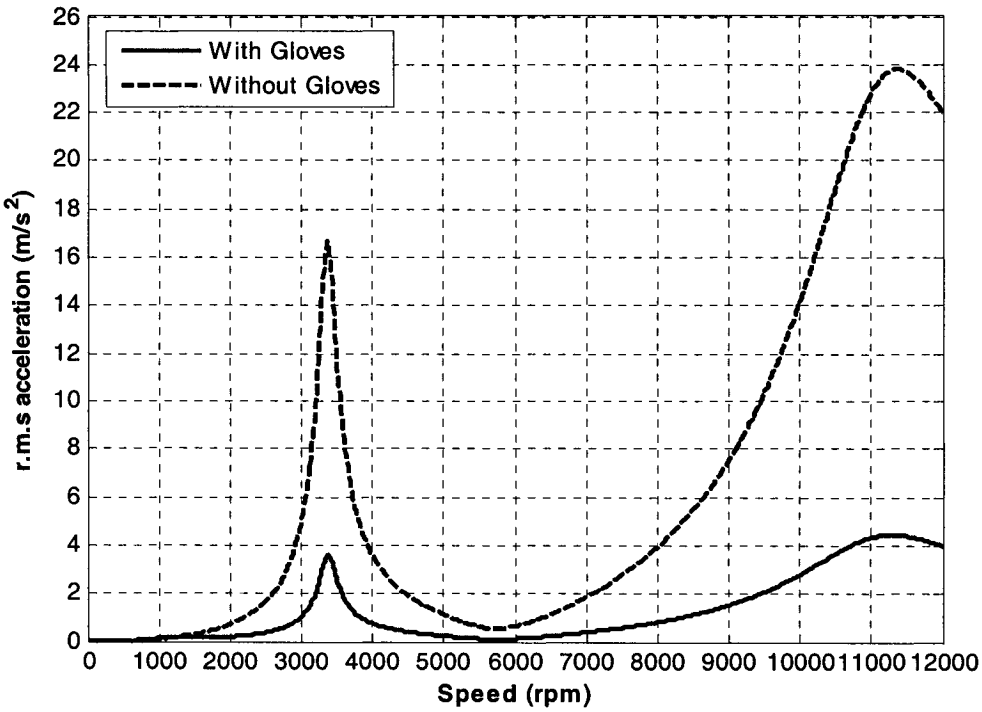

Figure 4.29: Influence of anti-vibration gloves on the rms acceleration response of the hand mass M_{hz1} along the Z-axis for mass unbalance of 76gm-mm

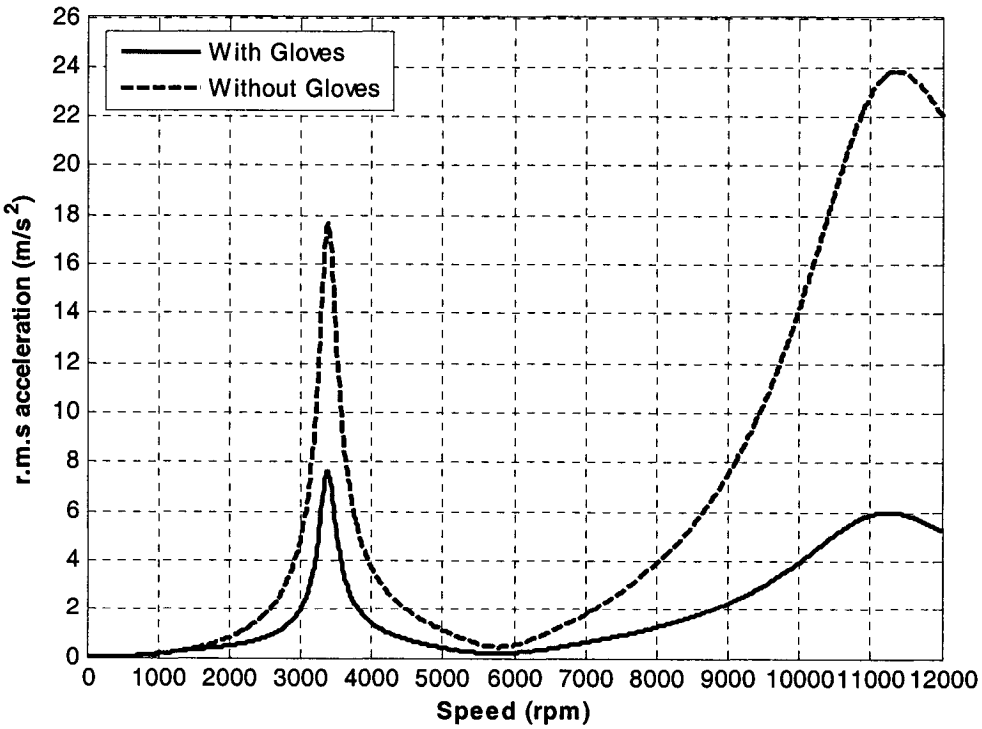

Figure 4.30: Influence of anti-vibration gloves on the rms acceleration response of the hand mass M_{hy1} along the Y-axis for mass unbalance of 76gm-mm

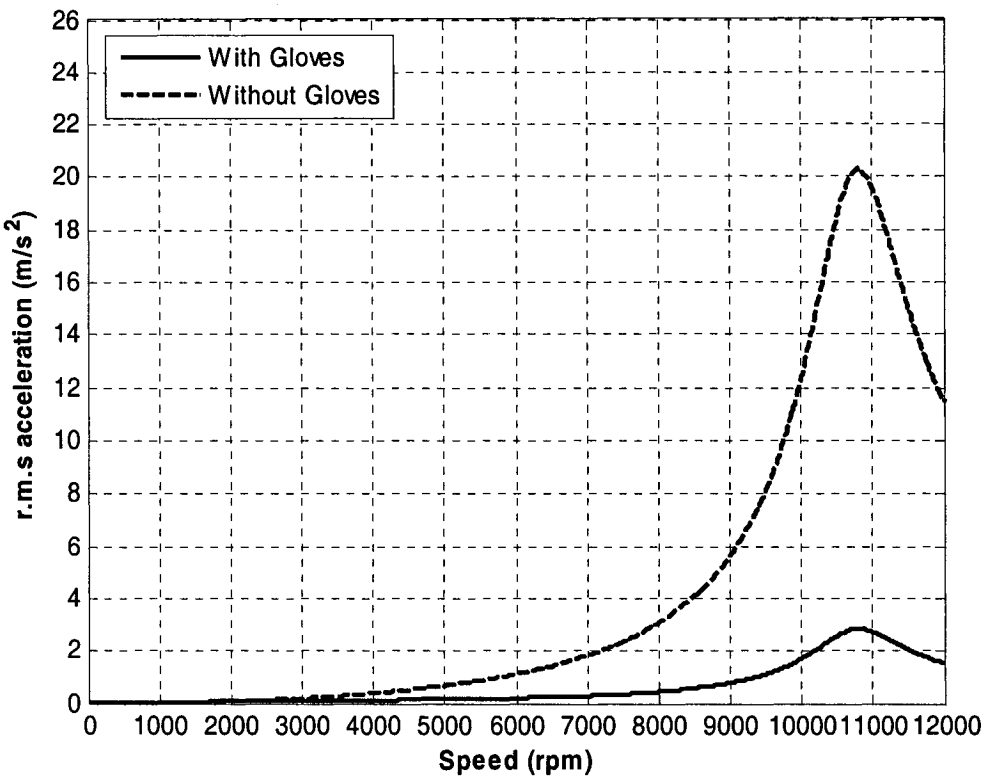

Figure 4.31: Influence of anti-vibration gloves on the rms acceleration response of the hand mass M_{hx1} along the X-axis for mass unbalance of 76gm-mm

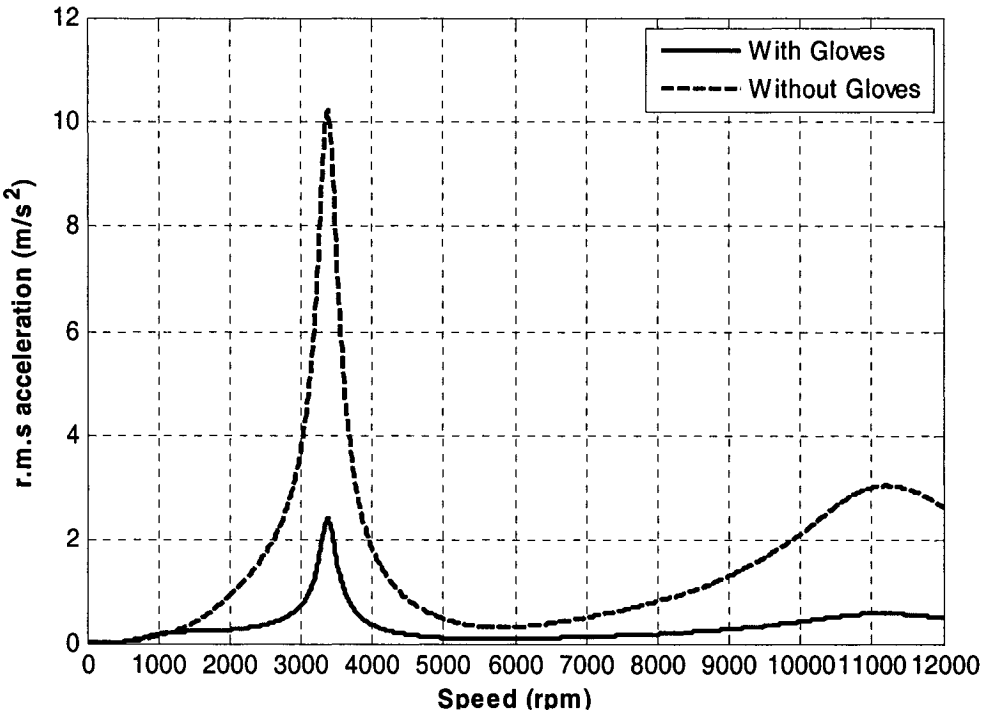

Figure 4.32: Influence of anti-vibration gloves on the rms acceleration response of the hand mass M_{hz2} along the Z-axis for mass unbalance of 76gm-mm

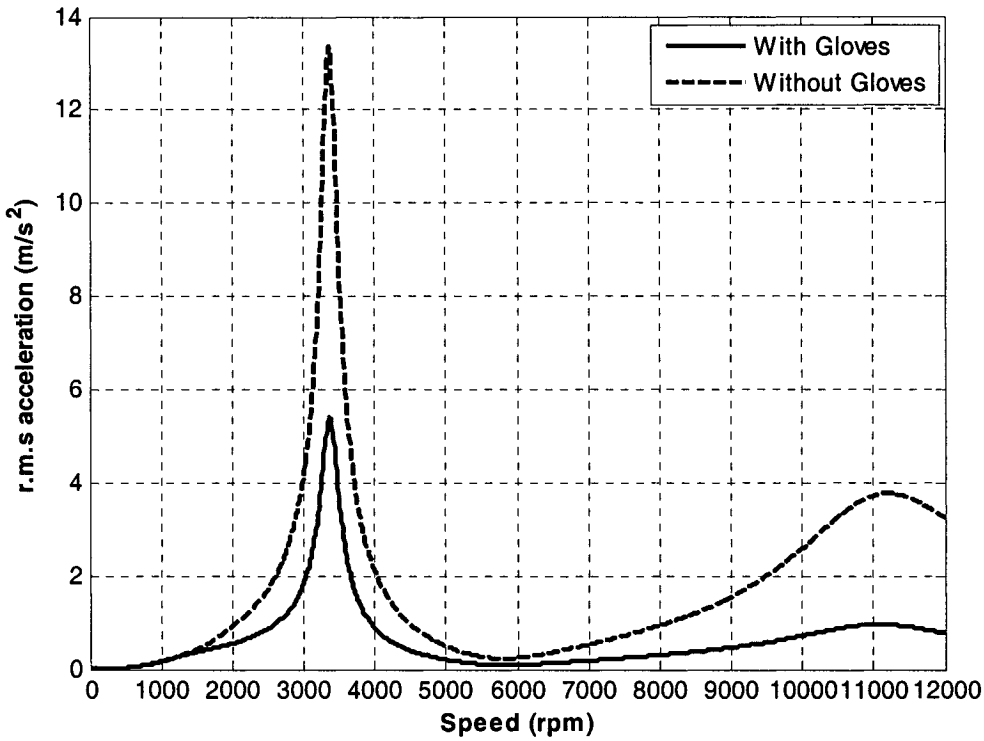

Figure 4.33: Influence of anti-vibration gloves on the rms acceleration response of the hand mass M_{hy2} along the Y-axis for mass unbalance of 76gm-mm

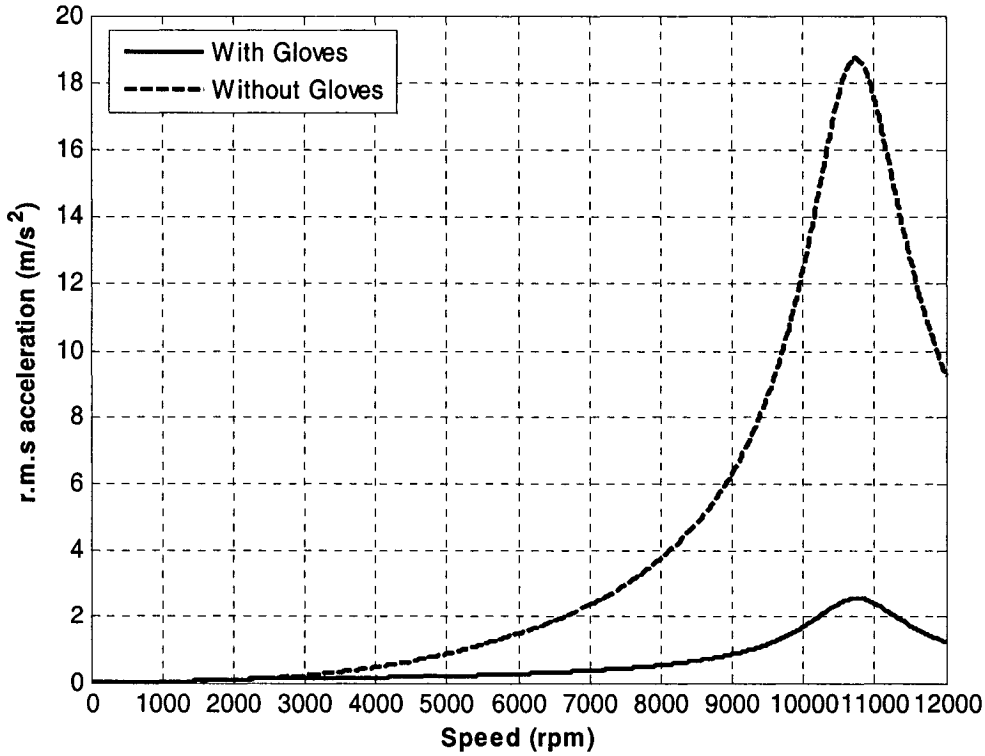

Figure 4.34: Influence of anti-vibration gloves on the rms acceleration response of the hand mass M_{hx2} along the X-axis for mass unbalance of 76gm-mm

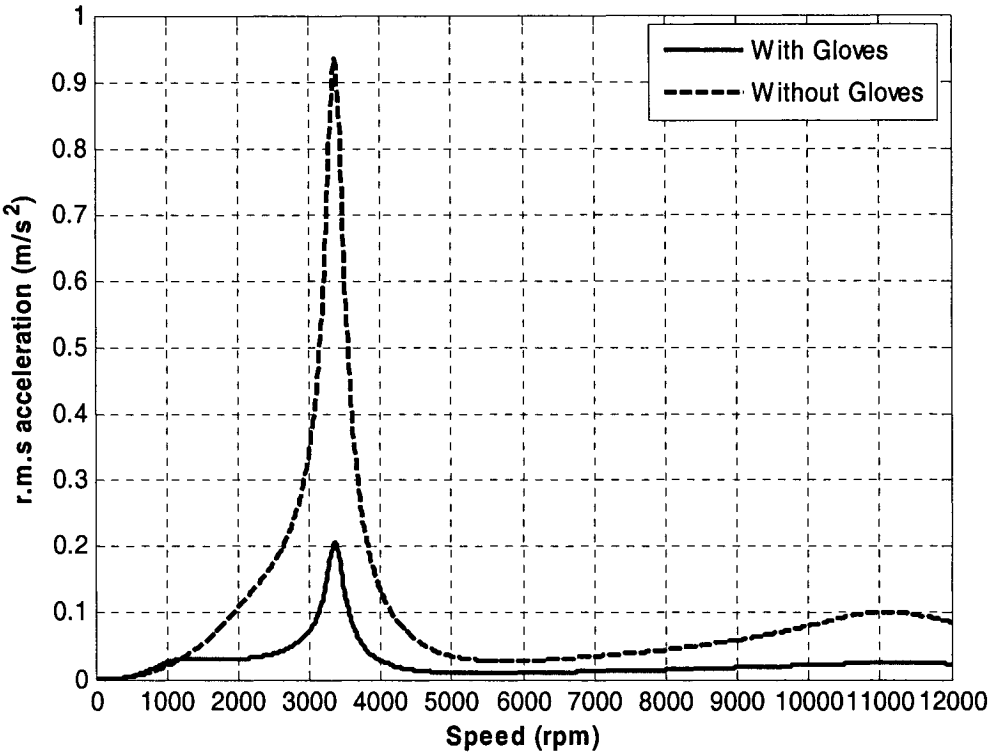

Figure 4.35: Influence of anti-vibration gloves on the rms acceleration response of the hand mass M_{hz3} along the Z-axis for mass unbalance of 76gm-mm

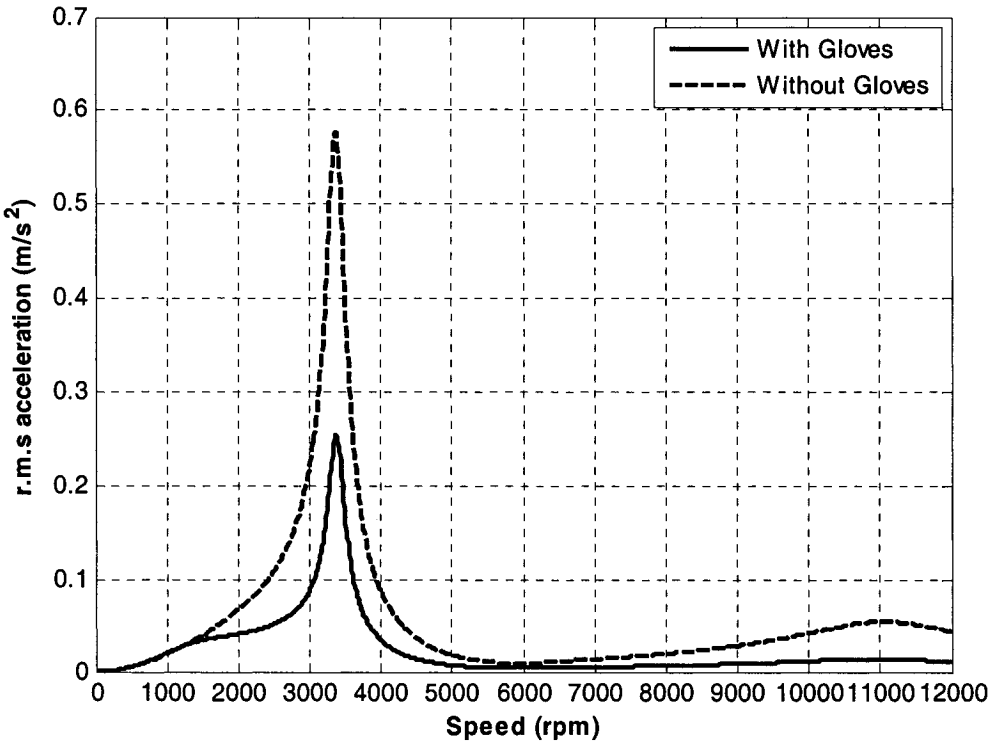

Figure 4.36: Influence of anti-vibration gloves on the rms acceleration response of the hand mass M_{hy3} along the Y-axis for mass unbalance of 76gm-mm

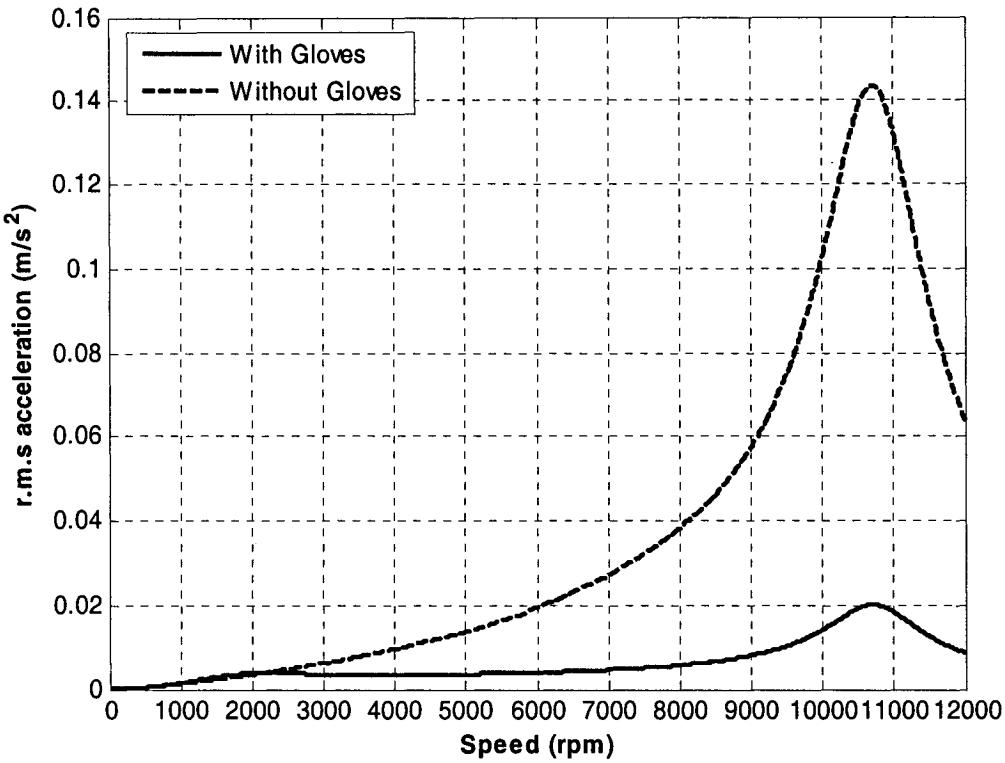

Figure 4.37: Influence of anti-vibration gloves on the rms acceleration response of the hand mass M_{hx3} along the X-axis for mass unbalance of 76gm-mm

4.10 Force Transmission to the Base

When using a hand-held power tool, the operator's hand, arm and shoulder are subjected to forces generated by the tool in use. Excessive load of this type may cause fatigue or, at worst, result in damage to the operator's musculoskeletal system. The magnitude of forces transmitted to the operator's hand structure depend on the type of tool and the task performed. When designing and selecting tools this load effect should be minimum. Analyses are performed to determine the forces transmitted to the base (shoulder) with and without the anti-vibration gloves as a function of the mass unbalance and the rotational speed upto a maximum of 12000 rpm. While the effects of applied grip and push force together with the cutting forces are neglected, the forces transmitted are derived from:

$$F_{tz3} = K_{hz3}(z_3 - z_2) + C_{hz3}(\dot{z}_3 - \dot{z}_2) \tag{4.32}$$

$$F_{ty3} = K_{hy3}(y_3 - y_2) + C_{hy3}(\dot{y}_3 - \dot{y}_2) \tag{4.33}$$

$$F_{tx3} = K_{hx3}(x_3 - x_2) + C_{hx3}(\dot{x}_3 - \dot{x}_2) \tag{4.34}$$

where F_{tz3}, F_{ty3} and F_{tx3} are the forces transmitted to the base along the Z-, Y- and X-axes, respectively.

As the mass unbalance increases the amount of force transmitted to the base also increases. This trend is observed along all the three axes (Z, Y and X), as shown in Figures 4.38 to 4.43. Figures 4.38 and 4.39 present the magnitudes of force transmitted to the base along the Z-axis without and with anti-vibration gloves. The results show two resonant peaks, around 3370 rpm and 11065 rpm, for the model without the glove, which correspond to the two primary natural frequencies, namely 56.19 Hz and 184.43 Hz. The amount of force transmitted to the base is significantly reduced by the anti-vibration gloves, as shown in Figure 4.39. The addition of the glove however, yields an additional resonant peak near 1000 rpm, which correspond to the natural frequency of 16.18 Hz of the coupled hand-glove-tool model along the Z-axis.

These simulation results clearly indicate that the amount of force transmitted to the base is significantly reduced by using the anti-vibration gloves. The magnitudes of transmitted forces are very small since the dynamic forces generated by the dynamic interactions among the tool components, cutting forces, and grip and push force, are neglected. The responses attained along the Y- and X-axes also reveal similar trends in the forces transmitted to the base, as shown in Figures 4.40 to 4.43. The responses along the Y- and X-axes show additional peaks in transmitted forces near 1300 and 1600 rpm, respectively, which are associated with the vibration mode related to the glove material.

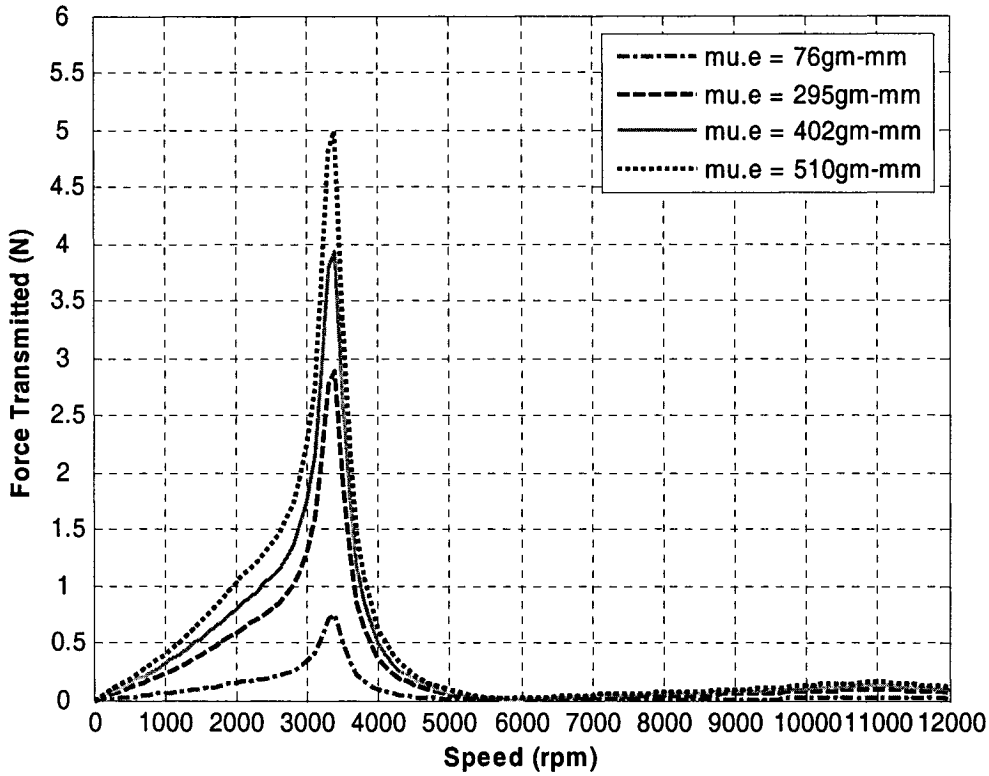

Figure 4.38: Influence of mass unbalance on the force transmitted to the base along the Z-axis with out anti-vibration gloves

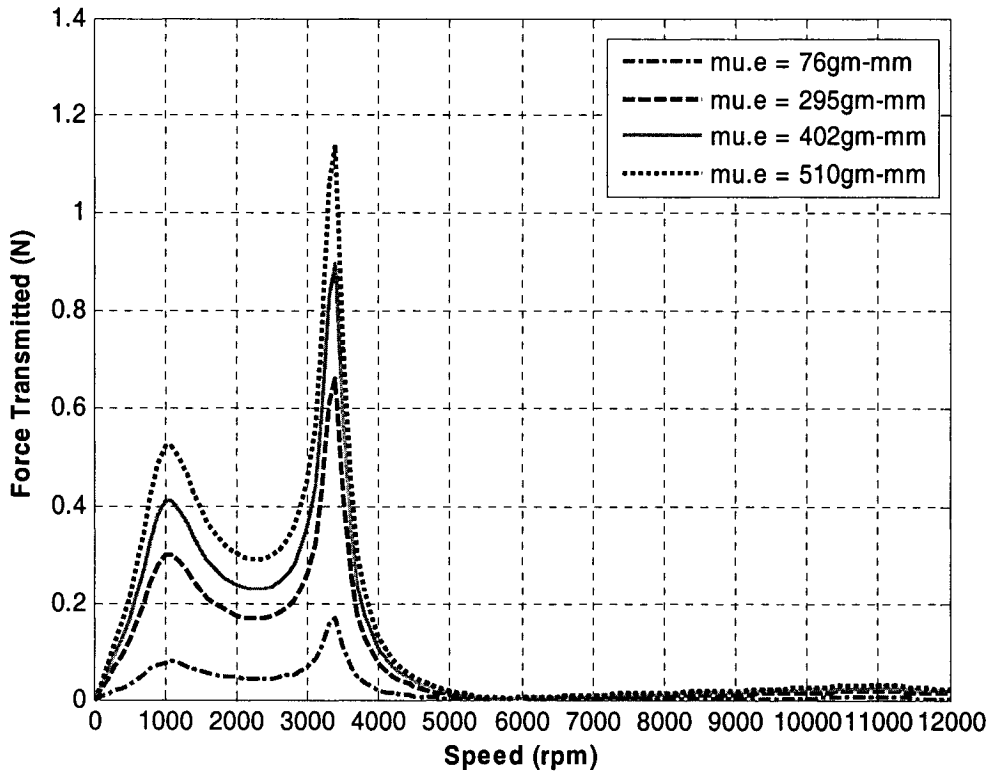

Figure 4.39: Influence of mass unbalance on the force transmitted to the base along the Z-axis with anti-vibration gloves

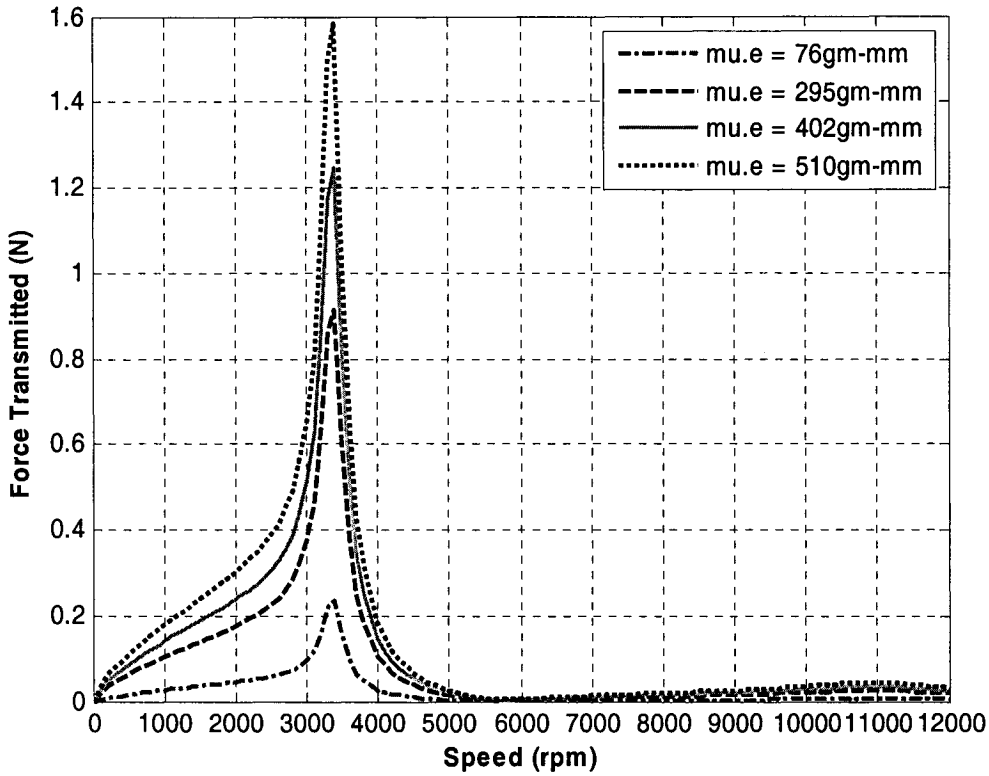

Figure 4.40: Influence of mass unbalance on the force transmitted to the base along the Y-axis with out anti-vibration gloves

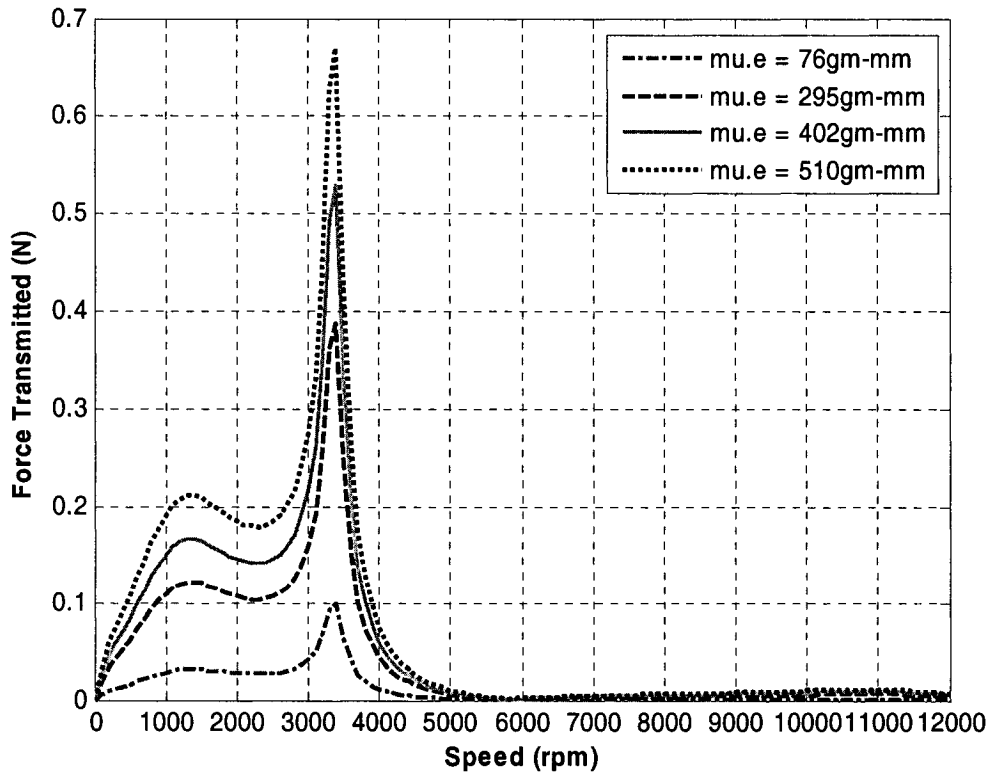

Figure 4.41: Influence of mass unbalance on the force transmitted to the base along the Y-axis with anti-vibration gloves

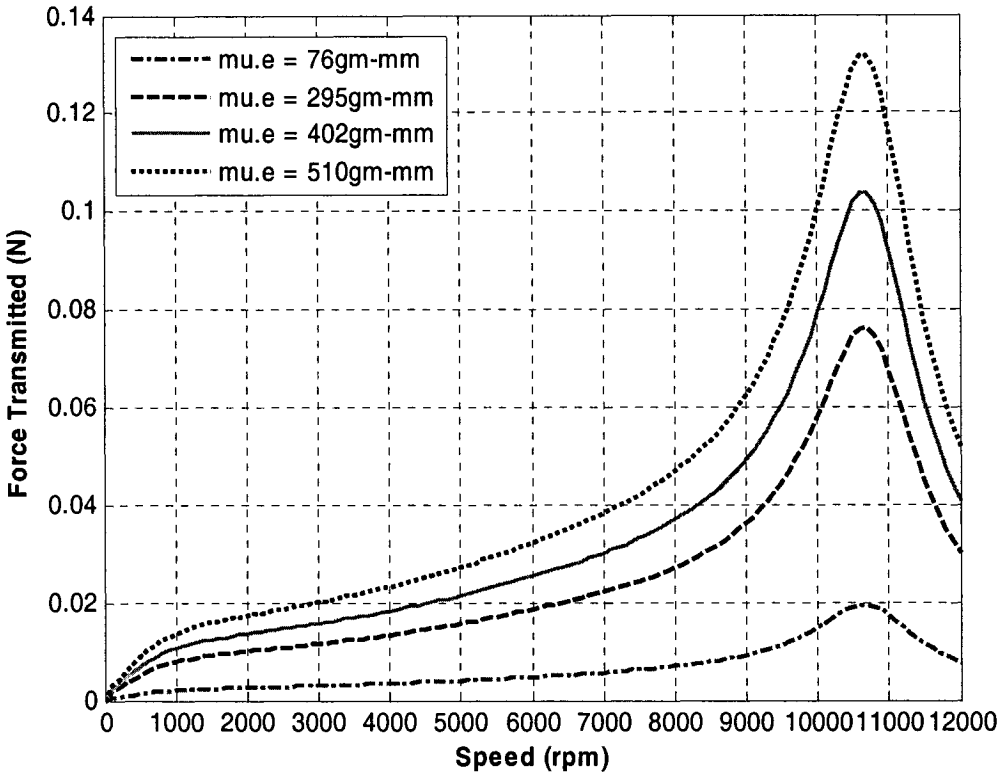

Figure 4.42: Influence of mass unbalance on the force transmitted to the base along the X-axis with out anti-vibration gloves

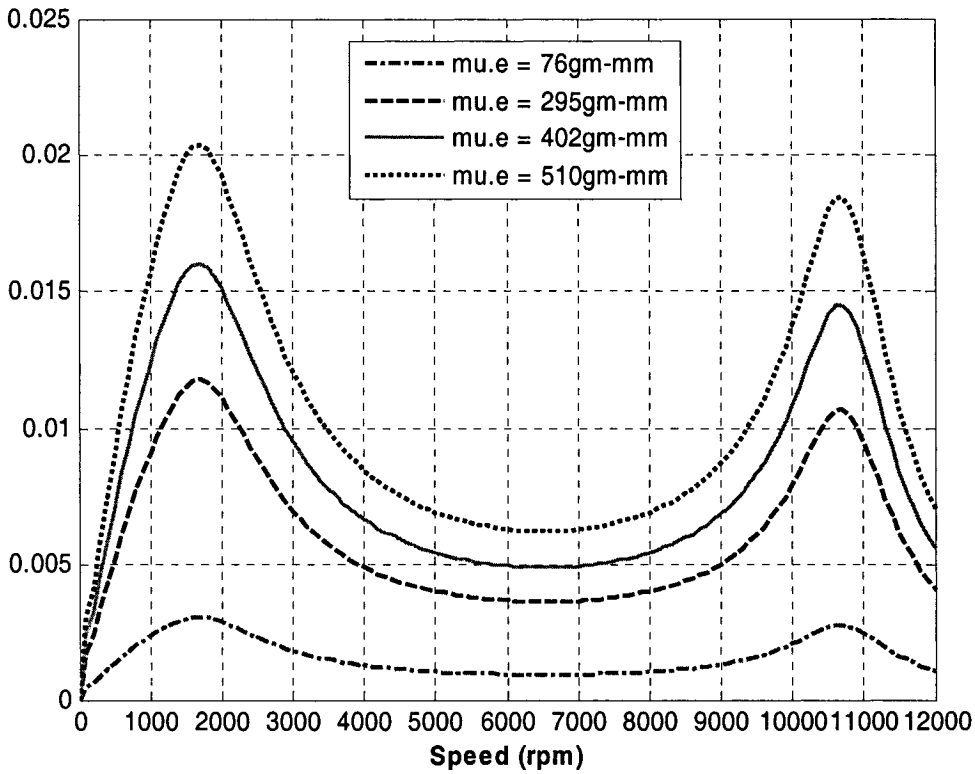

Figure 4.43: Influence of mass unbalance on the force transmitted to the base along the X-axis with anti-vibration gloves

4.11 Energy Dissipated by the Hand-Arm System

The majority of the studies and all current national and international standards regarding hand-transmitted vibration use tool handle acceleration as a measure to quantify the severity of vibration and to assess the risk of the exposure [42, 102]. A few investigators have suggested that the vibration energy absorption (VEA) may be a significant etiologic factor with regards to the vibration injuries, and that VEA may provide a better indication of vibration-induced injuries [103-105]. The human hand and arm is a complex visco-elastic system capable of storing both potential and kinetic energy. Potential energy is stored as a result of the relative compression or extension of the tissues, while the kinetic energy results from motions of various tissues in the hand and the arm [106]. In an ideal system, i.e., without damping, the vibration results in the transfer of energy between the hand-arm system and the tool handle and the average transfer of energy would be zero. The human hand-arm system, however, absorbs significant amount of energy, which can be attributed to its high damping properties.

4.11.1 Determination of Energy Dissipated by Viscous Damper

The energy dissipated per cycle in viscous damper given by:

$$W_d = \int_0^{\tau} F_d \, dx \tag{4.35}$$

where $F_d = C\dot{X}$ for a viscous damper and , and $\tau = \frac{2\pi}{\omega}$ is the period.

For the viscous damper subject to harmonic motion, $x(t) = X\sin(\omega t - \phi)$, the energy dissipated by the damper in a cycle can be expressed as [107]:

$$W_d = \pi C \omega X^2 \tag{4.36}$$

The total energy dissipated by the hand-arm system can be computed from the sum of individual dampers with viscous damping coefficients of C_{h3}, C_{h4} and C_{h5}. The total energy absorbed by the human hand and arm model is thus expressed as :

$$W_{Chi} = \sum_{k=3}^{5} W_{Chik};\ i = X, Y \text{ and } Z \tag{4.37}$$

where W_{Chi} is the total energy dissipated into the hand-arm system along the i-axis (i = X, Y and Z), and W_{Chik} represents the energy absorbed due to damping element C_{hik} (k=3, 4, 5) along the i-axis.

The equations of motion of hand-tool models with and without the gloves are solved to compute the relative motions across the damping elements, C_{hik}. The total energy absorbed into the hand-arm system is then evaluated using equations (4.36) and (4.37). The analyses are performed for the human hand-arm models with and without the anti-vibration glove while subject to mass unbalance of 76 gm-mm in the entire range of operating speed upto a maximum of 12000 rpm. Figures 4.44 to 4.46 illustrate comparisons of the amount of energy dissipated into the hand-arm system along the Z-, Y- and X-axes, respectively, with and without the anit-vibration gloves. From the results, it can be concluded that the energy dissipation can be significantly reduced by introducing the anti-vibration gloves between the hand mass M_{h1} and the tool body mass M_b. The dissipated energy response along the Z-axis reveals two resonant peaks at 3370

rpm and 11000 rpm, which correspond to the primary natural frequencies of the tool. The glove, however, causes a small power peak at a lower speed around 970 rpm, as observed in the case of transmitted force. Similar results are also obtained along the Y- and X-axes, as shown in Figures 4.45-4.46.

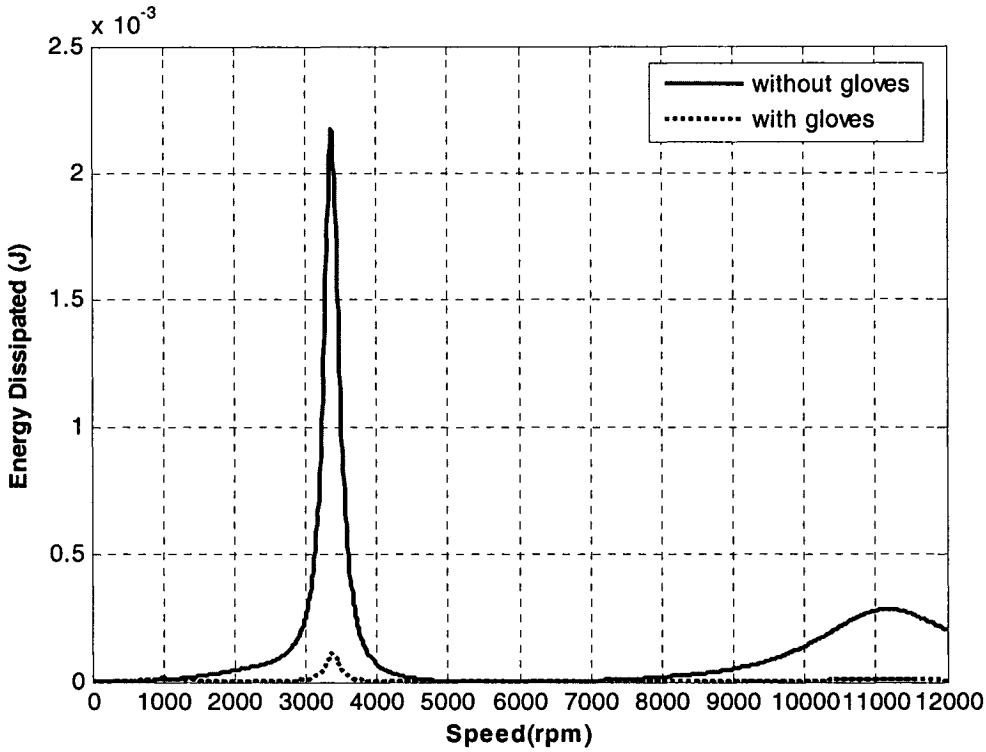

Figure 4.44: Influence of anti-vibration gloves on the energy dissipated by the hand-arm system along the Z-axis for mass unbalance of 76 gm-mm

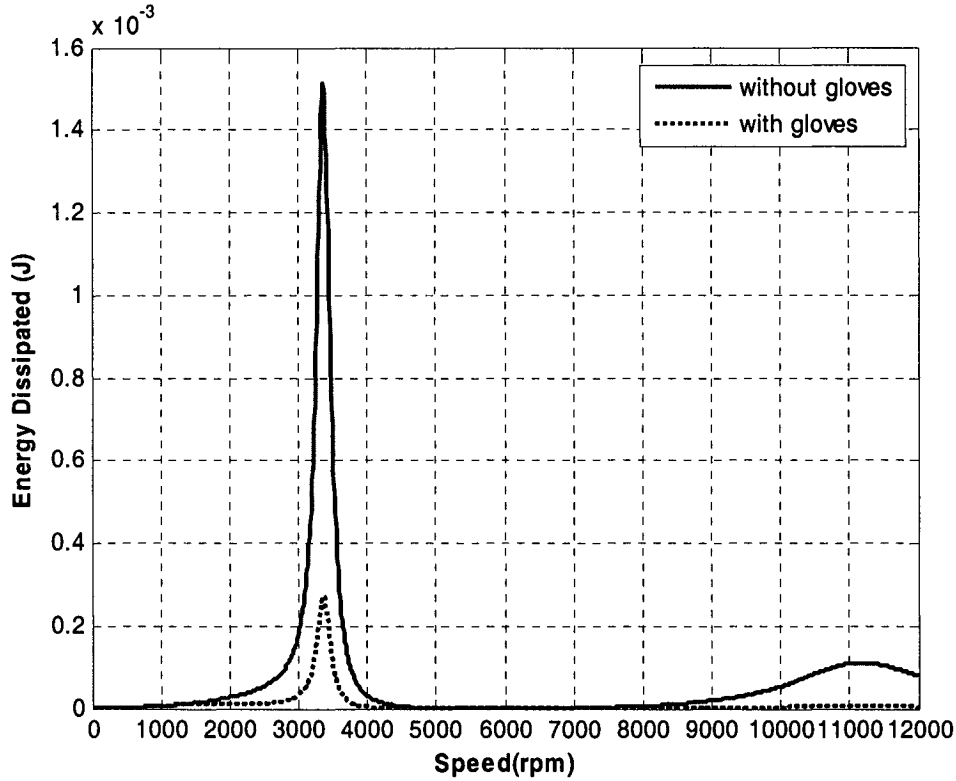

Figure 4.45: Influence of anti-vibration gloves on the energy dissipated by the hand-arm system along the Y-axis for mass unbalance of 76 gm-mm

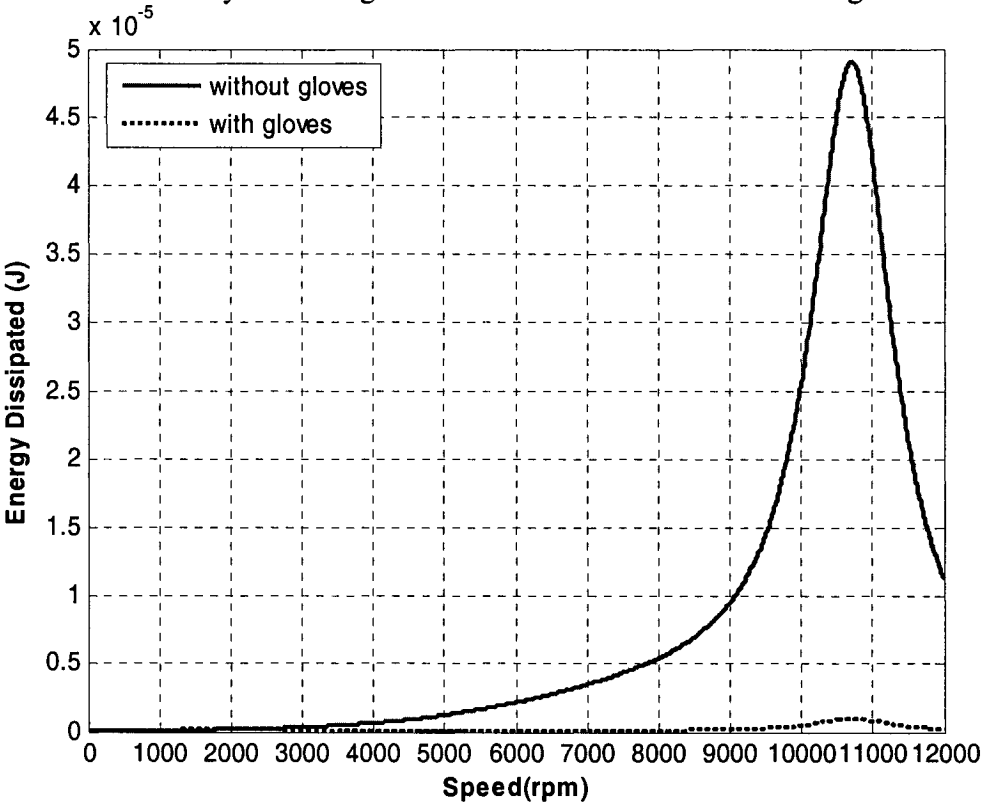

Figure 4.46: Influence of anti-vibration gloves on the energy dissipated by the hand-arm system along the X-axis for mass unbalance of 76 gm-mm

4.12 Summary

A coupled hand-tool model is developed and analyzed for different values of mass unbalance to derive the responses in terms of rms accelerations at the hand-tool interface, forces transmitted to the base (shoulder), energy dissipated and accelerations of different masses of the hand-arm model. The results show increasing rms acceleration responses with increasing mass unbalance, irrespective of the axis of vibration and the speed. The influence of damping properties of the bearings, the effect of variation in machine casing weight on the magnitudes of transmitted vibration is investigated. The vibration performance of the coupled-hand tool model, when anti-vibration gloves are used is also investigated. The results suggest that the magnitude of hand-transmitted vibration can be considerably reduced by employing anti-vibration gloves. The human hand-arm system's capacity of absorbing vibration energy is further investigated.

CHAPTER 5
CONCLUSIONS AND RECOMMENDATIONS FOR FUTURE WORK

5.1 Major Highlights of the Study

The major focus of this dissertation research involved the dynamic response characterization of a hand-held grinder coupled with the human hand and arm through analytical means. The primary purpose of the model was to study the characteristics of transmitted vibration and forces as a function of the mass unbalance, and to identify means for reducing the severity of transmitted vibrations. It also focuses on the changes in responses with variations in the selected design parameters, such as machine casing weight and bearing damping. Moreover, it focuses on the bio-dynamic modeling of the human hand-arm system on the basis of the standardized Driving Point Mechanical Impedance data. Driving Point Mechanical Impedance of human hand-arm is derived from the driving point excitation velocity and the resultant force generated. The vibration response characteristics of the hand-arm and the anti-vibration gloves are also studied. The major highlights of this investigation are summarized as follows:

1) The spindle-disc assembly of a hand-held grinder is characterized by a five degrees-of-freedom model developed along the three orthogonal directions (X-, Y- and Z-axes).
2) The essential parameters of the proposed model were identified in the laboratory through simple experiments and curve-fitting.
3) A human hand-arm model, characterized by a two-degrees-of-freedom lumped parameter system, is developed along all the three orthogonal directions

(x_h-, y_h – and z_h – axes) and the model parameters are identified using mechanical impedance data and nonlinear programming based optimization technique.

4) A coupled hand-tool model is derived analytically which is characterized by 14 degrees-of-freedom, to describe its motion along the X-,Y- and Z-axes. The model is developed specifically to study the contributions due to mass unbalance of the grinding wheel.

5) A parametric study is undertaken to study the influence of the mass unbalance, bearing damping and machine casing weight on the nature of transmitted vibration.

6) The effect of anti-vibration glove on the magnitudes of the hand-transmitted vibration is studied through development and analysis of a coupled hand-glove-tool model, characterized by 17 degrees-of-freedom, to describe its motion along the three orthogonal directions.

7) The human hand-arm system's capacity of absorbing vibration energy is studied.

5.2 Conclusions

On the basis of results obtained from the studies conducted in this thesis, the following major conclusions are drawn:

1) The gyroscopic effects of the rotary spindle and the disc are insignificant on the hand-transmitted vibration, when an in-plane mass unbalance is considered.

2) The optimization technique of reducing the error between the measured and calculated DPMI (Driving Point Mechanical Impedance) can be conveniently used to identify the parameters of the hand-arm vibration models. The model structure, provided in ISO-10068 [50] can be appropriately considered as a two-DOF system

along each axis. The considerations of the three-DOF model, as recommended, yields frequencies that donot correspond with those observed from the DPMI response.

3) The measured vibration data revealed various resonances of the hand-arm system which were identified in the 30-35 Hz, 30-40 Hz, and 100-110 Hz frequency ranges along the z_h-, y_h- and x_h-axes, respectively. The damped frequencies of the proposed model, identified from the complex eigenvalue analysis, were observed to lie close to the above frequency ranges. Furthermore, the eigenvalue analysis revealed that the human hand and arm is a highly damped system.
4) The magnitudes of the hand-transmitted vibration increased significantly with increase in the mass unbalance.
5) The response of the hand mass, which is in contact with the power tool, is larger than the response of the hand mass which is located at the base.
6) An increase in bearing damping could yield lower magnitudes of hand-transmitted vibration at the resonant frequencies.
7) An increase in machine casing weight can reduce the magnitude of hand-transmitted vibration, but a heavier machine would be undesirable.
8) The addition of anti-vibration glove material yields most significant reduction in the transmitted vibration, specifically at higher operating speeds. The gloves, however, cause slight amplifications of vibrations at lower speeds in the 1000-1600 rpm, depending upon the axes of measurement.
9) The proposed model could be effectively applied to assess and select the properties of the glove materials.

10) The proposed model can also be applied to study alternative measures of hand-transmitted vibration, specifically the forces transmitted to the upper body structure and energy dissipated within the hand-arm system.

11) The amount of hand-transmitted vibration can be reduced by using anti-vibration gloves.

12) The anti-vibration gloves also offer considerable potential in reducing the amounts of energy absorbed and forces transmitted.

5.3 Recommendations for Future Work

1) Consider the biological properties of the hand-arm system in the study; flexibility of the shaft, disc assembly; nonlinear properties of the bearings; and the conditions due to many intrinsic and extrinsic variables.

2) Develop and integrate the model of an auto-balancer incorporating freely oscillating balls within a guide way.

3) Identify optimal glove parameters, such that effective attenuation of vibration may be realized in the entire frequency range.

4) Determine if any relation exists between the energy absorbing properties of the hand-arm system and the risk assessment.

REFERENCES

1. Brammer A.J., Relations Between Vibration Exposure and the Development of the Vibration Syndrome, In : Brammer and Taylor (eds) Vibration Effects on the Hand and Arm in Industry. New York, John Wiley and Sons, pp. 283-290, 1982.
2. Reynolds D.D. and Soedel W., Dynamic Response of the Hand-Arm System to a Sinusoidal Input, Journal of Sound and Vibration, 21, pp. 339-353, 1972.
3. Reynolds D.D. and Jokel C.R., Hand-arm Vibration-An Engineering Approach, American Industrial Hygiene Association Journal, 35, pp. 613-620, 1974.
4. Griffin M.J., Hand-Arm Vibration Standards and Dose-Effect Relationship. In: Brammer A.J., Taylor W. (eds) Vibration Effects on the Hand and Arm in Industry. Wiley and Sons, New York, pp. 259-268, 1982.
5. Griffin M.J., Handbook of Human Vibration, Academic Press, London, 1990.
6. Griffin M.J., Macfarlane C.R. and Norman C.D., The Transmission of Vibration to the Hand and the Influence of Gloves, In: Vibration Effects on the Hand and Arm in Industry, Brammer A.J. and Taylor W. eds, John Wiley and Sons, New York, pp. 103-116, 1982.
7. Politschuk A.P. and Obilivin V.N., Methods of Reducing the Efforts of Noise and Vibration on Power Saw Operators. Proceedings of the International Occupational Hand-Arm Vibration Conference, Cincinnati (OH), 1977, pp. 230-232.
8. Suggs C.W., Abrams C.F. Jr. and Cundiff J.S., Attenuation of High Frequency Vibration in Chain Saws, Journal of Sound and Vibration, 2(6), 1968.

9. Suggs C.W. and Hanks J.M., Resilient Hand grips, In Brammer A.J. and Taylor W. eds., Vibration Effects on the Hand and Arm in Industry, New York, Wiley, pp.333-337, 1982.

10. Cherian T., Control of Hand Transmitted Vibration through Development and Analysis of a Human Hand-Arm-Isolator Model, M.A.Sc. Thesis Concordia University, 1994.

11. Hewitt S., Assessing the Performance of Anti-Vibration Gloves- A Possible Alternative to ISO 10819, 1996. Annals of Occupational Hygiene, 42, pp. 245-252, 1998.

12. Rens G., Dubrulle P. and Malchaire J., Efficiency of Conventional Gloves Against Vibration, Annals of Occupational Hygiene, Vol 31, No.2, pp. 249-254, 1987.

13. Gurram R., Rakheja S. and Gouw G.J., Vibration Transmission Characteristics of the Hand-Arm and Gloves, International Journal of Industrial Ergonomics, 13, pp. 217-234, 1994.

14. Rajalingham C., Bhat R.B. and Rakheja S., Automatic Balancing of Flexible Vertical Rotors Using a Guided Ball, International Journal of Mechanical Sciences, 40(9), pp. 825-834, 1998.

15. Wasserman D.E., Taylor W. and Curry M.G., Proceedings of the International Occupational Hand-Arm Conference, Cincinnati, Ohio, USA, 1977.

16. Wasserman D.E., Taylor W. and Curry M.G. (eds), Industrial Vibration- An overview, Journal of American Society of Safety Engineers, 19, pp 38-43, 1974.

17. Brammer A.J., Exposure of the Hand to Vibration in Industry, NRCC Document No.22844, Ottawa, Canada, 1984.

18. Bednal A.W., Hand-Arm Vibration in Great Britain, Proceedings of the Fifth International Conference on Low Frequency Noise and Vibration, Multi-Science Publishing Co., Oxford, pp. 13-20, 1987.

19. Gurram R., A study of Vibration Response Characteristics of the Human Hand Arm System, Ph.D Dissertation, Concordia University, 1993.

20. Radwin R.G., Armstrong T.J. and Van Bergeijk E., Hand-Arm Vibration and Work-Related Disorders of the Upper Limb. In: Pelmear P.L., Wasserman D.E., editors. Hand-Arm Vibration. Beverly Farms, MA: OEM Press, pp. 122-152, 1998.

21. Lundstrom R., Centralized European Hand-Arm Vibration Database, 1998.

22. NIOSH. Criteria for a Recommended Standard: Occupational Exposure to Hand-Arm Vibration. National Institute for Occupational Safety and Health, pp. 89-106, 1989.

23. Taylor W., Wasserman D., Behrens V., Reynolds D.D. and Samueloff S., Effect of Air Hammer on the Hands of Stone Cutters. The Limestone Quarries of Bedford, Indiana, Revisited. British Journal of Industrial Medicine, 41, pp. 289-295, 1984.

24. Oliver T.P., Pethybridge, R.J. and Lumley K.P.S., Vibration White Finger in Dockyard Workers, Arhiv za Higijenu rada Toksikologiju, 30, pp. 683-693, 1979.

25. Taylor W., Wilcox.T and Wasserman D., Health Hazard Evaluation Report, Neenah Foundry Company, Wisconsic, NIOSH report, HHE 80, pp. 189-870, 1981.

26. Agate J.N., Druett H.A. and Tombleson J.B.L., Raynaud's Phenomenon in Grinders of Small Metal Castings, British Journal of Industrial Medicine, 1946.

27. Matsumato T., Harada N., Yamada S. and Kobayashi S., On Vibration Hazards of Chipping Hammer Operations in an Iron Foundry, Japan Journal of Industrial Health 23, pp. 51-60, 1981.

28. Chatterjee D.S., Petrie A. and Taylor W., Prevalence of Vibration Induced White Finger in Fluorsparmines in Weardale, British Journal of Industrial Medicine, 35, pp. 208-218, 1978.

29. Robert J., Mereau P., Cavelier C. and Chameaud J., Occupational Angioneurotic Problems Caused by Hand Tool Vibrations, Archives des Maladies Professionnelles de Medecine du Travail et de Securite Sociale, 38, pp.437-455, 1977.

30. Matsumoto T., Yamada S. and Harada N., A Comparative Study of Vibration Hazards among Operators of Vibrating Tools in Certain Industries, Arhiv za Higijenu rada Toksikologiju, 30, pp. 701-707, 1979.

31. Behrens V., Taylor W., Wilcox T., Miday R., Spaeth S. and Burg J., Vibration Syndrome in Chipping and Grinding Workers-III.Epidemiology, Journal of Occupational Medicine, 26(10), pp. 769-773, 1984.

32. Bovenzi M., Petronio L. and Di Marino F., Epidemiological Survey of Shipyard Workers Exposed to Hand Arm Vibration, International Archives of Occupational and Environmental Health, 46, pp. 251-256, 1980.

33. Walker D.D., Jones B., Ogston S., Tasker E.G., Robinson A.J., A Study of White Finger in the Gas Industry, British Journal of Industrial Medicine, 42, pp. 672-677.

34. Pelmear P.L., Taylor W. and Pearson J.C.G., Raynaud's Phenomenon in Grinders, In Taylor W and Pelmear P L (eds), The Vibration White Finger in Industry, Academic Press, London, pp. 21-30, 1975.

35. Starck J.P., Farkilla M.A., Aatola S., Pyykko I. and Markonen O., Vibration Syndrome and Vibration in Pedestal Grinders, British Journal of Industrial Medicine, 40, 426-433, 1983.

36. Iwata H., Effects of Rock Drills on Operators (Part I and II), Industrial Health, 6, pp. 28-46, 1968.

37. Brubaker R.L., Mackenzie C.J.G. and Hutton S.G., Vibration Induced White Finger among Selected Underground Rock Drillers in British Columbia, Scandinavian Journal of Work Environment and Health, 12(4), pp. 296-300, 1986.

38. Pelmear P.L., Taylor W. and Pearson J.C.G., Raynoud's Phenomenon in Grinders, In :Taylor W and pelmear P.L (eds), The Vibration White Finger in Industry, Academic press, London, pp.21-30, 1975.

39. Engstrom K. and Dandanell R., Exposure Conditions and Raynaud's Phenomenon among Reivetres in the Aircraft Industry, Scandinavian Journal of Work Environment and Health, 12(4), pp. 293-295, 1986.

40. Brammer A.J. and Taylor W., Vibration Effects On The Hand and Arm in Industry: An Introduction and Review, John Wiley & Sons, NewYork, 1982.

41. ISO-5349, Guidelines for Measurement and Assessment of Human Exposure to Hand-Transmitted Vibration, 1986.

42. ISO 5349-1, Mechanical Vibration-Measurement and Evaluation of Human Exposure to Hand-Transmitted Vibration, 2001.

43. ISO-8727, Mechanical Vibration and Shock-Human Exposure-Biodynamic Coordinate Systems. International Standards Organization, 1997.

44. Ikeda K., Ishizuka H., Sawada A. and Urushiyama K., Vibration Acceleration Magnitudes of Hand-Held Tools and Work pieces. Industrial Health, 36, pp. 197-208, 1998.

45. Bitsch J., Donati P., Poirot R. and Roure L., Elaboration of a Standard Procedure for the Measurement of Vibration Emitted by Percussive Tools: Application to Breakers, Scandinavian Journal of Work Environment and Health, pp. 347-350, 1986.

46. BSI 6842, British Standard Guide to the Measurement and Evaluation of Human Exposure to Vibration Transmitted to the Hand, British Standards Institution, London, England, 1987.

47. ANSI S3.34, The American National Standards Institute's Guide for the Measurement and Evaluation of Human Exposure to Vibration Transmitted to the Hand, 1986.

48. ACGIH, Threshold Limit Values(TLV) and Biological Exposure Indices for 1988-1989. Cincinnati OH, American Conference of Governmental Industrial Hygienists, pp. 83-88.

49. Miwa T., Vibration-Isolation Systems for Hand-Held Vibrating Tools, In Brammer A.J. and Taylor W. eds., Vibration Effects on the Hand and Arm in Industry, New York, Wiley, pp. 303-310, 1982.

50. ISO-10068, Mechanical Vibration and Shock-Free, Mechanical Impedance of the Human Hand-Arm System at the Driving Point, 1998.

51. Reynolds D.D. and Falkenberg, R.J., A Study of the Hand Vibration on Chipping and Grinding Operators, part II: Four-degree-of-freedom Lumped Parameter Model

of the Vibration Response of the Human Hand, Journal of Sound and Vibration, 95, pp. 499-514, 1984.

52. Burström L., Measurement of the Impedance of the Hand and Arm, International Archives of Occupational and Environmental Health, 62, pp. 431-439, 1990.

53. Burström L., The Influence of Biodynamic Factors on the Mechanical Impedance of the Hand and Arm. International Archives of Occupational and Environmental Health, 69, pp. 437-446, 1997.

54. Abrams C.F Jr. and Suggs C.W., Chain Saw Vibration, Isolation and Transmission through the Human Arm, Transactions of the ASAE, pp. 423-425, 1969.

55. Abrams C.F., A Study of the Transmission of High Frequency Vibration in the Human Arm., Masters Thesis. North Carolina University, Raleigh, 1968.

56. Reynolds D.D., and Angevine E.N., Hand Arm Vibration, part II: Vibration Transmission Characteristics of the Hand and Arm, Journal of sound and Vibration, 51(2), pp. 255-265, 1977.

57. Pyykkő I., Färkkilä M., Toivanen, J., Korhonen O. and Hyvarinen J., Transmission of Vibration in the Hand-Arm System with Special Reference to Change in Compression Force and Acceleration, Scandinavian Journal of Work, Environment and Health, 2, pp. 87-95, 1976.

58. Rodriguez J., Fredericks TK., Vibration Transmission Characteristics of Subjects Exposed to Uniaxial Vibrations at the Fingers. In: Lee GCH, editor. Advances in Occupational Ergonomics and Safety. Amsterdam: IOS Press, pp. 327-331, 1999.

59. Gurram R., Rakheja S. and Brammer A.J., Driving-point Mechanical Impedance of the Human Hand-Arm System: Synthesis and Model Development, Journal of Sound and Vibration, 180, pp. 437-458, 1995.

60. Suggs C.W., and Mishoe J.W., Hand-Arm Vibration: Vibrational Responses of the Human Hand, Journal of Sound and Vibration, 53 (Pt II), pp. 545-558, 1977.

61. Suggs, C.W. and Mishoe J.W., Hand-Arm Vibration: Implications Drawn From Lumped Parameter Models, Proceedings of the 3rd International Hand-Arm Vibration Conference, Ohio, USA, pp. 136-141, 1977.

62. Reynolds D.D. and Angevine E.N., Hand Arm Vibration, part II: Vibration Transmission Characteristics of the Hand and Arm, Journal of Sound and Vibration, 51(2), pp. 255-265, 1977.

63. Miwa T., Yonekawa Y., Nara A., Kanada K. and Baba K., Vibration Isolation Gloves for Portable Vibrating Tools part 4: Vibration Isolation Gloves, Industrial Health (Japan), 17, pp. 141-152, 1979.

64. Meltzer G., Proceedings of the International Symposium on Man under Vibration Suffering and Protection: A Vibration Model for the Human Hand-Arm system, Udine, Italy, pp. 210-221, 1979.

65. Daikoku M. and Ishikawa F., Proceedings of Fifth International Conference on Hand-Arm Vibration: Mechanical Impedance and Vibration Model of Hand-Arm System, Kanzawa, Japan ,1990.

66. Reynolds D.D. and Soedel W., Dynamic Response of the Hand-Arm System to a Sinusoidal Input, Journal of Sound and Vibration 21, pp. 339-353, 1972.

67. Wood L.A., Suggs C.W. and Abrams C.F., Hand-Arm Vibration. Part III: A Distributed Parameter Dynamic Model of the Human Hand-Arm System, Journal of Sound and Vibration 57, pp. 157-169,1978.

68. Rakheja S., Wu J. Z., Dong R.G. and Schopper A W., A Comparison of Biodynamic Models of the Human Hand-Arm System for Applications to Hand-Held Power Tools, Journal of Sound and Vibration, 249(1), pp. 55-82, 2002.

69. Van Bergeijk E., Selection of Power Tools and Mechanical Assists for Control of Occupational Hand and Wrist Injuries. In: American Conference of Governmental Industrial Hygienists Staff. Ergonomic Interventions to Prevent Musculoskeletal Injuries in Industry. Chelsea, MI:Lewis Publishers, 1987.

70. Armstrong T., Hansen D.J., Kennedy K.W., Repetitive Trauma Disorders:Job Evaluation and Design. The Human Factors Society, 28, pp. 325-6, 1986.

71. Kihlberg S.K., Lindbeck L., Pneumatic Tool Torque Reaction-Reaction Forces, Displacement, Muscle Activity and Discomfort in the Hand-Arm System. Applied Ergonomics, 24, pp. 165-173, 1993.

72. Malkin S., Grinding Technology, Theory and Applications of Machining with Abrasives, 1989.

73. Leist T.H. and Lemon J.R., Practical Approaches to obtain Improved Machine Stability, Industrial Diamond Review, 30, No.353, pp.129-135, 1970.

74. Inoue H., Chattering Phenomena in Grinding, Bullet in of the Japan Society of Precisional Engineering, 3, pp.67-71, 1969.

75. Hoshi T. and Koumoto Y., Mechanism of Vibration in Plunge-cut Cylindrical Grinding, Proceedings of the 5th International Conference on Production Engineering pp. 314, Tokyo, 1984.

76. Colding B., How Stiffness Affecting Grinding Performance, Machinery (NY), March 1970, pp. 57.

77. Koenigsberger T., Machine Tool Structures, Volume-1, 1970.

78. Burstrom L., Measurement of the Mechanical Energy Absorption in the Hand and Arm whilst using Vibration Tools, Ph.D Dissertation, Lulea University of Technology.

79. Green I. and Etsion I., Stiffness and Damping characteristics of Elastomer O-rings Secondary Seals Subjected to Reciprocating Twist, International Conference on Fluid Sealing, pp. 221-229, 1984.

80. Erwin Kramer., Dynamics of Rotors and Foundations, Newyork: Springer-Verlag, 1993.

81. Tiwari M., Gupta K. and Prakash O., Dynamic response of an unbalanced Rotor Supported on Ball Bearings, Journal of Sound and Vibration, 238(5), 757-779, 2000.

82. Tamura H. and Tsuda Y., On the static Running Accuracy of Ball Bearings, Bulletin of the Japan Society of Mechanical Engineering, 28, pp. 1240-1246, 1985.

83. Aatola S., Transmission of Vibration to the Wrist and Compression of Frequency Response and Comparison of Frequency Estimators, Journal of Sound and Vibration, 131(3), pp. 497-507, 1989.

84. Lundstrom R. and Bustrom L., Mechanical Impedance of the Human Hand-Arm System, International Journal of Industrial Ergonomics, 3, pp. 235-242, 1989.

85. Reynolds D.D., Hand-arm vibration: A Review of Three Years Research, Proceedings of the 3rd International Hand-Arm Vibration Conference, Ohio, USA, pp. 99-129, 1977.

86. Suggs C.W., Modeling of the Dynamic Characteristic of the Hand-Arm System, In: Taylor W and Pelmear P.L.(eds), The Vibration Syndrome, Academic press, London, pp. 169-186, 1974.

87. Marcotte P., Aldien Y., Boileau P.-É., Rakheja S. and Boutin J., Effect of Handle Size and Hand–Handle Contact Force on the Biodynamic Response of the Hand–Arm System under z_h-axis vibration, Journal of Sound and Vibration, pp. 1-21, 2004.

88. Chaffin D.B. and Anderson B.J., Occupational Biomechanics, John Wiley and Sons, New York, 1984.

89. Newland D.E., Mechanical Vibration Analysis and Computation, Newyork, Wiley, 1989.

90. Foss K.A., Co-ordinates which Uncouple the Equations of Motion of Damped Linear Dynamic Systems, Journal of Applied Mechanics, pp. 361-364, 1958.

91. Reynolds D.D. and Wilson F.L., Mechanical Tests Stand for Measuring the Vibration of Chain Saw Handles During Cutting Operations, Vibration Effects on the Hand and Arm in Industry. Edited by Brammer A.J. and Taylor W., 1982.

92. Sorensson A. and Lundstrom R., Transmission of Vibration to the Hand. Journal of Low Frequency Noise,Vibration and Active Control, 11, pp. 14-22, 1992.

93. Ahmed Yousef E., Study of Hand Transmitted Vibration from a Hand-Held Rotary Power Tool, M.A.Sc. Thesis Concordia University, 2003.

94. Lindell H., Vibration Reduction on Hand-Held Grinders by Automatic Balancing, Central European Journal of Public Health, 4(1), pp. 43-45, 1996.

95. Suggs C.W. and Abrams Jr., C.F., Vibration Isolation of Power Tools Operators, Proceedings of the 27th Annual Meeting of the Human Factors Society, 1983.

96. Christ E., Anti-Vibration Gloves; Performance Tests. Die Berufsgenossenschaft, 1982

97. Goel V.K. and Rim Kwan., Role of Gloves in Reducing Vibration: Analysis for Pneumatic Chipping Hammer, American Industrial Hygiene Association Journal, 48(1), pp. 9-14, 1987.

98. Strack J., Pekkarinen J. and Chun Chang L., 1990.Transmission of Vibration from Tool Handle to Wrist and to Head. The Kurume Medical Journal, 37:s1-s11.

99. ISO 10819, Mechanical Vibration and Shock-Hand-Arm Vibration-Method for the Measurement and Evaluation of the Vibration Transmissibility of Gloves at the Palm of the Hand, 1996.

100. INRS., Cathierde Notes Documentaries, ND 409-110-83, pp. 47-52,1983.

101. Clarke J.B. and Dalby W., Noise Vibration Control, 16, pp. 146-149, 1985.

102. ANSI-S3.34. Guide for the Measurement and Evaluation of Human Exposure to Vibration Transmitted to the Hand. New York: American National Standards Institute, 1986.

103. Pradko F., Lee R.A. and Greene J.D., Human Vibration-Response Theory, American Society of Mechanical Engineers, Paper No.65-WA/HUF-19, 1965.

104. Lidstrom IM., Vibration Injury in Rock drillers, Chiselers and Grinders. Some Views on the Relationship between the Quantity of Energy Absorbed and the Risk of Occurrence of Vibration Injury. Proceedings of the International Conference on Hand-Arm Vibration, Cincinnati, OH, USA., pp.77-83, 1977.

105. Cundiff J.S., Energy Dissipation in Human Hand-Arm exposed to Random Vibration, Journal of the Acoustal Society of America, 59, pp. 212-214, 1976.

106. Reynolds D.D. and Jokel C., Hand-Arm Vibration-An Engineering Approach, American Industrial Hygiene Association Journal, 35, pp. 613-622, 1974.

107. William T Thomson., Theory of Vibration with Applications, 1993, pp. 67-69.

APPENDIX A

MASS, STIFFNESS AND DAMPING MATRIX OF 14 DEGREE-OF-FREEDOM HAND-GRINDER MODEL

A.1 Along the Z-axis

Mass Matrix

$$[\mathrm{M}] = \begin{bmatrix} M & 0 & 0 & 0 & 0 \\ 0 & I_y & 0 & 0 & 0 \\ 0 & 0 & M_b & 0 & 0 \\ 0 & 0 & 0 & M_{hz2} & 0 \\ 0 & 0 & 0 & 0 & M_{hz3} \end{bmatrix}$$

Stiffness Matrix

$$[\mathrm{K}] = \begin{bmatrix} 2(K_{bz1}+K_{bz2}+K_o+K_{sr}) & 2(a_1K_{bz1}+b_1K_{bz2}+c_1K_o+d_1K_{sr}) & -2(K_{bz1}+K_{bz2}+K_o+K_{sr}) & 0 & 0 \\ 2(a_1K_{bz1}+b_1K_{bz2}+c_1K_o+d_1K_{sr}) & 2(a_1^2K_{bz1}+b_1^2K_{bz2}+c_1^2K_o+d_1^2K_{sr}) & -2(a_1K_{bz1}+b_1K_{bz2}+c_1K_o+d_1K_{sr}) & 0 & 0 \\ -2(K_{bz1}+K_{bz2}+K_o+K_{sr}) & -2(a_1K_{bz1}+b_1K_{bz2}+c_1K_o+d_1K_{sr}) & 2(K_{bz1}+K_{bz2}+K_o+K_{sr})+K_{hz1} & -K_{hz1} & 0 \\ 0 & 0 & -K_{hz1} & K_{hz1}+K_{hz2} & -K_{hz2} \\ 0 & 0 & 0 & -K_{hz2} & K_{hz2}+K_{hz3} \end{bmatrix}$$

Damping Matrix

$$[C]=\begin{bmatrix} 2(C_{bz1}+C_{bz2}+C_o+C_{sr}) & 2(a_1C_{bz1}+b_1C_{bz2}+c_1C_o+d_1C_{sr}) & -2(C_{bz1}+C_{bz2}+C_o+C_{sr}) & 0 & 0 \\ 2(a_1C_{bz1}+b_1C_{bz2}+c_1C_o+d_1C_{sr}) & 2(a_1^2C_{bz1}+b_1^2C_{bz2}+c_1^2C_o+d_1^2C_{sr}) & -2(a_1C_{bz1}+b_1C_{bz2}+c_1C_o+d_1C_{sr}) & 0 & 0 \\ -2(C_{bz1}+C_{bz2}+C_o+C_{sr}) & -2(a_1C_{bz1}+b_1C_{bz2}+c_1C_o+d_1C_{sr}) & 2(C_{bz1}+C_{bz2}+C_o+C_{sr})+C_{hz1} & -C_{hz1} & 0 \\ 0 & 0 & -C_{hz1} & C_{hz1}+C_{hz2} & -C_{hz2} \\ 0 & 0 & 0 & -C_{hz2} & C_{hz2}+C_{hz3} \end{bmatrix}$$

A.2 Along the Y-axis

Mass Matrix

$$[M]=\begin{bmatrix} M & 0 & 0 & 0 & 0 \\ 0 & I_z & 0 & 0 & 0 \\ 0 & 0 & M_b & 0 & 0 \\ 0 & 0 & 0 & M_{hy2} & 0 \\ 0 & 0 & 0 & 0 & M_{hy3} \end{bmatrix}$$

Stiffness Matrix

$$[K]=\begin{bmatrix} 2(K_{by1}+K_{by2}+K_o+K_{sr}) & -2(a_1K_{by1}+b_1K_{by2}+c_1K_o+d_1K_{sr}) & -2(K_{by1}+K_{by2}+K_o+K_{sr}) & 0 & 0 \\ -2(a_1K_{by1}+b_1K_{by2}+c_1K_o+d_1K_{sr}) & 2(a_1^2K_{by1}+b_1^2K_{by2}+c_1^2K_o+d_1^2K_{sr}) & 2(a_1K_{by1}+b_1K_{by2}+c_1K_o+d_1K_{sr}) & 0 & 0 \\ -2(K_{by1}+K_{by2}+K_o+K_{sr}) & 2(a_1K_{by1}+b_1K_{by2}+c_1K_o+d_1K_{sr}) & 2(K_{by1}+K_{by2}+K_o+K_{sr})+K_{hy1} & -K_{hy1} & 0 \\ 0 & 0 & -K_{hy1} & K_{hy1}+K_{hy2} & -K_{hy2} \\ 0 & 0 & 0 & -K_{hy2} & K_{hy2}+K_{hy3} \end{bmatrix}$$

Damping Matrix

$$[C]=\begin{bmatrix} 2(C_{by1}+C_{by2}+C_o+C_{sr}) & -2(a_1C_{by1}+b_1C_{by2}+c_1C_o+d_1C_{sr}) & -2(C_{by1}+C_{by2}+C_o+C_{sr}) & 0 & 0 \\ -2(a_1C_{by1}+b_1C_{by2}+c_1C_o+d_1C_{sr}) & 2(a_1^2C_{by1}+b_1^2C_{by2}+c_1^2C_o+d_1^2C_{sr}) & 2(a_1C_{by1}+b_1C_{by2}+c_1C_o+d_1C_{sr}) & 0 & 0 \\ -2(C_{by1}+C_{by2}+C_o+C_{sr}) & 2(a_1C_{by1}+b_1C_{by2}+c_1C_o+d_1C_{sr}) & 2(C_{by1}+C_{by2}+C_o+C_{sr})+C_{hy1} & -C_{hy1} & 0 \\ 0 & 0 & -C_{hy1} & C_{hy1}+C_{hy2} & -C_{hy2} \\ 0 & 0 & 0 & -C_{hy2} & C_{hy2}+C_{hy3} \end{bmatrix}$$

A.3 Along the X-axis

Mass Matrix

$$[\mathrm{M}] = \begin{bmatrix} M & 0 & 0 & 0 \\ 0 & M_b & 0 & 0 \\ 0 & 0 & M_{hx1} & 0 \\ 0 & 0 & 0 & M_{hx2} \end{bmatrix}$$

Stiffness Matrix

$$[\mathrm{K}] = \begin{bmatrix} (K_{bx1}+K_{bx2}+K_o+K_{sr}) & -(K_{bx1}+K_{bx2}+K_o+K_{sr}) & 0 & 0 \\ -(K_{bx1}+K_{bx2}+K_o+K_{sr}) & (K_{bx1}+K_{bx2}+K_o+K_{sr}+K_{hx1}) & -K_{hx1} & 0 \\ 0 & -K_{hx1} & (K_{hx1}+K_{hx2}) & -K_{hx2} \\ 0 & 0 & -K_{hx2} & (K_{hx2}+K_{hx3}) \end{bmatrix}$$

Damping Matrix

$$[\mathrm{C}] = \begin{bmatrix} (C_{bx1}+C_{bx2}+C_o+C_{sr}) & -(C_{bx1}+C_{bx2}+C_o+C_{sr}) & 0 & 0 \\ -(C_{bx1}+C_{bx2}+C_o+C_{sr}) & (C_{bx1}+C_{bx2}+C_o+C_{sr}+C_{hx1}) & -C_{hx1} & 0 \\ 0 & -C_{hx1} & (C_{hx1}+C_{hx2}) & -C_{hx2} \\ 0 & 0 & -C_{hx2} & (C_{hx2}+C_{hx3}) \end{bmatrix}$$

APPENDIX B

EIGEN VECTORS OF 14 DEGREE-OF-FREEDOM HAND-GRINDER MODEL

Along the Z-axis:

	Mode-1	Mode-2	Mode-3	Mode-4	Mode-5
z_d	-0.5791	-0.03362	0.090754	0.026105	0.031818
β	0.010466	0.022763	-0.97348	-0.99965	0.99949
z_b	-0.57872	-0.032796	0.058388	-0.0037115	-0.0036359
z_2	-0.57294	-0.020804	-0.20171	0.0022369	0.00013077
z_3	-0.036817	0.99842	0.0011917	-6.1467e-006	-3.2057e-008

Natural Frequency for mode-1: 1.9210 (Hz)

Natural Frequency for mode-2: 11.6144 (Hz)

Natural Frequency for mode-3: 39.4959 (Hz)

Natural Frequency for mode-4: 56.5590 (Hz)

Natural Frequency for mode-5: 185.6951 (Hz)

Along the Y-axis:

	Mode-1	Mode-2	Mode-3	Mode-4	Mode-5
y_d	-0.58127	-0.074641	0.063538	0.026398	0.031816
α	0.01187	0.025482	-0.92848	-0.99964	0.99949
y_b	-0.58084	-0.073714	0.033374	-0.0034488	-0.0036123
y_2	-0.5671	-0.044872	-0.36439	0.0041756	0.00018956
y_3	-0.054891	0.99314	0.0012245	-8.3562e-006	-3.4356e-008

Natural Frequency for mode-1: 2.0419 (Hz)

Natural Frequency for mode-2: 8.2987(Hz)

Natural Frequency for mode-3: 43.8650 (Hz)

Natural Frequency for mode-4: 56.4296(Hz)

Natural Frequency for mode-5: 185.66 (Hz)

Along the X-axis:

	Mode-1	Mode-2	Mode-3	Mode-4
x_d	0.57761	-0.025277	-0.14074	-0.9848
x_b	0.57757	-0.025212	-0.055518	0.12021
x_2	0.57662	-0.023463	0.98849	-0.12539
x_3	0.017204	0.99909	-0.00012315	8.4136e-006

Natural Frequency for mode-1: 1.3321 (Hz)

Natural Frequency for mode-2: 8.6368 (Hz)

Natural Frequency for mode-3: 132.2935 (Hz)

Natural Frequency for mode-4: 180.0871(Hz)

APPENDIX C

MASS, STIFFNESS AND DAMPING MATRIX OF 17 DEGREE-OF-FREEDOM HAND-GRINDER MODEL WITH ANTI-VIBRATION GLOVES

C.1 Along the Z-axis

Mass Matrix

$$\begin{bmatrix} M & 0 & 0 & 0 & 0 & 0 \\ 0 & I_y & 0 & 0 & 0 & 0 \\ 0 & 0 & M_b & 0 & 0 & 0 \\ 0 & 0 & 0 & M_{hz1} & 0 & 0 \\ 0 & 0 & 0 & 0 & M_{hz2} & 0 \\ 0 & 0 & 0 & 0 & 0 & M_{hz3} \end{bmatrix}$$

Stiffness Matrix

$$[K]=\begin{bmatrix} 2(K_{bz1}+K_{bz2}+K_o+K_{sr}) & 2(a_1K_{bz1}+b_1K_{bz2}+c_1K_o+d_1K_{sr}) & -2(K_{bz1}+K_{bz2}+K_o+K_{sr}) & 0 & 0 & 0 \\ 2(a_1K_{bz1}+b_1K_{bz2}+c_1K_o+d_1K_{sr}) & 2(a_1^2K_{bz1}+b_1^2K_{bz2}+c_1^2K_o+d_1^2K_{sr}) & -2(a_1K_{bz1}+b_1K_{bz2}+c_1K_o+d_1K_{sr}) & 0 & 0 & 0 \\ -2(K_{bz1}+K_{bz2}+K_o+K_{sr}) & -2(a_1K_{bz1}+b_1K_{bz2}+c_1K_o+d_1K_{sr}) & 2(K_{bz1}+K_{bz2}+K_o+K_{sr})+K_{hzg} & -K_{hzg} & 0 & 0 \\ 0 & 0 & -K_{hzg} & (K_{hzg}+K_{hz1}) & -K_{hz1} & 0 \\ 0 & 0 & 0 & -K_{hz1} & (K_{hz1}+K_{hz2}) & -K_{hz2} \\ 0 & 0 & 0 & 0 & -K_{hz2} & (K_{hz2}+K_{hz3}) \end{bmatrix}$$

Damping Matrix

$$[C]=\begin{bmatrix} 2(C_{bz1}+C_{bz2}+C_o+C_{sr}) & 2(a_1C_{bz1}+b_1C_{bz2}+c_1C_o+d_1C_{sr}) & -2(C_{bz1}+C_{bz2}+C_o+C_{sr}) & 0 & 0 & 0 \\ 2(a_1C_{bz1}+b_1C_{bz2}+c_1C_o+d_1C_{sr}) & 2(a_1^2C_{bz1}+b_1^2C_{bz2}+c_1^2C_o+d_1^2C_{sr}) & -2(a_1C_{bz1}+b_1C_{bz2}+c_1C_o+d_1C_{sr}) & 0 & 0 & 0 \\ -2(C_{bz1}+C_{bz2}+C_o+C_{sr}) & -2(a_1C_{bz1}+b_1C_{bz2}+c_1C_o+d_1C_{sr}) & 2(C_{bz1}+C_{bz2}+C_o+C_{sr})+C_{hzg} & -C_{hzg} & 0 & 0 \\ 0 & 0 & -C_{hzg} & (C_{hzg}+C_{hz1}) & -C_{hz1} & 0 \\ 0 & 0 & 0 & -C_{hz1} & (C_{hz1}+C_{hz2}) & -C_{hz2} \\ 0 & 0 & 0 & 0 & -C_{hz2} & (C_{hz2}+C_{hz3}) \end{bmatrix}$$

C.2 Along the Y-axis

Mass Matrix

$$[M]=\begin{bmatrix} M & 0 & 0 & 0 & 0 & 0 \\ 0 & I_z & 0 & 0 & 0 & 0 \\ 0 & 0 & M_b & 0 & 0 & 0 \\ 0 & 0 & 0 & M_{y1} & 0 & 0 \\ 0 & 0 & 0 & 0 & M_{hy2} & 0 \\ 0 & 0 & 0 & 0 & 0 & M_{hy3} \end{bmatrix}$$

Stiffness Matrix

$$[K] = \begin{bmatrix} 2(K_{by1}+K_{by2}+K_o+K_{sr}) & -2(a_1K_{by1}+b_1K_{by2}+c_1K_o+d_1K_{sr}) & -2(K_{by1}+K_{by2}+K_o+K_{sr}) & 0 & 0 & 0 \\ -2(a_1K_{by1}+b_1K_{by2}+c_1K_o+d_1K_{sr}) & 2(a_1^2K_{by1}+b_1^2K_{by2}+c_1^2K_o+d_1^2K_{sr}) & 2(a_1K_{by1}+b_1K_{by2}+c_1K_o+d_1K_{sr}) & 0 & 0 & 0 \\ -2(K_{by1}+K_{by2}+K_o+K_{sr}) & 2(a_1K_{by1}+b_1K_{by2}+c_1K_o+d_1K_{sr}) & 2(K_{by1}+K_{by2}+K_o+K_{sr})+K_{hyg} & -K_{hyg} & 0 & 0 \\ 0 & 0 & -K_{hyg} & (K_{hyg}+K_{hy1}) & -K_{hy1} & 0 \\ 0 & 0 & 0 & -K_{hy1} & (K_{hy1}+K_{hy2}) & -K_{hy2} \\ 0 & 0 & 0 & 0 & -K_{hy2} & (K_{hy2}+K_{hy3}) \end{bmatrix}$$

Damping Matrix

$$[C] = \begin{bmatrix} 2(C_{by1}+C_{by2}+C_o+C_{sr}) & -2(a_1C_{by1}+b_1C_{by2}+c_1C_o+d_1C_{sr}) & -2(C_{by1}+C_{by2}+C_o+C_{sr}) & 0 & 0 & 0 \\ -2(a_1C_{by1}+b_1C_{by2}+c_1C_o+d_1C_{sr}) & 2(a_1^2C_{by1}+b_1^2C_{by2}+c_1^2C_o+d_1^2C_{sr}) & 2(a_1C_{by1}+b_1C_{by2}+c_1C_o+d_1C_{sr}) & 0 & 0 & 0 \\ -2(C_{by1}+C_{by2}+C_o+C_{sr}) & 2(a_1C_{by1}+b_1C_{by2}+c_1C_o+d_1C_{sr}) & 2(C_{by1}+C_{by2}+C_o+C_{sr})+C_{hyg} & -C_{hyg} & 0 & 0 \\ 0 & 0 & -C_{hyg} & (C_{hyg}+C_{hy1}) & -C_{hy1} & 0 \\ 0 & 0 & 0 & -C_{hy1} & (C_{hy1}+C_{hy2}) & -C_{hy2} \\ 0 & 0 & 0 & 0 & -C_{hy2} & (C_{hy2}+C_{hy3}) \end{bmatrix}$$

C.3 Along the X-axis

Mass Matrix

$$[\mathrm{M}] = \begin{bmatrix} M & 0 & 0 & 0 & 0 \\ 0 & M_b & 0 & 0 & 0 \\ 0 & 0 & M_{hx1} & 0 & 0 \\ 0 & 0 & 0 & M_{hx2} & 0 \\ 0 & 0 & 0 & 0 & M_{hx3} \end{bmatrix}$$

Stiffness Matrix

$$[\mathrm{K}] = \begin{bmatrix} (K_{bx1}+K_{bx2}+K_o+K_{sr}) & -(K_{bx1}+K_{bx2}+K_o+K_{sr}) & 0 & 0 & 0 \\ -(K_{bx1}+K_{bx2}+K_o+K_{sr}) & (K_{bx1}+K_{bx2}+K_o+K_{sr}) & -K_{hxg} & 0 & 0 \\ 0 & -K_{hxg} & (K_{hxg}+K_{hx1}) & -K_{hx1} & 0 \\ 0 & 0 & -K_{hx1} & (K_{hx1}+K_{hx2}) & -K_{hx2} \\ 0 & 0 & 0 & -K_{hx2} & (K_{hx2}+K_{hx3}) \end{bmatrix}$$

Damping Matrix

$$[\mathrm{C}] = \begin{bmatrix} (C_{bx1}+C_{bx2}+C_o+C_{sr}) & -(C_{bx1}+C_{bx2}+C_o+C_{sr}) & 0 & 0 & 0 \\ -(C_{bx1}+C_{bx2}+C_o+C_{sr}) & (C_{bx1}+C_{bx2}+C_o+C_{sr}) & -C_{hxg} & 0 & 0 \\ 0 & -C_{hxg} & (C_{hxg}+C_{hx1}) & -C_{hx1} & 0 \\ 0 & 0 & -C_{hx1} & (C_{hx1}+C_{hx2}) & -C_{hx2} \\ 0 & 0 & 0 & -C_{hx2} & (C_{hx2}+C_{hx3}) \end{bmatrix}$$

APPENDIX D

EIGEN VECTORS OF 17 DEGREE-OF-FREEDOM HAND-GRINDER MODEL WITH ANTI-VIBRATION GLOVES

Along the Z-axis:

	Mode-1	Mode-2	Mode-3	Mode-4	Mode-5	Mode-6
z_d	-0.50999	-0.049521	-0.23469	-0.026773	0.005415	0.031815
β	0.0087103	0.033411	0.40291	0.99964	0.24854	0.99949
z_b	-0.50967	-0.048311	-0.22026	0.0031119	0.0078515	-0.0036035
z_1	-0.49192	0.016701	0.50906	0.00054607	-0.96344	0.00040631
z_2	-0.48693	0.034063	0.6885	-0.00033471	0.09957	-1.4621e-005
z_3	-0.031242	0.99632	-0.029773	9.2978e-007	-6.6236e-005	3.586e-009

Natural Frequency for mode-1: 1.8675 (Hz)

Natural Frequency for mode-2: 11.5944 (Hz)

Natural Frequency for mode-3: 18.1502 (Hz)

Natural Frequency for mode-4: 56.2652 (Hz)

Natural Frequency for mode-5: 113.1017 (Hz)

Natural Frequency for mode-6: 185.6497 (Hz)

Along the Y-axis:

	Mode-1	Mode-2	Mode-3	Mode-4	Mode-5	Mode-6
y_d	-0.51239	-0.075484	-0.10432	-0.026784	0.0047012	0.031815
α	0.0097557	0.025649	0.37249	0.99964	0.36904	0.99949
y_b	-0.51204	-0.074551	-0.091226	0.0031022	0.011882	-0.0036033
y_1	-0.49216	-0.023459	0.50289	0.00084721	-0.89761	0.00033232
y_2	-0.48043	0.0059382	0.76751	-0.0010397	0.24071	-1.7441e-005
y_3	-0.0463	0.99373	-0.0083329	2.0935e-006	-0.00018534	3.1616e-009

Natural Frequency for mode-1: 1.9717 (Hz)

Natural Frequency for mode-2: 8.2795 (Hz)

Natural Frequency for mode-3: 25.3552 (Hz)

Natural Frequency for mode-4: 56.2604 (Hz)

Natural Frequency for mode-5: 90.3678 (Hz)

Natural Frequency for mode-6: 185.6493 (Hz)

Along the X-axis:

	Mode-1	Mode-2	Mode-3	Mode-4	Mode-5
x_d	0.50439	-0.025764	0.075283	-0.99353	-0.0047567
x_b	0.50437	-0.025698	0.072585	0.11248	0.0026789
x_1	0.49588	-0.0065629	-0.68085	0.010877	-0.86568
x_2	0.49506	-0.0047631	-0.72492	-0.011532	0.50056
x_3	0.014753	0.9993	0.0016376	7.7997e-007	-2.4094e-005

Natural Frequency for mode-1: 1.2979 (Hz)

Natural Frequency for mode-2: 8.6345 (Hz)

Natural Frequency for mode-3: 32.1816 (Hz)

Natural Frequency for mode-4: 179.3755 (Hz)

Natural Frequency for mode-5: 212.5588 (Hz)